THE EUROPEAN
PHYSICAL JOURNAL C

Searches for physics beyond the standard model with the M_{T2} variable in hadronic final states with and without disappearing tracks in proton–proton collisions at $\sqrt{s} = 13$ TeV

CMS Collaboration[*]

CERN, 1211 Geneva 23, Switzerland

Abstract Two related searches for phenomena beyond the standard model (BSM) are performed using events with hadronic jets and significant transverse momentum imbalance. The results are based on a sample of proton–proton collisions at a center-of-mass energy of 13 TeV, collected by the CMS experiment at the LHC in 2016–2018 and corresponding to an integrated luminosity of 137 fb^{-1}. The first search is inclusive, based on signal regions defined by the hadronic energy in the event, the jet multiplicity, the number of jets identified as originating from bottom quarks, and the value of the kinematic variable M_{T2} for events with at least two jets. For events with exactly one jet, the transverse momentum of the jet is used instead. The second search looks in addition for disappearing tracks produced by BSM long-lived charged particles that decay within the volume of the tracking detector. No excess event yield is observed above the predicted standard model background. This is used to constrain a range of BSM models that predict the following: the pair production of gluinos and squarks in the context of supersymmetry models conserving R-parity, with or without intermediate long-lived charginos produced in the decay chain; the resonant production of a colored scalar state decaying to a massive Dirac fermion and a quark; or the pair production of scalar and vector leptoquarks each decaying to a neutrino and a top, bottom, or light-flavor quark. In most of the cases, the results obtained are the most stringent constraints to date.

1 Introduction

We present results of two related searches for physics beyond the standard model (BSM) in events with jets and significant transverse momentum imbalance. These are based on a data set of proton–proton (pp) collisions at $\sqrt{s} = 13$ TeV, collected with the CMS detector at the CERN LHC in

2016–2018, and corresponding to an integrated luminosity of 137 fb^{-1}.

The first is an inclusive search that exploits the transverse momentum imbalance as inferred from the kinematic variable M_{T2} [1], defined in Sect. 3.1, in events with at least two hadronic jets, or the transverse momentum (p_T) of the jet in events with just one jet. Similar searches were previously conducted by both the ATLAS [2–7] and CMS [8–12] Collaborations. Our analysis builds on the work presented in Refs. [9,11], using improved methods to estimate the background from standard model (SM) processes, in particular the multijet background arising from instrumental effects. Event counts in bins of the number of jets (N_j), the number of jets identified as originating from the fragmentation of a bottom quark (b-tagged jets, N_b), the scalar p_T sum of all selected jets (H_T), and the M_{T2} variable or the p_T of the single jet, are compared against estimates of the background from SM processes, as derived from dedicated data control samples.

The second search aims at extending the sensitivity of the inclusive search for scenarios where the mass spectrum of potential new particles is compressed. In such scenarios, some theoretical models [13,14] predict the existence of long-lived charged particles that can be identified as disappearing tracks, when they decay within the volume of the tracking detector and their charged decay products are below the p_T detection threshold. Such signatures are rare in the SM and are often dominated by instrumental effects. The presence of disappearing tracks is exploited in order to suppress the background from SM processes, and to enhance the sensitivity towards these scenarios. Similar analyses were previously conducted by both the ATLAS [15,16] and CMS [17–20] Collaborations. We use events with at least two jets, and the M_{T2} variable to further suppress the background from SM processes. Event counts in bins of N_j, H_T, disappearing track length, and disappearing track p_T are compared against estimates of the background from SM processes derived from dedicated data control samples.

[*] e-mail: cms-publication-committee-chair@cern.ch

The results are interpreted in the context of simplified models [21–25] of R-parity [26] conserving supersymmetry (SUSY) [27–34] where gluinos and squarks are pair-produced and the lightest SUSY particle is a neutralino.

The results of the inclusive M_{T2} search are also interpreted in the context of a BSM scenario where a colored scalar state ϕ is resonantly produced through coupling to quarks, and decays to an invisible massive Dirac fermion ψ and an SM quark. This is referred to as the mono-ϕ model. It has been recently proposed as an explanation of an excess in data in regions with low jet multiplicities, identified in the context of a reinterpretation [35,36] of the results of the previous inclusive M_{T2} search [9] as well as of other similar searches by both the ATLAS [6,7] and CMS [8,37] Collaborations.

Finally, the inclusive M_{T2} search is interpreted using models of leptoquark (LQ) pair production, similarly to Ref. [11]. Leptoquarks are hypothetical particles with quantum numbers of both quarks and leptons [38]. The spin of an LQ state is either 0 (scalar LQ or LQ_S) or 1 (vector LQ or LQ_V). Leptoquarks appear in BSM theories such as grand unified theories [38–41], technicolor models [42–45], compositeness scenarios [46,47], and R-parity violating SUSY [27–34,48], and have been suggested as an explanation of the anomalies observed in flavor physics [49–55] by the BaBar [56,57], Belle [58–62], and LHCb [63–68] Collaborations. The best fit model of Refs. [54,55] predicts an LQ_V with a mass of $\mathcal{O}$ (TeV) decaying with 50% branching fraction to either a top quark and a neutrino (tν) or a bottom quark and a τ lepton (bτ), which would be expected to be visible at the LHC. The final states and kinematic variables resulting from the pair production of LQ_S, each decaying to a quark and a neutrino, are the same as those considered in searches for squark pair production in R-parity conserving SUSY, assuming that the squark decays directly to a quark and a massless neutralino [11,69]. The decay products of LQ_V are also found to have similar kinematic properties [11,69]. Therefore, as the search presented in this paper is already optimized for squark pair production, it is also sensitive to LQ pair production. The LQ production with decays to a quark and a neutrino has been constrained using LHC data by both the ATLAS [70–72] and CMS [11,73–77] Collaborations, either by reinterpreting the existing squark searches, or considering scenarios with mixed branching fractions where an LQ also decays to a quark and a charged lepton. The same signatures have been previously covered at the Fermilab Tevatron by the CDF (e.g., in Refs. [78–80]) and D0 (e.g., in Refs. [81–83]) Collaborations. Constraints have been placed by direct searches for single LQ production performed at HERA by the H1 [84] and ZEUS [85] Collaborations. Finally, searches for LQs decaying to bτ have been performed by the ATLAS [86], CMS [87,88], CDF [89,90], and D0 [91] Collaborations.

After a brief description of the CMS detector in Sect. 2, the event selection and categorization as well as details of the Monte Carlo (MC) simulation are presented in Sect. 3. Section 4 describes the SM background estimation. Results and their interpretations are presented in Sects. 5 and 6, respectively. Finally, a summary is provided in Sect. 7.

2 The CMS detector

The central feature of the CMS apparatus is a superconducting solenoid of 6 m internal diameter providing a magnetic field of 3.8 T. Within the solenoid volume are a silicon pixel and strip tracker, a lead tungstate crystal electromagnetic calorimeter, and a brass and scintillator hadron calorimeter, each composed of a barrel and two endcap sections. Forward calorimeters extend the pseudorapidity (η) coverage provided by the barrel and endcap detectors. Muons are measured in gas-ionization detectors embedded in the steel flux-return yoke outside the solenoid. The first level of the CMS trigger system, composed of custom hardware processors, uses information from the calorimeters and muon detectors to select the most interesting events in a fixed time interval of less than 4 µs. The high-level trigger processor farm further decreases the event rate from around 100 kHz to about 1 kHz, before data storage. A more detailed description of the CMS detector and trigger system, together with a definition of the coordinate system used and the relevant kinematic variables, can be found in Refs. [92,93]. The pixel tracker was upgraded before the start of the data taking period in 2017, providing one additional layer of measurements compared to the older tracker [94].

3 Event selection and Monte Carlo simulation

3.1 Event selection

Events are processed using the particle-flow (PF) algorithm [95], which aims at reconstructing and identifying each individual particle in an event, with an optimal combination of information from the elements of the CMS detector. The particles reconstructed with this algorithm are hereafter referred to as PF candidates. The physics objects and the event preselection are similar to those described in Ref. [9]; they are summarized in Table 1, and described in detail below. We select events with at least one reconstructed vertex and at least one jet, and veto events with an isolated lepton (e or µ) or an isolated charged PF candidate. The isolated charged PF candidate veto is designed to provide additional rejection against events with electrons and muons, as well as to reject hadronic τ decays.

Jets are formed by clustering PF candidates using the anti-k_T algorithm [97,98] and are corrected for contributions from event pileup [99] and the effects of nonuniform detector

Table 1 Summary of the trigger requirements and the kinematic offline event preselection requirements on the reconstructed physics objects, for both the inclusive M_{T2} search and the search for disappearing tracks. Here R is the distance parameter of the anti-k_{T} algorithm. To veto leptons and tracks, the transverse mass M_{T} is determined using the veto object and the $\vec{p}_{\mathrm{T}}^{\mathrm{miss}}$. The variable $p_{\mathrm{T}}^{\mathrm{sum}}$ is a measure of object isolation and it denotes the p_{T} sum of all additional PF candidates in a cone around the lepton or the track. The size of the cone is listed in the table in units of $\Delta R \equiv \sqrt{(\Delta\phi)^2 + (\Delta\eta)^2}$. The lepton (track) p_{T} is denoted as $p_{\mathrm{T}}^{\mathrm{lep}}$ ($p_{\mathrm{T}}^{\mathrm{track}}$). Further details of the lepton selection are given in Refs. [9,96]. The ith-highest p_{T} jet is denoted as j_{i}

Trigger	2016:
	$p_{\mathrm{T}}^{\mathrm{miss}} > 120$ GeV and $H_{\mathrm{T}}^{\mathrm{miss}} > 120$ GeV, or
	$H_{\mathrm{T}} > 300$ GeV and $p_{\mathrm{T}}^{\mathrm{miss}} > 110$ GeV, or
	$H_{\mathrm{T}} > 900$ GeV, or jet $p_{\mathrm{T}} > 450$ GeV
	2017 and 2018:
	$p_{\mathrm{T}}^{\mathrm{miss}} > 120$ GeV and $H_{\mathrm{T}}^{\mathrm{miss}} > 120$ GeV, or
	$H_{\mathrm{T}} > 60$ GeV and $p_{\mathrm{T}}^{\mathrm{miss}} > 120$ GeV and $H_{\mathrm{T}}^{\mathrm{miss}} > 120$ GeV, or
	$H_{\mathrm{T}} > 500$ GeV and $p_{\mathrm{T}}^{\mathrm{miss}} > 100$ GeV and $H_{\mathrm{T}}^{\mathrm{miss}} > 100$ GeV, or
	$H_{\mathrm{T}} > 800$ GeV and $p_{\mathrm{T}}^{\mathrm{miss}} > 75$ GeV and $H_{\mathrm{T}}^{\mathrm{miss}} > 75$ GeV, or
	$H_{\mathrm{T}} > 1050$ GeV, or jet $p_{\mathrm{T}} > 500$ GeV
Jet selection	$R = 0.4$, $p_{\mathrm{T}} > 30$ GeV, $|\eta| < 2.4$
b-tagged jet selection	$p_{\mathrm{T}} > 20$ GeV, $|\eta| < 2.4$ and b tag
H_{T}	$H_{\mathrm{T}} > 250$ GeV
$p_{\mathrm{T}}^{\mathrm{miss}}$	$p_{\mathrm{T}}^{\mathrm{miss}} > 250$ GeV for $H_{\mathrm{T}} < 1200$ GeV or $N_{\mathrm{j}} = 1$, else $p_{\mathrm{T}}^{\mathrm{miss}} > 30$ GeV
	$\Delta\phi_{\mathrm{min}} = \Delta\phi\left(\vec{p}_{\mathrm{T}}^{\mathrm{miss}}, j_{1,2,3,4}\right) > 0.3$
	$|\vec{p}_{\mathrm{T}}^{\mathrm{miss}} - \vec{H}_{\mathrm{T}}^{\mathrm{miss}}|/p_{\mathrm{T}}^{\mathrm{miss}} < 0.5$
M_{T2} (if $N_{\mathrm{j}} \geq 2$)	Inclusive M_{T2} search:
	$M_{\mathrm{T2}} > 200$ GeV for $H_{\mathrm{T}} < 1500$ GeV, else $M_{\mathrm{T2}} > 400$ GeV
	Disappearing tracks search:
	$M_{\mathrm{T2}} > 200$ GeV
$p_{\mathrm{T}}^{\mathrm{sum}}$ cone (isolation)	Veto e or μ: $\Delta R = \min(0.2, \max(10 \text{ GeV}/p_{\mathrm{T}}^{\mathrm{lep}}, 0.05))$
	Veto track: $\Delta R = 0.3$
Veto electron	$p_{\mathrm{T}} > 10$ GeV, $|\eta| < 2.4$, $p_{\mathrm{T}}^{\mathrm{sum}} < 0.1\, p_{\mathrm{T}}^{\mathrm{lep}}$
Veto electron track	$p_{\mathrm{T}} > 5$ GeV, $|\eta| < 2.4$, $M_{\mathrm{T}} < 100$ GeV, $p_{\mathrm{T}}^{\mathrm{sum}} < 0.2\, p_{\mathrm{T}}^{\mathrm{lep}}$
Veto muon	$p_{\mathrm{T}} > 10$ GeV, $|\eta| < 2.4$, $p_{\mathrm{T}}^{\mathrm{sum}} < 0.2\, p_{\mathrm{T}}^{\mathrm{lep}}$
Veto muon track	$p_{\mathrm{T}} > 5$ GeV, $|\eta| < 2.4$, $M_{\mathrm{T}} < 100$ GeV, $p_{\mathrm{T}}^{\mathrm{sum}} < 0.2\, p_{\mathrm{T}}^{\mathrm{lep}}$
Veto track	$p_{\mathrm{T}} > 10$ GeV, $|\eta| < 2.4$, $M_{\mathrm{T}} < 100$ GeV, $p_{\mathrm{T}}^{\mathrm{sum}} < 0.1\, p_{\mathrm{T}}^{\mathrm{track}}$

response [100,101]. Only jets passing the selection criteria in Table 1 are used for counting and for the determination of kinematic variables. In particular, we consider jets with $p_{\mathrm{T}} > 30$ GeV and $|\eta| < 2.4$, unless otherwise stated. Jets that contain the decay of a bottom-flavored hadron are identified using a deep neural network algorithm [102] with a working point chosen such that the efficiency to identify a bottom quark jet is in the range 55–70% for jet p_{T} between 20 and 400 GeV. The misidentification rate is approximately 1–2% for light-flavor or gluon jets, and 10–15% for charm jets. We count b-tagged jets with $p_{\mathrm{T}} > 20$ GeV and $|\eta| < 2.4$. The minimum p_{T} threshold used for counting b-tagged jets is lowered to 20 GeV instead of 30, as used for N_{j}, in order to maximize the sensitivity towards BSM scenarios with bottom quarks.

The negative of the vector p_{T} sum of all selected jets is denoted by $\vec{H}_{\mathrm{T}}^{\mathrm{miss}}$, while the missing transverse momentum $\vec{p}_{\mathrm{T}}^{\mathrm{miss}}$ is defined as the negative of the vector p_{T} sum of all reconstructed PF candidates. Their magnitudes are referred to as $H_{\mathrm{T}}^{\mathrm{miss}}$ and $p_{\mathrm{T}}^{\mathrm{miss}}$, respectively. The $\vec{p}_{\mathrm{T}}^{\mathrm{miss}}$ is further adjusted

to reflect the jet energy corrections [100,101]. Events with possible contributions from beam halo processes or anomalous noise in the calorimeter are rejected using dedicated filters [103,104]. For events with at least two jets, we start with the pair having the largest dijet invariant mass and iteratively cluster all selected jets using an algorithm that minimizes the Lund distance measure [105,106] until two stable pseudo-jets are obtained. The resulting pseudo-jets together with the $\vec{p}_{\mathrm{T}}^{\mathrm{miss}}$ are used to calculate the kinematic variable M_{T2} [1] as:

$$M_{\mathrm{T2}} = \min_{\vec{p}_{\mathrm{T}}^{\mathrm{miss\,X(1)}} + \vec{p}_{\mathrm{T}}^{\mathrm{miss\,X(2)}} = \vec{p}_{\mathrm{T}}^{\mathrm{miss}}} \left[\max\left(M_{\mathrm{T}}^{(1)}, M_{\mathrm{T}}^{(2)} \right) \right], \quad (1)$$

where $\vec{p}_{\mathrm{T}}^{\mathrm{miss\,X}(i)}$ ($i = 1, 2$) are trial vectors obtained by decomposing $\vec{p}_{\mathrm{T}}^{\mathrm{miss}}$, and $M_{\mathrm{T}}^{(i)}$ are the transverse masses [107] obtained by pairing either of the trial vectors with one of the two pseudo-jets. The minimization is performed over all trial momenta satisfying the $\vec{p}_{\mathrm{T}}^{\mathrm{miss}}$ constraint. The background from multijet events (discussed in Sect. 4) is characterized by small values of M_{T2}, while processes with significant gen-

uine $\vec{p}_\mathrm{T}^\mathrm{miss}$ yield larger values of M_T2. More detailed discussions of the M_T2 variable properties are given in Refs. [96,108,109].

In both the inclusive M_T2 search and the search for disappearing tracks, collision events are selected using triggers with requirements on H_T, $p_\mathrm{T}^\mathrm{miss}$, $H_\mathrm{T}^\mathrm{miss}$, and jet p_T. The combined trigger efficiency, as measured in an orthogonal data sample of events with an isolated electron, is found to be >97% across the full kinematic range of the search. To suppress background from multijet production, we require $M_\mathrm{T2} > 200$ GeV in events with $N_\mathrm{j} \geq 2$. In the inclusive M_T2 search, this M_T2 threshold is increased to 400 GeV for events with $H_\mathrm{T} > 1500$ GeV to maintain multijet processes as a subdominant background in all search regions. In events with $N_\mathrm{j} = 1$, where M_T2 is not defined, we require $p_\mathrm{T}^\mathrm{jet} > 250$ GeV and $p_\mathrm{T}^\mathrm{miss} > 250$ GeV. As a protection against jet mismeasurement, we require the minimum difference in the azimuthal angle between the $\vec{p}_\mathrm{T}^\mathrm{miss}$ vector and the direction of each of the four p_T-leading jets, $\Delta\phi_\mathrm{min}$, to be greater than 0.3 radians, and the magnitude of the difference between $\vec{p}_\mathrm{T}^\mathrm{miss}$ and $\vec{H}_\mathrm{T}^\mathrm{miss}$ to be less than half of $p_\mathrm{T}^\mathrm{miss}$. For the determination of $\Delta\phi_\mathrm{min}$, we consider jets with $|\eta| < 4.7$. If fewer than four such jets are found, all are considered in the $\Delta\phi_\mathrm{min}$ calculation.

In the search for disappearing tracks, events are selected requiring in addition the presence of at least one disappearing track. These are defined as well-reconstructed isolated tracks with no measurement points in at least two of the outermost layers of the tracker and no associated energy deposits in the calorimeter. These tracks are predominantly not considered as candidates by the PF algorithm; as a result they are not included in the calculation of $\vec{p}_\mathrm{T}^\mathrm{miss}$.

3.2 Event categorization

3.2.1 Inclusive M_T2 search

Events containing at least two jets are categorized by the values of N_j, N_b, and H_T. Each category is referred to as a topological region. Signal regions are defined by further dividing topological regions into bins of M_T2. Events with only one jet are selected if the jet p_T is at least 250 GeV, and are classified according to the p_T of this jet and whether the event contains a b-tagged jet. The 282 search regions are summarized in Tables 12, 13, 14, 15, 16, 17, 18, 19, 20, 21, 22 and 23 in Appendix B.1. We also define *super signal regions*, covering a subset of the kinematic space of the full analysis with simpler inclusive selection criteria. The super signal regions can be used to obtain approximate interpretations of our result, as discussed in Sect. 5, where these regions are defined.

3.2.2 Search for disappearing tracks

In the following, the selected disappearing tracks are called short tracks (STs). We also define short track candidates (STCs) as disappearing tracks that are required to satisfy relaxed selection criteria on the track quality and isolation compared to an ST, but not the tight ones required for STs. Both STs and STCs are required to have no measurement points in at least two of the outermost layers of the tracker and no associated energy deposits in the calorimeter.

We select events with at least one ST and at least two jets, and we categorize them by the values of N_j and H_T. Disappearing tracks are categorized according to their length and p_T, in order to maximize the sensitivity to a range of lifetimes of potential BSM long-lived charged particles, and to distinguish tracks reconstructed with different precision. Two bins of p_T are defined as:

- $15 < p_\mathrm{T} < 50$ GeV,
- $p_\mathrm{T} > 50$ GeV.

Additionally, four track length categories are defined, depending on the number of layers of the tracking detector with a measurement:

- pixel tracks (P), having at least three layers with a measurement in the pixel tracking detector, and none in the strip tracking detector,
- medium length tracks (M), having less than seven layers with a measurement, and at least one outside of the pixel tracking detector,
- long tracks (L), having at least seven layers with a measurement.

For 2017–2018 data, we further split the P tracks into two categories:

- pixel tracks having three layers with a measurement (P3),
- pixel tracks having at least four layers with a measurement (P4).

For long (L) tracks, no categorization in bins of p_T is applied.

The full track selection requirements for both STs and STCs are listed in Table 11 of Appendix A, together with the track length categories they belong to. For signal STs, the track reconstruction and selection efficiency ranges from 50 to 65%, depending on the track length and the data taking period.

The 68 search regions (28 used for the categorization of the 2016 data set, and 40 for the 2017–2018 data set) are summarized in Tables 24 and 25 in Appendix B.2.

3.3 Monte Carlo simulation

The MC simulation is used to design the search, to help estimate SM backgrounds, and to evaluate the sensitivity to simplified models of BSM physics.

The main background samples (Z+jets, W+jets, $t\bar{t}$+jets, and multijet), as well as BSM signal samples, are generated at leading order (LO) precision with the MAD-GRAPH5_aMC@NLO 2 (2.2.2, or 2.4.2) generator [110]. Up to four, three, or two additional partons are considered in the matrix element calculations for the generation of the V+jets (V = W, Z), $t\bar{t}$+jets, and signal samples, respectively. Other background processes are also considered: $t\bar{t}$V samples with up to two additional partons in the matrix element calculations are generated at LO precision with the MADGRAPH5_aMC@NLO 2 generator, while single top quark samples are generated at next-to-leading order (NLO) precision with the MADGRAPH5_aMC@NLO 2 or POWHEG (v1.0, or v2.0) [111–115] generators. Finally, contributions from rarer processes such as diboson, triboson, and four top quark production, are also considered and found to be negligible. The expected yields of all samples are normalized using the most precise available cross section calculations, typically corresponding to NLO or next-to-NLO (NNLO) accuracy [110,113,115–119].

The detector response of SM samples and 2016 signal samples containing long-lived objects is modeled with the GEANT4 [120] program, while the CMS fast simulation framework [121,122] is used for other signal samples, and uncertainties are derived to account for the potential mismodeling of the event kinematics.

For all simulated samples, generators are interfaced with PYTHIA 8.2 (8.205, 8.212, 8.226, or 8.230) [123] for fragmentation and parton showering. For samples simulated at LO (NLO) precision, the MLM [124] (FxFx [125]) prescription is used to match partons from the matrix element calculation to those from the parton showers. The CUETP8M1 [126] PYTHIA 8.2 tune is used for the 2016 SM background and signal samples. For 2017 and 2018, the CP5 and CP2 tunes [127] are used for the SM background and signal samples, respectively. The NNPDF2.3LO (NNPDF2.3NLO) [128] parton distribution functions (PDFs) are used to generate the 2016 LO (NLO) samples, while the NNPDF3.1LO (NNPDF3.1NNLO) [129] PDFs are used for the 2017 and 2018 samples.

The output of the detector simulation is processed using the same chain of reconstruction algorithms as for collision data.

To improve on the MADGRAPH5_aMC@NLO modeling of the multiplicity of additional jets from initial-state radiation (ISR) in the 2016 sample, MADGRAPH5_aMC@NLO $t\bar{t}$ MC events are weighted based on the number of ISR jets (N_j^{ISR}) so as to make the jet multiplicity agree with data. The same reweighting procedure is applied to BSM MC events. The weighting factors are obtained from a control region enriched in $t\bar{t}$, defined as events with two leptons and exactly two b-tagged jets, and vary between 0.92 for $N_j^{\mathrm{ISR}} = 1$ and 0.51 for $N_j^{\mathrm{ISR}} \geq 6$. We take one half of the deviation from unity as the systematic uncertainty in these reweighting factors, to cover for the experimental uncertainties in their derivation and for differences between $t\bar{t}$ and BSM production. Owing to a better tuning of the MC generators, this reweighting procedure is not necessary for 2017 and 2018 MADGRAPH5_aMC@NLO $t\bar{t}$ MC samples, while it is still applied to BSM MC events.

To improve the modeling of the flavor of additional jets, the simulation of $t\bar{t}$ and $t\bar{t}$V events is corrected to account for the measured ratio of $t\bar{t}b\bar{b}/t\bar{t}jj$ cross sections reported in Ref. [130]. Specifically, simulated $t\bar{t}$ and $t\bar{t}$V events with two b quarks not originating from top quark decay are weighted to account for the CMS measurement of the ratio of cross sections $\sigma(t\bar{t}b\bar{b})/\sigma(t\bar{t}jj)$, which was found to be a factor of 1.7 ± 0.5 larger than the MC prediction [130].

4 Background estimation

4.1 Inclusive M_{T2} search

The backgrounds in jets-plus-$p_{\mathrm{T}}^{\mathrm{miss}}$ final states arise from three categories of SM processes.

- The lost-lepton (LL) background: events with a lepton from a W boson decay where the lepton is either out of acceptance, not reconstructed, not identified, or not isolated. This background originates mostly from W+jets and $t\bar{t}$+jets events, with smaller contributions from more rare processes, such as diboson or $t\bar{t}$V production.
- The irreducible background: Z+jets events, where the Z boson decays to neutrinos. This background is the most difficult to distinguish from the final states arising from potential signals. It is a major background in nearly all search regions, its importance decreasing with increasing N_b.
- The instrumental background: mostly multijet events with no genuine $p_{\mathrm{T}}^{\mathrm{miss}}$. These events enter a search region due to either significant jet momentum mismeasurements or sources of anomalous noise. This is a subdominant background compared to others, after events are selected, as described in Sect. 3.1.

The backgrounds are estimated from data control regions. In the presence of BSM physics, these control regions could be affected by signal contamination. Although the expected signal contamination is typically negligible, its potential

impact is accounted for in the interpretation of the results, as further described in Sect. 6.

4.1.1 Estimation of the background from events with leptonic W boson decays

The LL background is estimated from control regions with exactly one lepton candidate (e or μ) selected using the same triggers and preselection criteria used for the signal regions, with the exception of the lepton veto, which is inverted. The transverse mass M_T determined using the lepton candidate and the $\vec{p}_T^{\,\mathrm{miss}}$ is required to satisfy $M_T < 100$ GeV, in order to suppress the potential signal contamination of the control regions. Selected events are binned according to the same criteria as the search regions. The background in each signal bin, $N_{\mathrm{LL}}^{\mathrm{SR}}$, is obtained by scaling the number of events in the control region, $N_{1\ell}^{\mathrm{CR}}$, using transfer factors $R_{\mathrm{MC}}^{0\ell/1\ell}$, as detailed below:

- For events with $N_{\mathrm{j}} = 1$:

$$
\begin{aligned}
N_{\mathrm{LL}}^{\mathrm{SR}} &\left(p_T^{\mathrm{jet}}, N_{\mathrm{b}} \right) \\
&= N_{1\ell}^{\mathrm{CR}} \left(p_T^{\mathrm{jet}}, N_{\mathrm{b}} \right) \, R_{\mathrm{MC}}^{0\ell/1\ell} \left(p_T^{\mathrm{jet}}, N_{\mathrm{b}} \right) .
\end{aligned}
\tag{2}
$$

- For events with $N_{\mathrm{j}} \geq 2$:

$$
\begin{aligned}
N_{\mathrm{LL}}^{\mathrm{SR}} (\Omega, M_{\mathrm{T2}}) &= N_{1\ell}^{\mathrm{CR}} (\Omega, M_{\mathrm{T2}}) \\
&\times R_{\mathrm{MC}}^{0\ell/1\ell} (\Omega, M_{\mathrm{T2}}) \, k_{\mathrm{LL}} (M_{\mathrm{T2}}|\Omega) ,
\end{aligned}
\tag{3}
$$

where:

$$
\Omega \equiv \left(H_T, N_{\mathrm{j}}, N_{\mathrm{b}} \right) .
\tag{4}
$$

The single-lepton control regions have 1–2 times as many events as the corresponding signal regions. The factor $R_{\mathrm{MC}}^{0\ell/1\ell}$ accounts for lepton acceptance and efficiency, as well as the expected contribution from the decay of W bosons to hadrons through an intermediate τ lepton. It is obtained from MC simulation, and corrected for the measured differences in the lepton efficiencies between data and simulation.

For events with $N_{\mathrm{j}} \geq 2$, the factor k_{LL} is one, except at high M_{T2} values, where the single-lepton control sample has insufficient data to allow $N_{1\ell}^{\mathrm{CR}}$ to be measured in each (H_T, N_{j}, N_{b}, M_{T2}) bin. In such cases, $N_{1\ell}^{\mathrm{CR}}$ is integrated over the remaining M_{T2} bins of the same (H_T, N_{j}, N_{b}) region, and the distribution in M_{T2} across these bins is taken from simulation and applied through the factor k_{LL}.

The MC modeling of M_{T2} is checked in data, in single-lepton events with either $N_{\mathrm{b}} = 0$ or $N_{\mathrm{b}} \geq 1$, as shown in the left and right panels of Fig. 1, respectively. The predicted distributions in the comparison are obtained by summing all the relevant regions, after normalizing MC event yields to data and distributing events among the M_{T2} bins according to the expectation from simulation.

Uncertainties arising from the limited size of the control samples and from theoretical and experimental considerations are evaluated and propagated to the final estimate. The dominant uncertainty in $R_{\mathrm{MC}}^{0\ell/1\ell}$ is due to the modeling of the lepton efficiency (for electrons, muons, and hadronically decaying τ leptons) and jet energy scale (JES), and is of order 15–20%. The uncertainty in the M_{T2} extrapolation via k_{LL}, which is as large as 40%, arises primarily from the JES, the relative fractions of W+jets and t$\bar{\mathrm{t}}$+jets events, and the choice of the renormalization (μ_R) and factorization (μ_F) scales used in the event generation.

The uncertainties in the LL background prediction are summarized in Table 2 together with their typical size ranges across the search bins.

4.1.2 Estimation of the background from Z($\nu\bar{\nu}$) + jets

The Z $\rightarrow \nu\bar{\nu}$ background is estimated from a Z $\rightarrow \ell^+\ell^-$ ($\ell = $ e, μ) control sample selected using dilepton triggers. The trigger efficiency, measured from a sample of events in data with large H_T, is found to be greater than 97% in the selected kinematic range.

The leptons in the control sample are required to be of the same flavor and have opposite charge. The p_T of the leading and trailing leptons must be at least 100 and 30 GeV, respectively. Finally, the invariant mass of the lepton pair must be within 20 GeV of the Z boson mass.

After requiring that the p_T of the dilepton system is at least 200 GeV (corresponding to the $M_{\mathrm{T2}} > 200$ GeV requirement), the preselection requirements are applied based on kinematic variables recalculated after removing the dilepton system from the event to replicate the Z $\rightarrow \nu\bar{\nu}$ kinematic properties. For events with $N_{\mathrm{j}} = 1$, one control region is defined for each bin of jet p_T. For events with at least two jets, the selected events are binned in H_T, N_{j}, and N_{b}, but not in M_{T2}, to increase the dilepton event yield in each control region.

The contribution to each control region from flavor-symmetric processes, most importantly t$\bar{\mathrm{t}}$ production, is estimated using different-flavor (DF) eμ events obtained with the same selection criteria as same-flavor (SF) ee and μμ events. The background in each signal bin is then obtained using transfer factors.
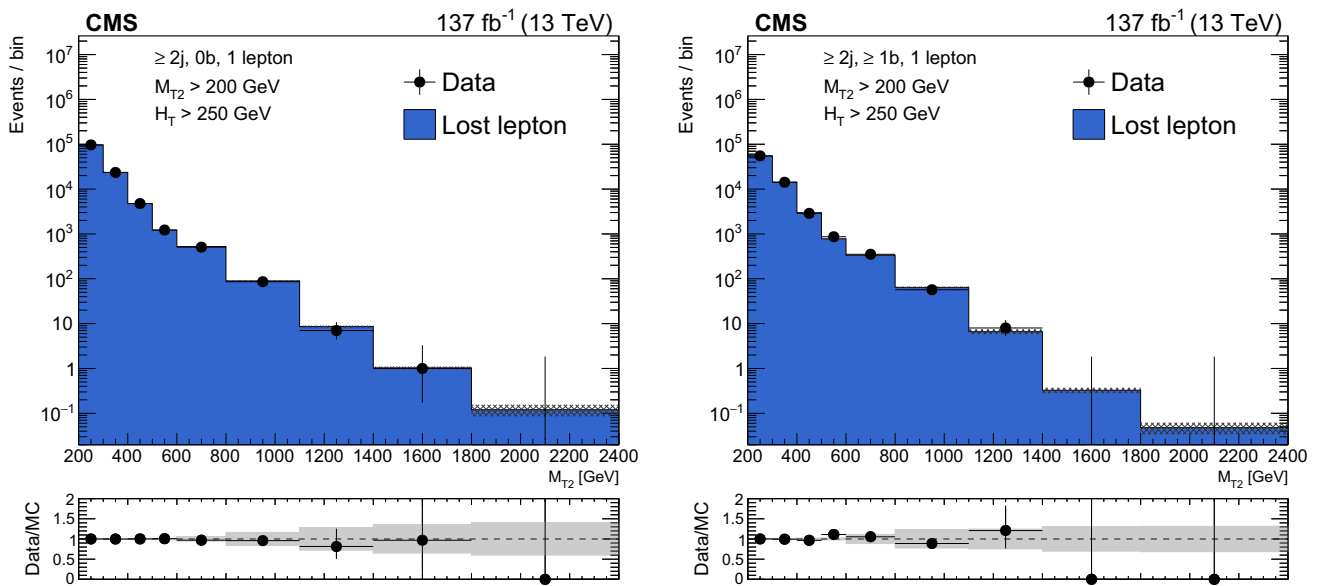
Fig. 1 Distributions of the M_{T2} variable in data and simulation for the single-lepton control region, after normalizing the simulation to data in bins of H_T, N_j, and N_b, for events with no b-tagged jets (left), and events with at least one b-tagged jet (right). The hatched bands on the top pan-

els show the MC statistical uncertainty, while the solid gray bands in the ratio plots show the systematic uncertainty in the M_{T2} shape. The bins have different widths, denoted by the horizontal bars

- For events with $N_j = 1$, according to:

$$
\begin{aligned}
N^{SR}_{Z\to\nu\bar{\nu}}\left(p^{jet}_T, N_b\right) = &\left[N^{CRSF}_{\ell\ell}\left(p^{jet}_T, N_b\right)\right.\\
&\left.- N^{CRDF}_{\ell\ell}\left(p^{jet}_T, N_b\right) R^{SF/DF}\right]\\
&\times R^{Z\to\nu\bar{\nu}/Z\to\ell^+\ell^-}_{MC}\left(p^{jet}_T, N_b\right).
\end{aligned}
$$ (5)

- For events with $N_j \geq 2$, according to:

$$
\begin{aligned}
N^{SR}_{Z\to\nu\bar{\nu}}\left(\Omega, M_{T2}\right) = &\left[N^{CRSF}_{\ell\ell}\left(\Omega\right)\right.\\
&\left.- N^{CRDF}_{\ell\ell}\left(\Omega\right) R^{SF/DF}\right]\\
&\times R^{Z\to\nu\bar{\nu}/Z\to\ell^+\ell^-}_{MC}\left(\Omega\right) k_{Z\to\nu\bar{\nu}}\left(M_{T2} \mid \Omega\right),
\end{aligned}
$$ (6)

where Ω is defined in Eq. (4).

Here $N^{CRSF}_{\ell\ell}$ and $N^{CRDF}_{\ell\ell}$ are the number of SF and DF events in the control region, while $R^{Z\to\nu\bar{\nu}/Z\to\ell^+\ell^-}_{MC}$ and $k_{Z\to\nu\bar{\nu}}$ are defined below. The factor $R^{SF/DF}$ accounts for the difference in acceptance and efficiency between SF and DF events. It is determined as the ratio of the number of SF to DF events in a $t\bar{t}$ enriched control sample, obtained with the same selection criteria as the $Z \to \ell^+\ell^-$ sample, but inverting the requirements on the p_T and the invariant mass of the lepton pair. A measured value of $R^{SF/DF} = 1.06 \pm 0.15$ is observed to be stable with respect to event kinematic variables, and is

Table 2 Summary of systematic uncertainties in the lost-lepton background prediction, together with their typical size ranges across the search bins

Source	Range (%)
Limited size of data control samples	5–100
Limited size of MC samples	0–50
e/μ efficiency	0–10
τ efficiency	0–3
b tagging efficiency	0–3
Jet energy scale	0–5
M_T (lepton, $\vec{p}^{miss}_T$) selection efficiency	0–3
M_{T2} shape uncertainty (if $k_{LL} \neq 1$)	0–40
μ_R and μ_F variation	0–5
$t\bar{t}b\bar{b}/t\bar{t}jj$ weight	0–25

applied in all regions. Figure 2 (left) shows $R^{SF/DF}$ measured as a function of the number of jets.

For events with $N_j = 1$, an estimate of the $Z \to \nu\bar{\nu}$ background in each search bin is obtained from the corresponding dilepton control region via the factor $R^{Z\to\nu\bar{\nu}/Z\to\ell^+\ell^-}_{MC}$, which accounts for the acceptance and efficiency to select the dilepton pair and the ratio of branching fractions for the $Z \to \ell^+\ell^-$ and $Z \to \nu\bar{\nu}$ decays. For events with at least two jets, an estimate of the $Z \to \nu\bar{\nu}$ background is obtained analogously in each (H_T, N_j, N_b) region, integrated over M_{T2}. The factor $R^{Z\to\nu\bar{\nu}/Z\to\ell^+\ell^-}_{MC}$ is obtained from simula-
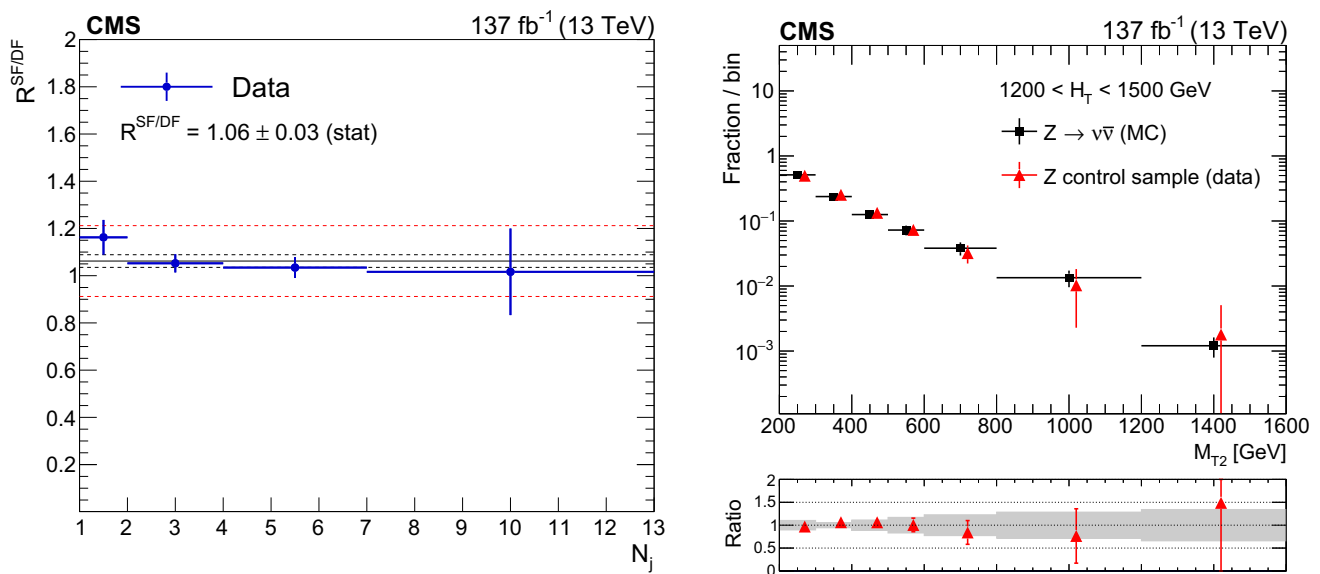
Fig. 2 (Left) Ratio $R^{\mathrm{SF/DF}}$ in data as a function of N_{j}. The solid black line enclosed by the red dashed lines corresponds to a value of 1.06 ± 0.15 that is observed to be stable with respect to event kinematic variables, while the two dashed black lines denote the statistical uncertainty in the $R^{\mathrm{SF/DF}}$ value. (Right) The shape of the M_{T2} distribution in

$Z \rightarrow \nu\bar{\nu}$ simulation compared to the one obtained from the $Z \rightarrow \ell^{+}\ell^{-}$ data control sample, in a region with $1200 < H_{\mathrm{T}} < 1500$ GeV and $N_{\mathrm{j}} \geq 2$, inclusive in N_{b}. The solid gray band on the ratio plot shows the systematic uncertainty in the M_{T2} shape. The bins have different widths, denoted by the horizontal bars

tion, including corrections for the differences in the lepton efficiencies between data and simulation.

For events with $N_{\mathrm{j}} \geq 2$, the factor $k_{Z \rightarrow \nu\bar{\nu}}$ accounts for the distribution in bins of M_{T2} of the estimated background in each $(H_{\mathrm{T}}, N_{\mathrm{j}}, N_{\mathrm{b}})$ region. This distribution is constructed using M_{T2} shape templates from dilepton data and $Z \rightarrow \nu\bar{\nu}$ simulation in each $(H_{\mathrm{T}}, N_{\mathrm{j}}, N_{\mathrm{b}})$ region. The templates obtained from data are used at low values of M_{T2}, where the amount of data is sufficient. On the other hand, at high values of M_{T2} we use the templates from simulation.

Studies with simulated samples have demonstrated that the shape of the M_{T2} distribution of the function $k_{Z \rightarrow \nu\bar{\nu}}$ is independent of N_{b} for a given H_{T} and N_{j} selection, and that the shape is also independent of N_{j} for $H_{\mathrm{T}} > 1500$ GeV. The dilepton control sample supports this observation. Therefore, functions $k_{Z \rightarrow \nu\bar{\nu}}$ are obtained for each $(H_{\mathrm{T}}, N_{\mathrm{j}})$ region, integrated over N_{b}. For $H_{\mathrm{T}} > 1500$ GeV, only one function $k_{Z \rightarrow \nu\bar{\nu}}$ is constructed, integrating also over N_{j}.

The MC modeling of the M_{T2} variable is validated in data using control samples enriched in $Z \rightarrow \ell^{+}\ell^{-}$ events, in each bin of H_{T}, as shown in the right panel of Fig. 2 for events with $1200 < H_{\mathrm{T}} < 1500$ GeV.

The largest uncertainty in the estimate of the invisible Z background in most regions results from the limited size of the dilepton control sample. The dominant uncertainty of about 5% in the ratio $R^{Z \rightarrow \nu\bar{\nu}/Z \rightarrow \ell^{+}\ell^{-}}_{\mathrm{MC}}$ reflects the uncertainty in the differences between the lepton efficiencies in data and simulation. The uncertainty in the $k_{Z \rightarrow \nu\bar{\nu}}$ factor arises from

Table 3 Summary of systematic uncertainties in the $Z \rightarrow \nu\bar{\nu}$ background prediction, together with their typical size ranges across the search bins

Source	Range (%)
Limited size of data control samples	5–100
Limited size of MC samples	0–50
Lepton efficiency	0–5
Jet energy scale	0–5
Uncertainty in $R^{\mathrm{SF/DF}}$	0–5
M_{T2} shape uncertainty (if $k_{Z \rightarrow \nu\bar{\nu}} \neq 1$)	0–40

data statistical uncertainty for bins at low values of M_{T2}, where the function $k_{Z \rightarrow \nu\bar{\nu}}$ is obtained from data, while for bins at high values of M_{T2}, where the function $k_{Z \rightarrow \nu\bar{\nu}}$ is obtained from simulation, it is due to the uncertainties in the JES and the choice of the μ_{R} and μ_{F}. These can result in effects as large as 40%.

The uncertainties in the $Z \rightarrow \nu\bar{\nu}$ background prediction are summarized in Table 3 together with their typical size ranges across the search bins.

4.1.3 Estimation of the multijet background

The background from SM events comprised uniquely of jets produced through the strong interaction (multijet events) is estimated from control regions in data selected using triggers

that require H_T to exceed thresholds ranging from 125 (180) to 900 (1050) GeV in 2016 (2017–2018) data samples. In addition, events are required to have at least two jets with $p_T > 10$ GeV.

The rebalance and smear (R&S) method used to estimate the multijet background consists of two steps. First, multijet data events are rebalanced by adjusting the p_T of the jets such that the resulting p_T^{miss} is approximately zero. This rebalancing is performed through a likelihood maximization, accounting for the jet energy resolution [100,101]. The output of the rebalancing step is an inclusive sample of multijet events with approximately zero p_T^{miss} that are used as a seed for the second step, the smearing. In the smearing step, the p_T of the rebalanced jets is smeared according to the jet response function, in order to model the instrumental effects that lead to nonzero p_T^{miss}. The smearing step is repeated many times for each rebalanced event. The output of each smearing step is an independent sample of events, which serves to populate the tails of kinematic distributions such as p_T^{miss} and M_{T2}, and to obtain a more precise estimate of the multijet background than would be possible using only simulation.

The method makes use of jet response templates, i.e., distributions of the ratio of reconstructed jet p_T to generator-level jet p_T. The templates are derived from simulation in bins of jet p_T and η, separately for b-tagged and non-b-tagged jets.

Table 4 Summary of systematic uncertainties in the multijet background prediction, together with their typical size ranges across the search bins

Source	Range (%)
Jet energy resolution	10–20
Tails of jet response in templates	17–25
σ_T^{soft} modeling	1–25
N_j modeling	1–19
N_b modeling	1–16

Systematic uncertainties are assessed to cover for the modeling of the core and of the tails of the jet response templates.

Of all jets in the event, a jet qualifies for use in the R&S procedure if it has $p_T > 10$ GeV, and if it is not identified as a jet from pileup [131] in the case that $p_T < 100$ GeV. All other jets are left unchanged but are still used in the calculation of $\vec{p}_T^{miss}$ and other jet-related quantities. An event with n qualifying jets is rebalanced by varying the p_T^{reb} of each jet, which is an estimate of the true jet p_T, to maximize the likelihood function

$$L = \prod_{i=1}^{n} P\left(p_{T,i}^{reco} \mid p_{T,i}^{reb}\right) G\left(\frac{p_{T,reb,x}^{miss}}{\sigma_T^{soft}}\right) G\left(\frac{p_{T,reb,y}^{miss}}{\sigma_T^{soft}}\right), \quad (7)$$
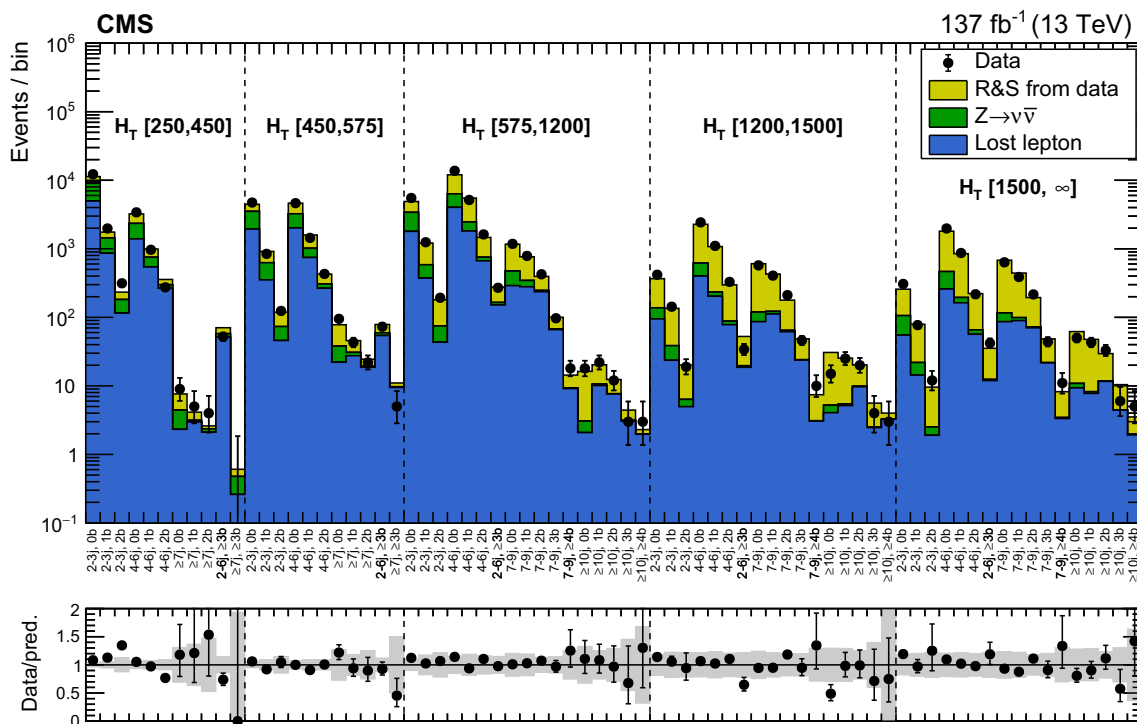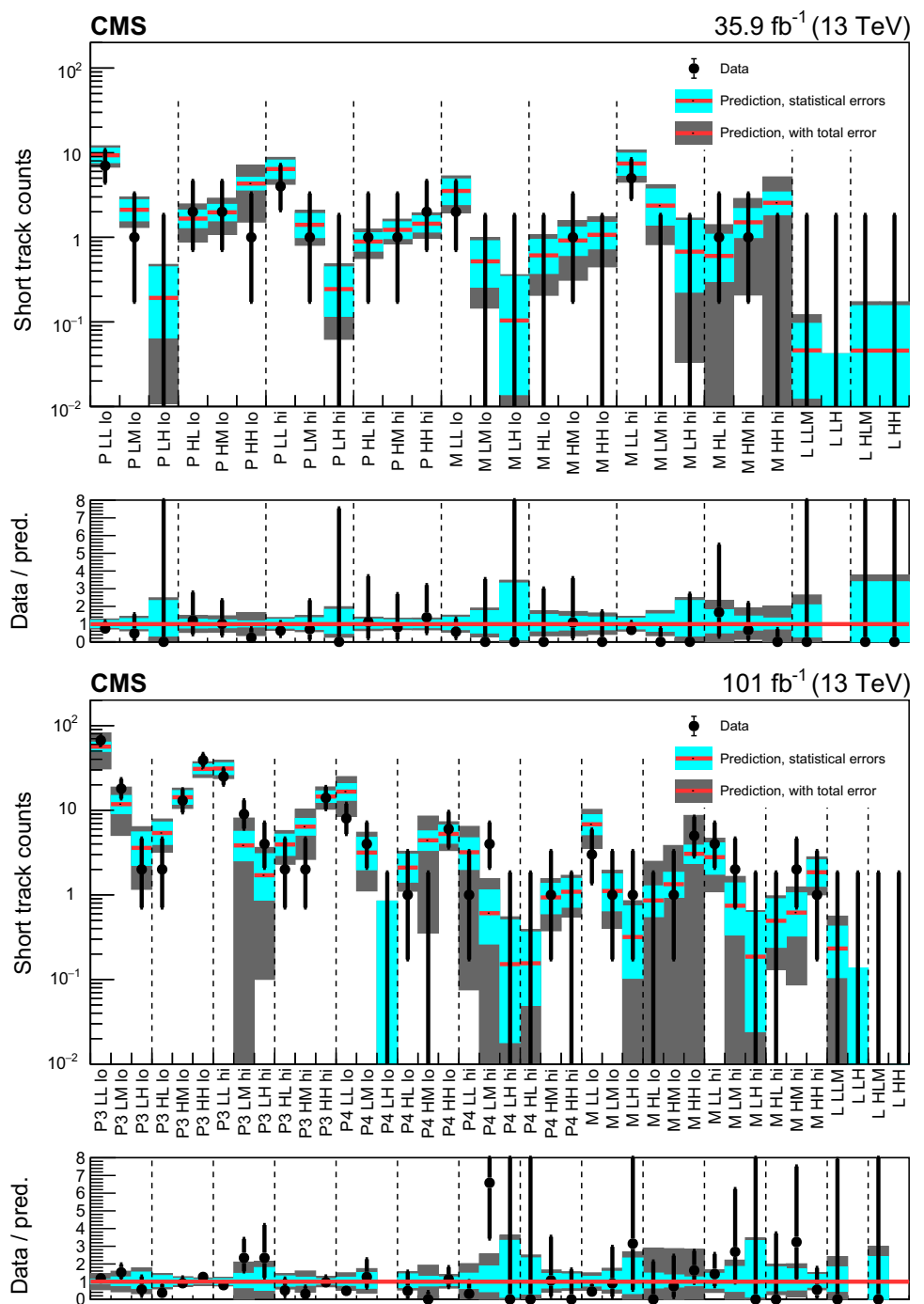

Fig. 3 Validation of the R&S multijet background prediction in control regions in data selected with $\Delta\phi_{min} < 0.3$. Electroweak backgrounds (LL and $Z \to \nu\bar{\nu}$) are estimated from data. In regions where the amount of data is insufficient to estimate the electroweak backgrounds, the cor-responding yields are taken directly from simulation. The bins on the horizontal axis correspond to the (H_T, N_j, N_b) topological regions. The gray band on the ratio plot represents the total uncertainty in the prediction

Fig. 4 Validation of the background prediction method in (upper) 2016 and (lower) 2017–2018 data with $100 < M_{\mathrm{T2}} < 200$ GeV, for the disappearing tracks search. The red histograms represent the predicted backgrounds, while the black markers are the observed data counts. The cyan bands represent the statistical uncertainty in the prediction. The gray bands represent the total uncertainty in the prediction. The labels on the x axes are explained in Tables 24 and 25 of Appendix B.2. Regions whose predictions use the same measurement of f_{short} are grouped by the vertical dashed lines. Bins with no entry in the ratio have zero predicted background

where

$$G(x) \equiv \mathrm{e}^{-x^2/2}, \tag{8}$$

and

$$\vec{p}_{\mathrm{T,reb}}^{\mathrm{miss}} \equiv \vec{p}_{\mathrm{T}}^{\mathrm{miss}} - \sum_{i=1}^{n} \left(\vec{p}_{\mathrm{T},i}^{\mathrm{reb}} - \vec{p}_{\mathrm{T},i}^{\mathrm{reco}} \right). \tag{9}$$

The term $\mathrm{P}(p_{\mathrm{T},i}^{\mathrm{reco}} | p_{\mathrm{T},i}^{\mathrm{reb}})$ in Eq. (7) is the probability for a jet with p_{T} of $p_{\mathrm{T},i}^{\mathrm{reb}}$ to be assigned a p_{T} of $p_{\mathrm{T},i}^{\mathrm{reco}}$ after reconstruc-

tion. This probability is taken directly from the jet response templates. The two $G(x)$ terms in Eq. (7) enforce an approximate balancing condition. The $\vec{p}_{\mathrm{T,reb}}^{\mathrm{miss}}$ terms in Eq. (7) represent the $\vec{p}_{\mathrm{T}}^{\mathrm{miss}}$ after rebalancing, and are obtained by simply propagating the changes in jet p_{T} from rebalancing to $\vec{p}_{\mathrm{T}}^{\mathrm{miss}}$. For the balancing of the x and y components of the $\vec{p}_{\mathrm{T}}^{\mathrm{miss}}$, we use $\sigma_{\mathrm{T}}^{\mathrm{soft}} = 20$ GeV, which is approximately the width of the distributions of the x and y components of $\vec{p}_{\mathrm{T}}^{\mathrm{miss}}$ in minimum bias events. This parameter represents the inherent

missing energy due to low-p_T jets, unclustered energy, and jets from pileup that cannot be eliminated by rebalancing. A systematic uncertainty is assessed to cover for the effects of the variation of σ_T^{soft}.

The rebalanced events are used as input to the smearing procedure, where the p_T of each qualifying jet is rescaled by a random factor drawn from the corresponding jet response template, and all kinematic quantities are recalculated accordingly.

The background from multijet events is estimated by applying the signal region selection requirements to the above rebalanced and smeared sample, except events are only used if $p_{T,\mathrm{reb}}^{\mathrm{miss}} < 100$ GeV to remove potential contamination from electroweak sources. This additional requirement is found to be fully efficient for multijet events, in simulation. Hence, no correction is applied to the prediction.

Systematic uncertainties are summarized in Table 4 together with their typical size ranges across the search bins.

The resulting background prediction is validated in data using control regions enriched in multijet events. The results of the validation in a control region selected by inverting the $\Delta\phi_{\mathrm{min}}$ requirement are shown in Fig. 3. The electroweak backgrounds (LL and $Z \to \nu\bar{\nu}$) in this control region are estimated from data using transfer factors from leptonic control regions as described above. In regions where the number of events in the data leptonic control regions are insufficient, the electroweak background is taken from simulation. The observation is found to agree with the prediction, within the uncertainties.

4.2 Search for disappearing tracks

In the search for disappearing tracks, the SM background consists of events with charged hadrons or leptons that interact in the tracker or are poorly reconstructed, as well as tracks built out of incorrect combinations of hits. The background is estimated from data, leveraging the orthogonal definition of STCs and selected STs (Sect. 3.2.2), as described by Eq. (10).

$$N_{\mathrm{ST}}^{\mathrm{est}} = f_{\mathrm{short}} N_{\mathrm{STC}}^{\mathrm{obs}}, \tag{10}$$

where N_{ST} is the number of selected short tracks, N_{STC} is the number of selected short track candidates, and f_{short} is defined as:

$$f_{\mathrm{short}} = N_{\mathrm{ST}}^{\mathrm{obs}} / N_{\mathrm{STC}}^{\mathrm{obs}}. \tag{11}$$

The f_{short} ratio is measured directly in data, in a control region of events selected using the same triggers and preselection criteria used for the signal regions, except the selection on p_T^{miss} is relaxed to $p_T^{\mathrm{miss}} > 30$ GeV for all H_T values, and the selection on M_{T2} is shifted to $60 < M_{T2} < 100$ GeV. We exploit the empirical invariance of this ratio with respect

Table 5 Summary of systematic uncertainties in the disappearing track background prediction, together with their typical size ranges across the search bins. The systematic uncertainties arising from the assumption of kinematic invariance of f_{short} and from the validation of the background prediction are always taken to be at least as large as the statistical uncertainties on the measured values of f_{short} and on the background prediction in the validation region, respectively

Source	Range (%)
Limited size of data control samples	1–100
Limited size of data f_{short} measurement samples	5–45
Kinematic invariance of f_{short}	10–80
Validation of background prediction	25–75

to the H_T and p_T^{miss} selection criteria, as observed in data control regions, to reduce the statistical uncertainty in the measurement. The f_{short} ratio is therefore measured in data separately for each N_j, track p_T, track length category, and inclusively in H_T. The f_{short} values are measured separately in 2016 and 2017–2018 data, mainly to account for the upgrade of the CMS tracking detector after 2016. Since a reliable measurement in data of the f_{short} ratio for long (L) tracks is not achievable because of the insufficient number of events, the value measured in data for medium (M) length tracks is used instead, after applying a correction based on simulation:

$$f_{\mathrm{short}}(\mathrm{L})_{\mathrm{data}}^{\mathrm{est}} = f_{\mathrm{short}}(\mathrm{M})_{\mathrm{data}} \, f_{\mathrm{short}}(\mathrm{L})_{\mathrm{MC}} / f_{\mathrm{short}}(\mathrm{M})_{\mathrm{MC}}. \tag{12}$$

A systematic uncertainty in the measured values of f_{short} is assigned to cover for the empirically motivated assumption of its invariance with respect to H_T and p_T^{miss}. Its size is determined by varying the H_T and p_T^{miss} selection requirements in data events with $60 < M_{T2} < 100$ GeV. For long tracks, a conservative systematic uncertainty of 100% is assigned, as a correction based on simulation is used and there are insufficient data to study the effect of H_T and p_T^{miss} variations.

The f_{short} ratio is then used to predict the expected background in events with $M_{T2} > 100$ GeV, as described in Eq. (10).

In the presence of BSM physics, the above-defined control regions could be affected by signal contamination. Although the expected signal contamination is typically negligible, its potential impact is accounted for in the interpretation of the results, as further described in Sect. 6.

The background prediction is validated in data in an intermediate M_{T2} region ($100 < M_{T2} < 200$ GeV). No excess event yield is observed. The event categorization in this validation region is identical to the signal region, allowing for a bin-by-bin validation of the background prediction.

Figure 4 shows the result of the background prediction validation in 2016 data and in 2017–2018 data. We find good agreement between the observation and the background pre-
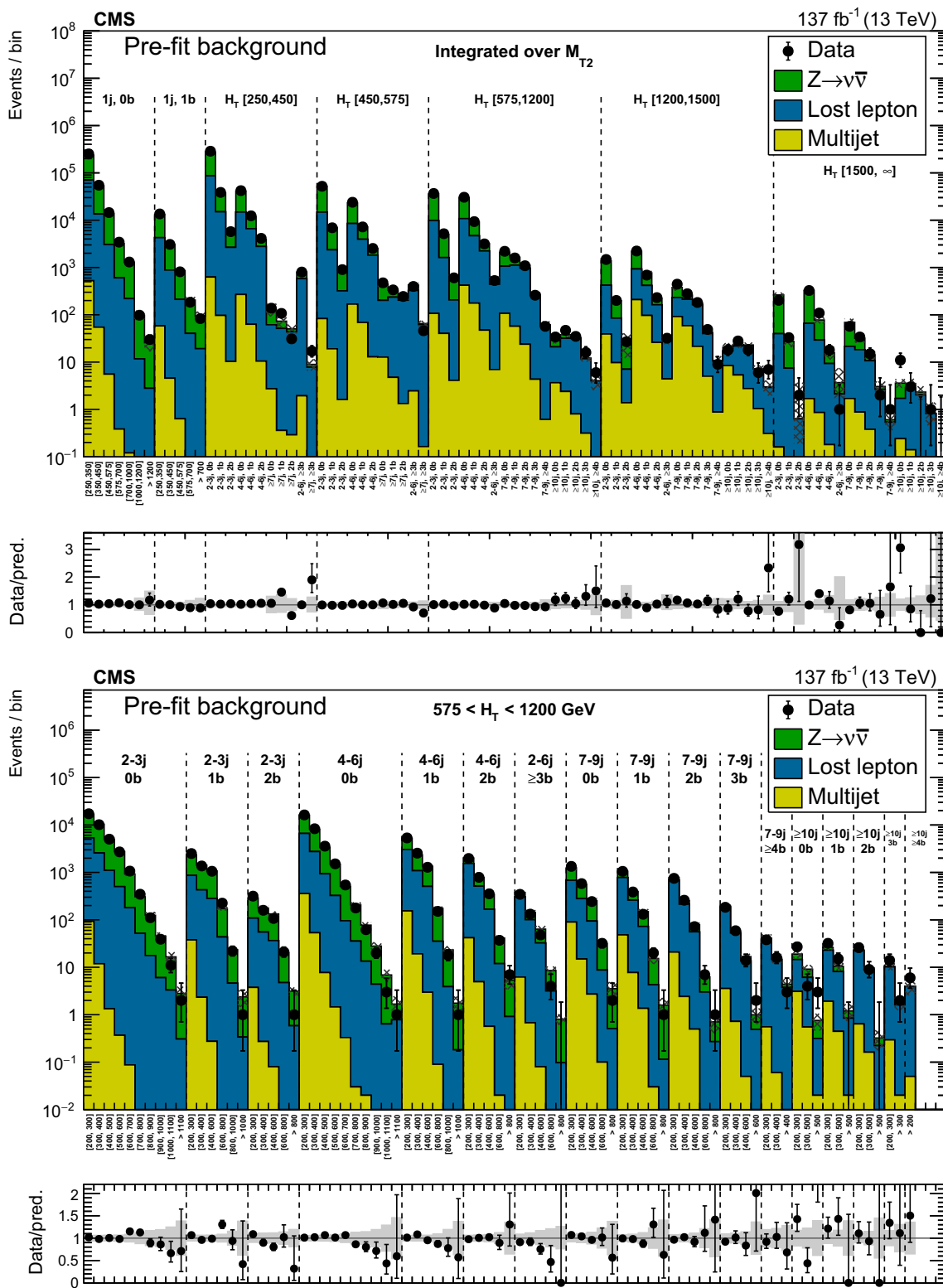
Fig. 5 (Upper) Comparison of the estimated (pre-fit) background and observed data events in each topological region. The hatched bands represent the full uncertainty in the background estimate. The monojet regions ($N_j = 1$) are identified by the labels "1j, 0b" and "1j, 1b", and are binned in jet p_T. The multijet regions are shown for each H_T region separately, and are labeled accordingly. The notations j, b are short for N_j, N_b. (Lower) Same for individual M_{T2} search bins in the medium-H_T region. On the x axis, the M_{T2} binning is shown in units of GeV

Table 6 Definitions of super signal regions, along with predictions, observed data, and the observed 95% CL upper limits on the number of signal events contributing to each region (N_{95}^{max}). The limits are shown as a range corresponding to an assumed uncertainty in the signal acceptance of 0 or 15% ($N_{95}^{\mathrm{max},0}$–$N_{95}^{\mathrm{max},15}$). A dash in the selection criteria means that no requirement is applied. All selection criteria as in the full analysis are applied. For regions with $N_{\mathrm{j}} = 1$, $H_{\mathrm{T}} \equiv p_{\mathrm{T}}^{\mathrm{jet}}$. The mono-$\phi$ super signal region corresponds to the subset of analysis bins identified in Refs. [35,36] as showing a significant excess in data based on the results of Ref. [9]

Region	N_{j}	N_{b}	H_{T} (GeV)	M_{T2} (GeV)	Prediction	Data	$N_{95}^{\mathrm{max},0}$–$N_{95}^{\mathrm{max},15}$
2j loose	≥ 2	–	> 1200	> 1200	37 ± 14	41	$26.0-27.2$
2j tight	≥ 2	–	> 1500	> 1400	$10.7^{+4.2}_{-4.1}$	13	$11.7-12.3$
4j loose	≥ 4	–	> 1200	> 1000	54 ± 13	72	$41.5-43.8$
4j tight	≥ 4	–	> 1500	> 1400	6.4 ± 2.5	10	$10.9-11.4$
7j loose	≥ 7	–	> 1200	> 600	63^{+13}_{-12}	72	$33.4-35.0$
7j tight	≥ 7	–	> 1500	> 800	$14.9^{+4.3}_{-4.2}$	14	$10.1-10.4$
10j loose	≥ 10	–	> 1200	> 400	17.3 ± 4.0	25	$18.6-19.5$
10j tight	≥ 10	–	> 1500	> 600	$3.6^{+1.2}_{-1.1}$	5	$6.8-7.1$
2b loose	≥ 2	≥ 2	> 1200	> 600	32.0 ± 4.5	33	$15.3-15.9$
2b tight	≥ 2	≥ 2	> 1500	> 600	$12.0^{+2.8}_{-2.7}$	12	$9.1-9.4$
3b loose	≥ 2	≥ 3	> 1200	> 400	17.6 ± 4.0	16	$10.0-10.3$
3b tight	≥ 2	≥ 3	> 1500	> 400	7.5 ± 2.1	5	$5.3-5.5$
4b loose	≥ 2	≥ 4	> 1200	> 400	2.1 ± 0.7	2	$4.2-4.4$
4b tight	≥ 2	≥ 4	> 1500	> 400	$0.8^{+0.4}_{-0.3}$	1	$3.5-3.6$
7j 3b loose	≥ 7	≥ 3	> 1200	> 400	$10.9^{+3.0}_{-2.9}$	8	$8.7-8.9$
7j 3b tight	≥ 7	≥ 3	> 1500	> 400	$4.6^{+2.0}_{-1.9}$	4	$5.5-5.7$
7j 4b loose	≥ 7	≥ 4	> 1200	> 400	1.7 ± 0.7	2	$4.3-4.5$
7j 4b tight	≥ 7	≥ 4	> 1500	> 400	0.7 ± 0.4	1	$3.6-3.7$
10j 4b loose	≥ 10	≥ 4	> 1200	> 400	$0.6^{+0.5}_{-0.4}$	1	$3.6-3.7$
10j 4b tight	≥ 10	≥ 4	> 1500	> 400	$0.1^{+0.5}_{-0.1}$	0	$2.0-2.1$
Mono-ϕ	$1-3$	0	$250-450$	$200-300$ (if $N_{\mathrm{j}} \geq 2$)	$(5.2 \pm 0.3) \times 10^5$	5.5×10^5	$(0.6-0.8) \times 10^5$

diction in the validation region. An additional systematic uncertainty is assigned to cover for discrepancies exceeding statistical uncertainties. The uncertainties in the background prediction are summarized in Table 5 together with their typical size ranges across the search bins.

5 Results

The data yields in the search regions are statistically compatible with the estimated backgrounds from SM processes.
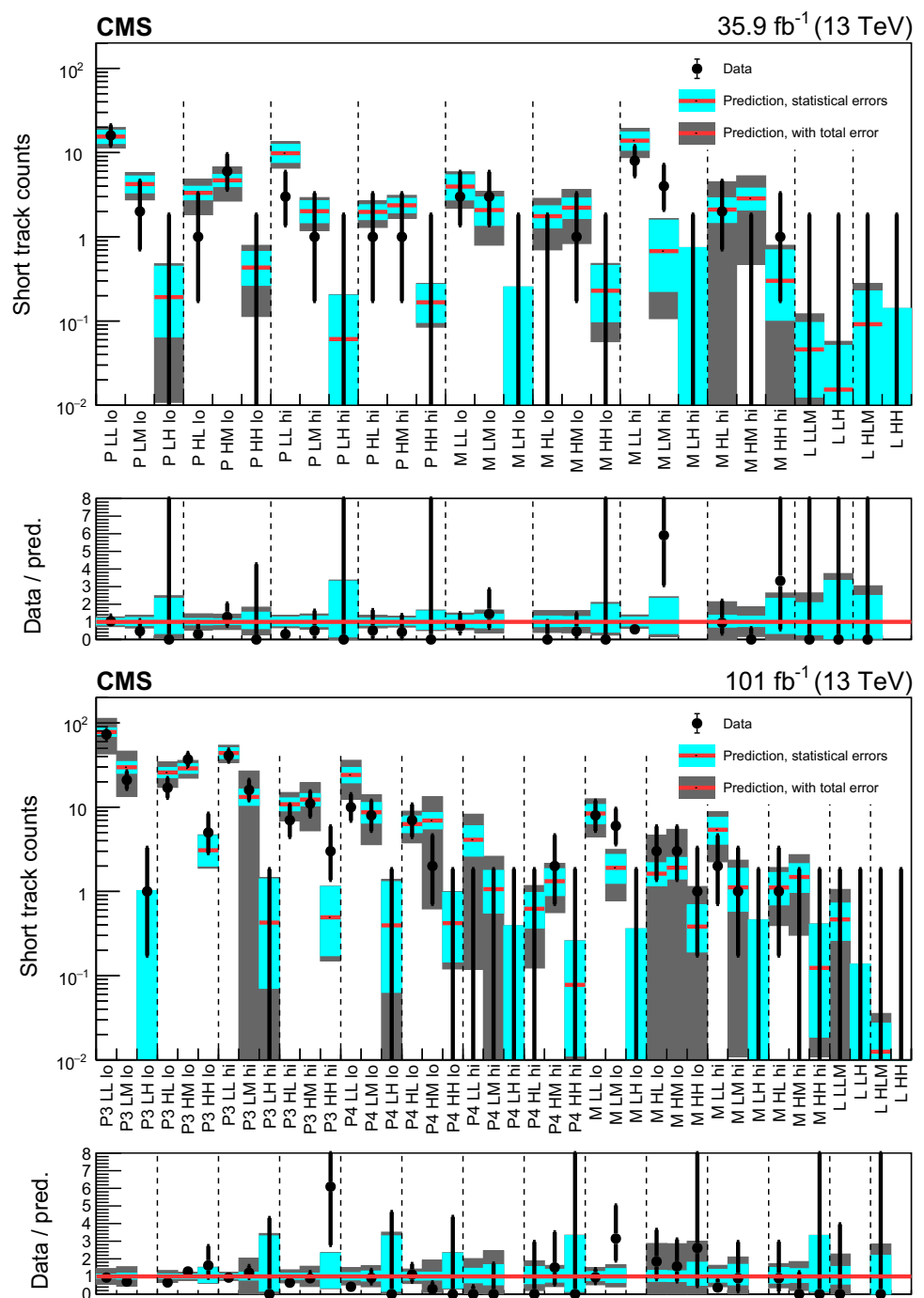
5.1 Inclusive M_{T2} search

A summary of the results of the M_{T2} inclusive search is shown in Fig. 5. Each bin in Fig. 5 (upper) corresponds to a single (H_{T}, N_{j}, N_{b}) topological region integrated over M_{T2}. Figure 5 (lower) breaks down the background estimates and observed data yields into M_{T2} bins for the region $575 < H_{\mathrm{T}} < 1200$ GeV: each bin corresponds to a single

M_{T2} bin, and vertical lines identify (H_{T}, N_{j}, N_{b}) topological regions. Distributions for the other H_{T} regions can be found in Figs. 23 and 24 in Appendix C.1. Background predictions and observed yields in all search regions are also summarized in Tables 12, 13, 14, 15, 16, 17, 18, 19, 20, 21, 22 and 23 in Appendix B.1. The background estimates and corresponding uncertainties rely exclusively on the inputs from control samples and simulation described in Sect. 4.1, prior to the fit to the data detailed in Sect. 6, and are referred to in the rest of the text as pre-fit background results.

To allow simpler reinterpretation, we also provide results for super signal regions, which cover subsets of the full analysis with simpler inclusive selection criteria and that can be used to obtain approximate interpretations of this search. The definitions of these regions are given in Table 6, with the predicted and observed number of events and the 95% confidence level (CL) upper limit on the number of signal events contributing to each region. Limits are set using a modified frequentist approach, employing the CL_{s} criterion and relying on asymptotic approximations to calculate the

Fig. 6 Comparison of the estimated (pre-fit) background and observed data events in (upper) each of the 2016 search regions, and in (lower) each of the 2017–2018 search regions, in the search for disappearing tracks. The red histogram represents the predicted background, while the black markers are the observed data counts. The cyan band represents the statistical uncertainty in the prediction. The gray band represents the total uncertainty. The labels on the x axes are explained in Tables 24 and 25 of Appendix B.2. Regions whose predictions use the same measurement of f_{short} are grouped by the vertical dashed lines. Bins with no entry in the ratio have zero pre-fit predicted background

distribution of the profile likelihood test-statistic used [132–135].

5.2 Search for disappearing tracks

The results of the search for disappearing tracks are shown in Fig. 6. Just as in the case of the inclusive search, the background estimates and the uncertainties rely exclusively on the inputs from control samples and simulation (Sect. 4.2), prior

to the fit to the data described in Sect. 6. We refer to them in the rest of the text as pre-fit background results. Background predictions and observed yields in all search regions are also summarized in Tables 24 and 25 in Appendix B.2.

6 Interpretation of the results

The measurements are interpreted in the context of models of new physics. Maximum likelihood fits to the data in

Fig. 7 (Upper) Diagrams for three scenarios of direct gluino pair production where each gluino undergoes a three-body decay to light-flavor (u, d, s, c) quarks, with different decay modes. For mixed-decay scenarios, we assume equal branching fraction for each decay mode. (Upper middle) Diagrams for the direct gluino pair production where gluinos decay to bottom and top quarks. (Lower middle) Diagrams for the direct pair production of light-flavor, bottom, and top squark pairs. (Lower) Diagrams for three alternate scenarios of direct top squark pair production with different decay modes. For mixed-decay scenarios, we assume equal branching fraction for each decay mode

the signal regions are carried out under either background-only or background+signal hypotheses. The uncertainties in the modeling of the backgrounds, summarized in Sect. 4, are inputs to the fitting procedure. The likelihoods are constructed as the product of Poisson probability density functions, one for each signal region, with additional log-normal constraint terms that account for the uncertainties in the background estimates and, if considered, in the signal yields.

The background+signal fits are used to set 95% CL upper limits on the cross sections for the signal models under con-

Fig. 8 Diagram for the mono-ϕ model, where a colored scalar ϕ is resonantly produced, and it decays to an invisible massive Dirac fermion ψ and an SM quark

Fig. 9 Diagrams for LQ pair production

Fig. 10 Diagrams for direct (left) gluino, (middle) light-flavor (u, d, s, c) squark, and (right) top squark pair production, where the directly produced gluinos and squarks can decay via a long-lived $\tilde{\chi}_1^\pm$. For gluinos, we assume a 1/3 decay branching fraction to each $\tilde{\chi}_1^0$, $\tilde{\chi}_1^+$, and $\tilde{\chi}_1^-$, and each gluino decays to light-flavor quarks. For squarks, we assume a 1/2 branching fraction for decays to $\tilde{\chi}_1^0$ and to the $\tilde{\chi}_1^\pm$ allowed by charge conservation. The mass of the $\tilde{\chi}_1^\pm$ is larger than the mass of the $\tilde{\chi}_1^0$ by hundreds of MeV. The $\tilde{\chi}_1^\pm$ decays to a $\tilde{\chi}_1^0$ via a pion, which is too soft to be detected

sideration. These limits are then used, in conjunction with the theoretical cross section calculations, to exclude ranges of masses for the BSM particles of the signal models. Before the fits are performed, the signal yields are corrected to account for the expected signal contamination of the data control regions used to estimate the SM background.

For the interpretation of the results, simplified BSM physics models [21–25] are used. Simplified models are defined by sets of hypothetical particles and sequences of their production and decay. The theoretical parameters are thus reduced to a small number of masses and cross sections, providing an effective tool to characterize potential signals of BSM physics.

The results of the inclusive M_{T2} search are used to constrain each of the simplified models of SUSY shown in Fig. 7. For each scenario of gluino (squark) pair production, the simplified models assume that all SUSY particles other than those shown in the corresponding diagram are too heavy to be produced directly, and that the gluino (squark) decays promptly. The models assume that each gluino (squark) decays with a 100% branching fraction into

Table 7 Systematic uncertainties in the signal yields for the simplified models of BSM physics. The large statistical uncertainties in the simulated signal sample come from a small number of bins with low acceptance, which are typically not among the most sensitive bins contributing to a given model benchmark point

Source	Range (%)
Integrated luminosity	2.3–2.5
Limited size of MC samples	1–100
b tagging efficiency, heavy flavors	0–40
b tagging efficiency, light flavors	0–20
Lepton efficiency	0–20
Jet energy scale	5
Fast simulation p_T^{miss} modeling	0–5
ISR modeling	0–30
μ_R and μ_F	5

the decay products depicted in Fig. 7. For models where the decays of the two gluinos or squarks in the same diagram differ, a 1/3 (1/2) branching fraction for each of the three
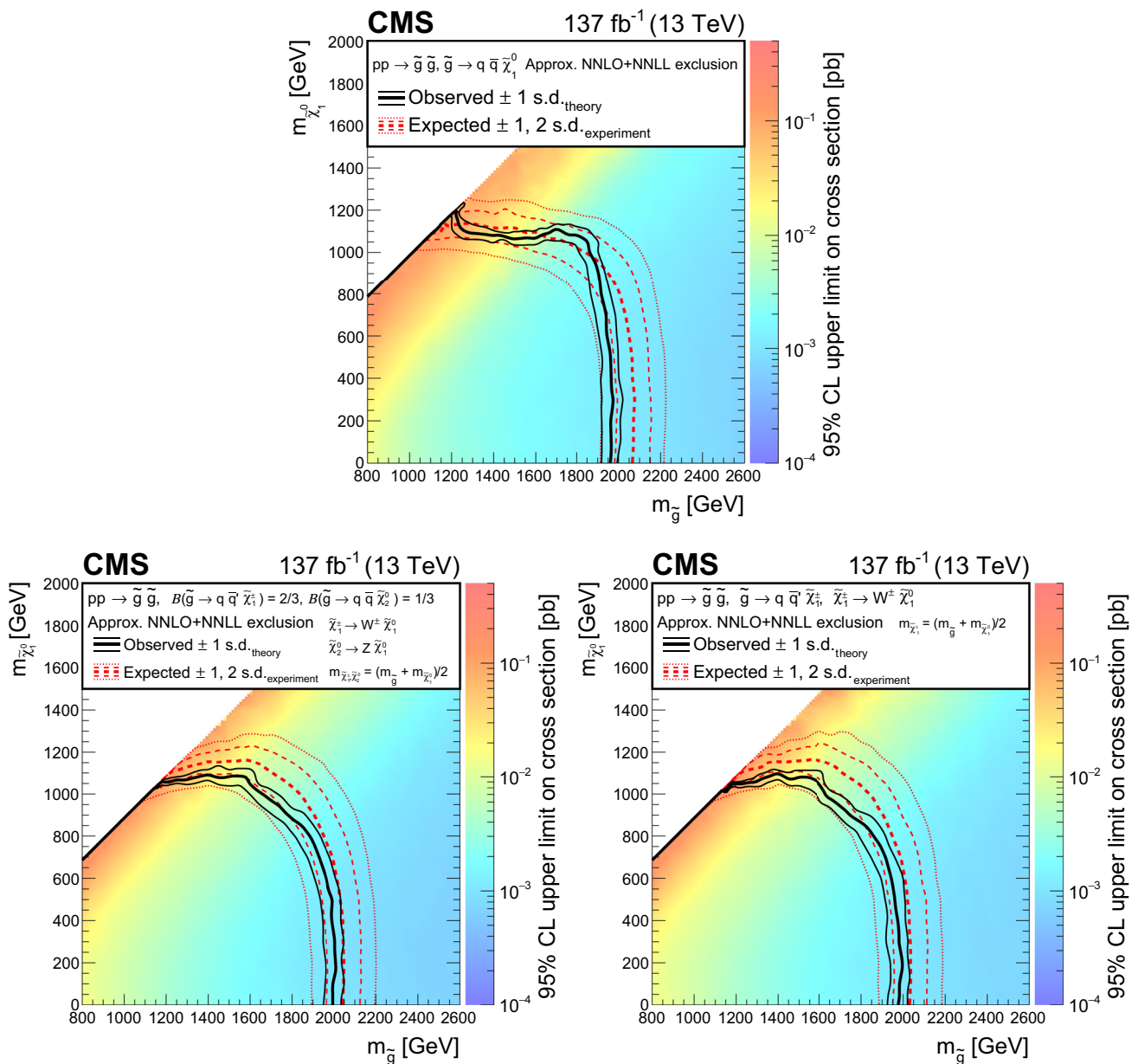
Fig. 11 Exclusion limits at 95% CL for direct gluino pair production, where (upper) $\tilde{g} \rightarrow q\bar{q}\tilde{\chi}_1^0$, (lower left) $\tilde{g} \rightarrow q\bar{q}\tilde{\chi}_2^0$ and $\tilde{\chi}_2^0 \rightarrow Z\tilde{\chi}_1^0$, or $\tilde{g} \rightarrow q\bar{q}'\tilde{\chi}_1^\pm$ and $\tilde{\chi}_1^\pm \rightarrow W^\pm\tilde{\chi}_1^0$, and (lower right) $\tilde{g} \rightarrow q\bar{q}'\tilde{\chi}_1^\pm$ and $\tilde{\chi}_1^\pm \rightarrow W^\pm\tilde{\chi}_1^0$ (with q = u, d, s, or c). For the scenarios where the gluinos decay via an intermediate $\tilde{\chi}_2^0$ or $\tilde{\chi}_1^\pm$, $\tilde{\chi}_2^0$ and $\tilde{\chi}_1^\pm$ are assumed to be mass-degenerate, with $m_{\tilde{\chi}_1^\pm, \tilde{\chi}_2^0} = 0.5(m_{\tilde{g}} + m_{\tilde{\chi}_1^0})$. The area enclosed by the thick black curve represents the observed exclusion region, while the dashed red lines indicate the expected limits and their ± 1 and ± 2 standard deviation (s.d.) ranges. The thin black lines show the effect of the theoretical uncertainties in the signal cross section. Signal cross sections are calculated at approximately NNLO+NNLL order in α_S [136–147], assuming 1/3 branching fraction ($\mathcal{B}$) for each decay mode in the mixed-decay scenarios, or unity branching fraction for the indicated decay

(two) decay modes is assumed. In particular, for the diagram of gluino pair production where the decays of the two gluinos differ, each gluino can decay via a $\tilde{\chi}_2^0$, $\tilde{\chi}_1^+$, or $\tilde{\chi}_1^-$. For scenarios with top squarks decaying into top quarks, the polarization of the top quark can be model dependent and a function of the top squark and neutralino mixing matrices.

To maintain independence of any particular model realization, events are generated with unpolarized top quarks. Signal cross sections are calculated at approximately NNLO+NNLL (next-to-next-to-leading-logarithm) order in α_S [136–147]. For direct light-flavor squark pair production we assume either one single squark, or eight degenerate squarks ($\tilde{q}_L + \tilde{q}_R$,
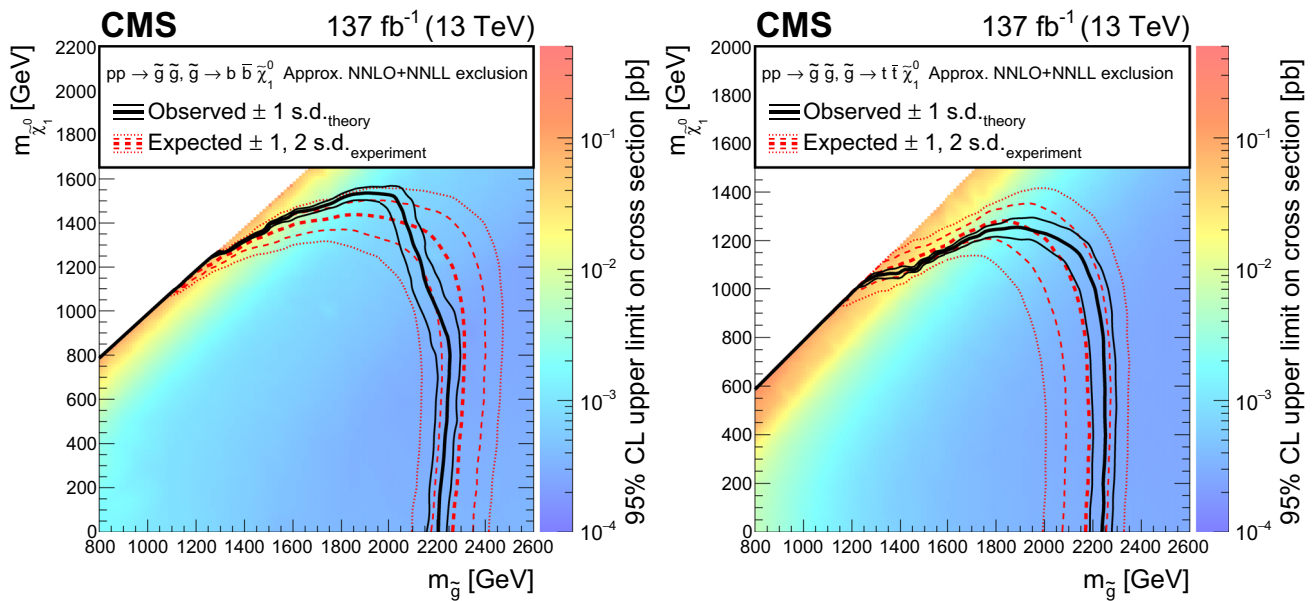
Fig. 12 Exclusion limits at 95% CL for direct gluino pair production where the gluinos decay to (left) bottom quarks and (right) top quarks. The area enclosed by the thick black curve represents the observed exclusion region, while the dashed red lines indicate the expected limits and their ± 1 and ± 2 standard deviation (s.d.) ranges. The thin black lines show the effect of the theoretical uncertainties in the signal cross section. Signal cross sections are calculated at approximately NNLO+NNLL order in α_S [136–147], assuming unity branching fraction for the indicated decay

with $\tilde{q} = \tilde{u}, \tilde{d}, \tilde{s}, \tilde{c}$). For direct bottom and top squark pair production, we assume one single squark.

The mono-ϕ model depicted in Fig. 8, that was recently proposed [35,36] based on a reinterpretation of the results of Refs. [6–9,37], is also probed by the inclusive M_{T2} search. In this case, the cross section for the signal is only calculated at LO order in α_S.

Another interpretation of the inclusive M_{T2} results places cross section limits on LQ pair production (depicted in Fig. 9) as a function of the LQ mass, similarly to Ref. [11]. We consider production of either LQ_S or LQ_V. In each case, we assume that only one LQ state is within mass reach of the LHC, and that the LQ decays with 100% branching fraction to a neutrino and a single type of quark: a light-flavor quark (q = u, d, s, or c), a bottom quark, or a top quark. The cross sections for LQ_S (LQ_V) pair production are computed to NLO (LO) order in α_S following Ref. [55]. The LQ_S pair production cross section depends only on the LQ mass. For LQ_V, additional constraints are imposed by unitarity at high energy scales, leading to model dependent solutions and thus production cross sections. In the model of Ref. [55], developed to explain the flavor physics anomalies, the additional relevant parameter for the LQ_V pair production cross section is κ, a dimensionless coupling that is 1 in the Yang–Mills case and 0 in the minimal coupling case. We consider both values. For $\kappa = 1$, the cross section for the LQ_V pair production is a factor 5–20 times larger than that of LQ_S, depending on the

LQ mass. In the LQ_V model, other free parameters are g_{t_L} and g_{b_L}, the couplings of the LQ_V to $t\nu$ and $b\tau$ pairs, respectively. However, g_{t_L} and g_{b_L} do not affect the cross section or the kinematics for the LQ_V pair production, and we assume $g_{t_L} = g_{b_L} = 0.1$, as predicted to explain the flavor physics anomalies.

The results of the search for disappearing tracks are used to constrain simplified models of SUSY where gluinos and squarks are produced in pairs, and each one decays either directly to the lightest neutralino ($\tilde{\chi}_1^0$), or first to a long-lived chargino ($\tilde{\chi}_1^\pm$) as shown in Fig. 10. All possible decays are assumed to occur with equal probability. Thus, the gluino branching fraction is 1/3 each for the decay to $\tilde{\chi}_1^0$, $\tilde{\chi}_1^+$, and $\tilde{\chi}_1^-$, and the squark branching fraction is 1/2 to $\tilde{\chi}_1^0$ and 1/2 to the $\tilde{\chi}_1^\pm$ of opposite charge. The $\tilde{\chi}_1^\pm$ and $\tilde{\chi}_1^0$ are assumed to be wino-like, and their masses to differ by a few hundred MeV [13,14]. Thus, the phase space for the decay of the $\tilde{\chi}_1^\pm$ to a $\tilde{\chi}_1^0$ and a charged pion is small. As a consequence, the $\tilde{\chi}_1^\pm$ has lifetime of the order of a few nanoseconds, and the momentum of the pion originating from its decay does not exceed a few hundred MeV. Hence, the final state shows negligible dependence on small variations of the mass difference between $\tilde{\chi}_1^\pm$ and $\tilde{\chi}_1^0$. Lifetimes of the $\tilde{\chi}_1^\pm$ are probed in the range $c\tau_0(\tilde{\chi}_1^\pm) = 1$–2000 cm.

Uncertainties in the signal yield for the simplified models considered are listed in Table 7. The sources of uncertainty and the methods used to evaluate their effect on the inter-
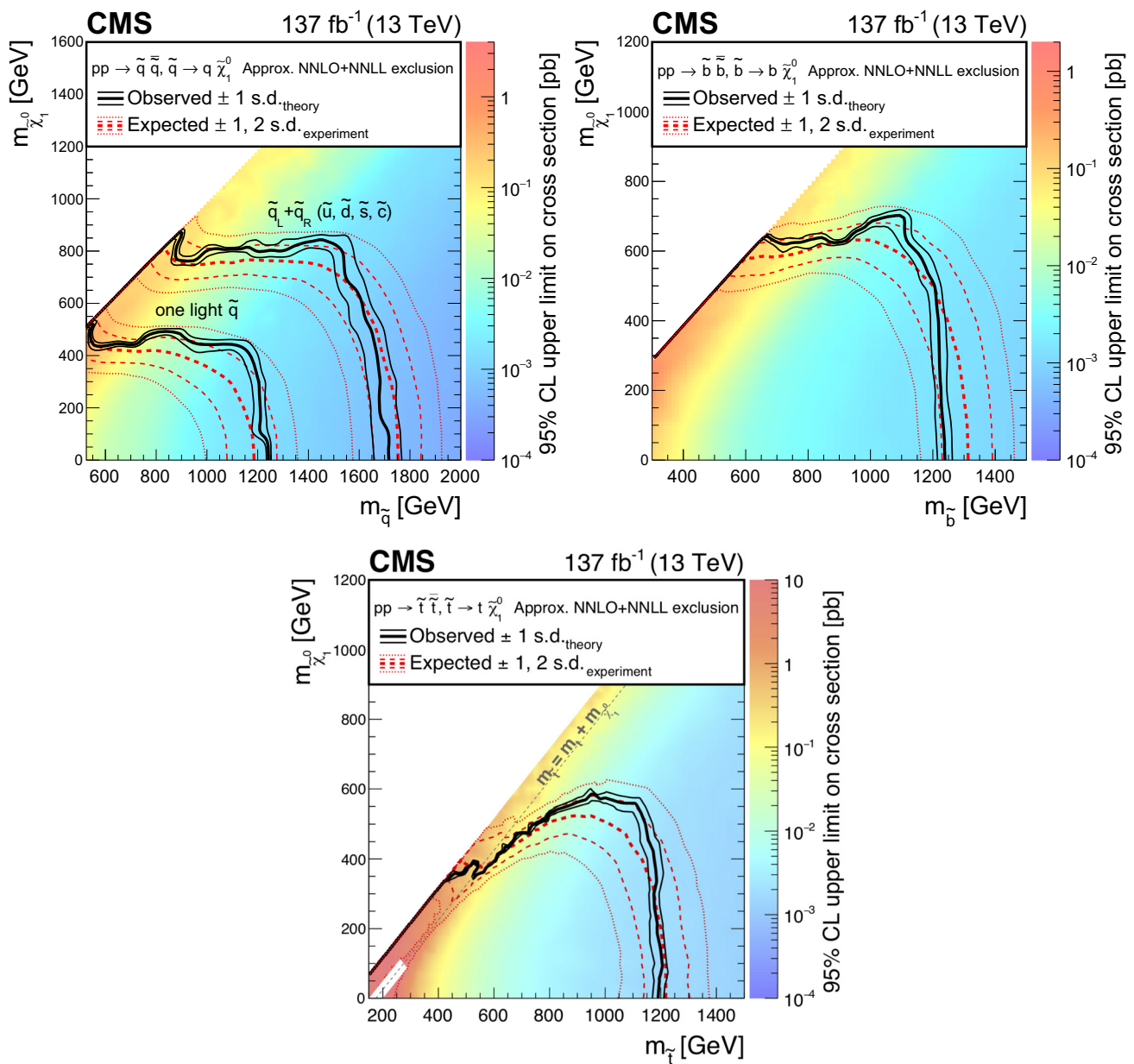
Fig. 13 Exclusion limit at 95% CL for (upper left) light-flavor squark pair production, (upper right) bottom squark pair production, and (lower) top squark pair production. The area enclosed by the thick black curve represents the observed exclusion region, while the dashed red lines indicate the expected limits and their ± 1 and ± 2 standard deviation (s.d.) ranges. The thin black lines show the effect of the theoretical uncertainties in the signal cross section. The white diagonal band in the top squark pair production exclusion limit corresponds to the region $|m_{\tilde{t}} - m_t - m_{\tilde{\chi}_1^0}| < 25$ GeV and small $m_{\tilde{\chi}_1^0}$. Here the efficiency of the selection is a strong function of $m_{\tilde{t}} - m_{\tilde{\chi}_1^0}$, and as a result the precise determination of the cross section upper limit is uncertain because of the finite granularity of the available MC samples in this region of the $(m_{\tilde{t}}, m_{\tilde{\chi}_1^0})$ plane. In the same exclusion limit, the dashed black diagonal line corresponds to $m_{\tilde{t}} = m_t + m_{\tilde{\chi}_1^0}$. Signal cross sections are calculated at approximately NNLO+NNLL order in α_S [136–147], assuming unity branching fraction for the indicated decay

pretation are the same as those discussed in Refs. [9,96]. For each data sample corresponding to the different periods of data taking (2016, 2017, and 2018), uncertainties in the luminosity measurement [148–150], ISR modeling, fast simulation p_T^{miss} distributions, and b tagging and lep-

ton efficiencies are treated as correlated across search bins. Uncertainties in fast simulation p_T^{miss} distributions, b tagging, and lepton efficiencies are treated as correlated also across data samples. The remaining uncertainties are taken as uncorrelated. In the search for disappearing tracks, all
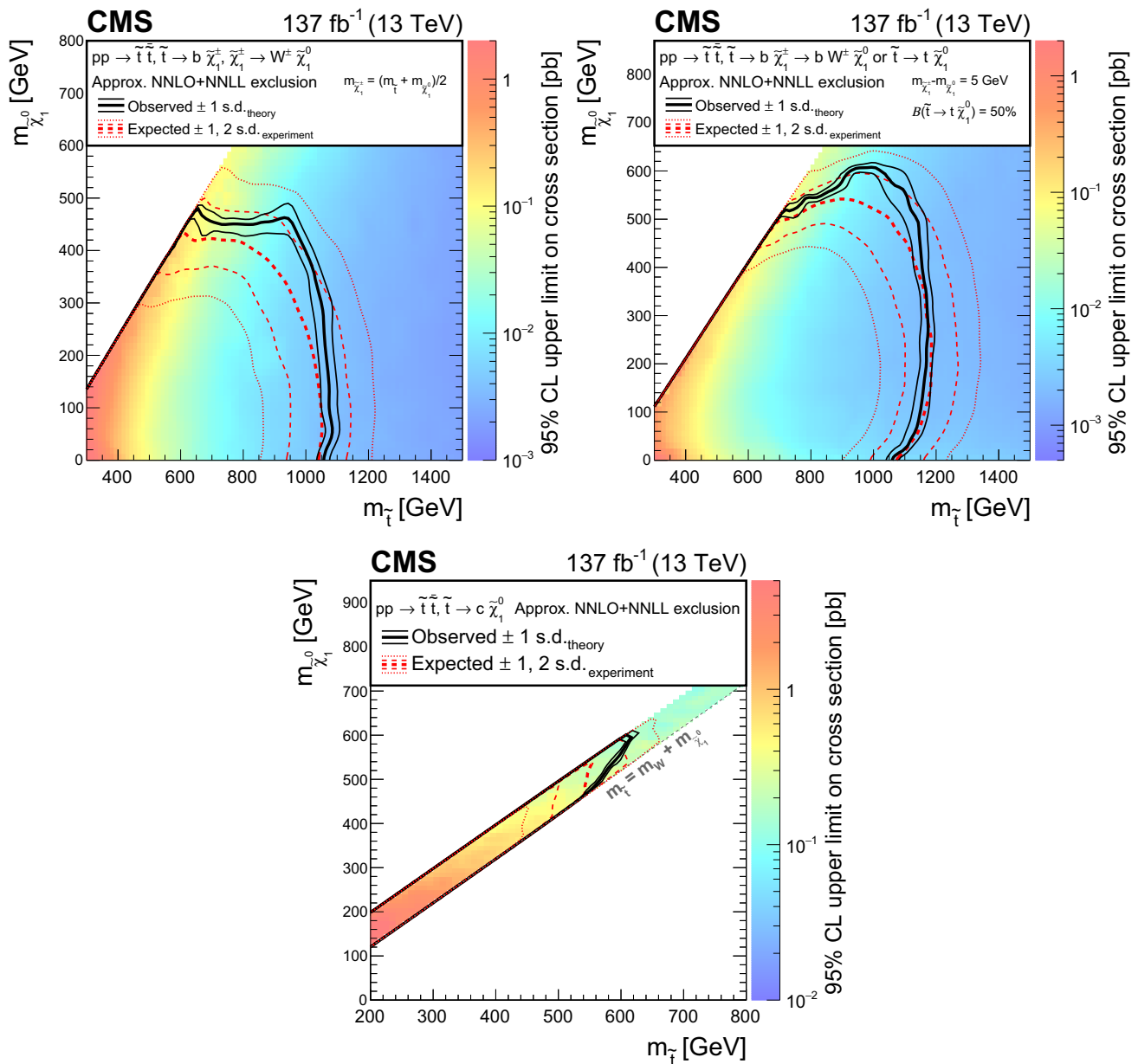
Fig. 14 Exclusion limit at 95% CL for top squark pair production for different decay modes of the top squark. (Upper left) For the scenario where $pp \to \tilde{t}\bar{\tilde{t}} \to b\bar{b}\tilde{\chi}_1^\pm \tilde{\chi}_1^\mp$, $\tilde{\chi}_1^\pm \to W^\pm \tilde{\chi}_1^0$, the mass of the chargino is chosen to be half way in between the masses of the top squark and the neutralino. (Upper right) A mixed-decay scenario, $pp \to \tilde{t}\bar{\tilde{t}}$ with equal branching fractions for the top squark decays $\tilde{t} \to t\tilde{\chi}_1^0$ and $\tilde{t} \to b\tilde{\chi}_1^+$, $\tilde{\chi}_1^+ \to W^{*+}\tilde{\chi}_1^0$, is also considered, with the chargino mass chosen such that $\Delta m\left(\tilde{\chi}_1^\pm, \tilde{\chi}_1^0\right) = 5$ GeV. (Lower) Finally, we also consider a compressed spectrum scenario where $pp \to \tilde{t}\bar{\tilde{t}} \to c\bar{c}\tilde{\chi}_1^0\tilde{\chi}_1^0$. In this scenario,

mass ranges are considered where the $\tilde{t} \to c\tilde{\chi}_1^0$ branching fraction can be significant. The area enclosed by the thick black curve represents the observed exclusion region, while the dashed red lines indicate the expected limits and their ± 1 and ± 2 standard deviation (s.d.) ranges. The thin black lines show the effect of the theoretical uncertainties in the signal cross section. Signal cross sections are calculated at approximately NNLO+NNLL order in α_S [136–147], assuming 50% branching fraction ($\mathcal{B}$) for each decay mode in the mixed-decay scenarios, or unity branching fraction for the indicated decay

other tagging and lepton efficiencies are neglected. Other uncertainties associated with the modeling of disappearing tracks are treated as correlated across search bins. Specifically, an uncertainty in the signal yield is assigned, equal

to one half of the track selection inefficiency: 25 (17.5)% for P (M and L) tracks in 2016, and 10% for tracks of all lengths in 2017–2018. Additionally, a 6% uncertainty in the 2017–2018 signal yield is assigned to account for inaccu-

Table 8 Summary of the observed 95% CL exclusion limits on the masses of SUSY particles for different simplified model scenarios. The highest limits on the mass of the directly produced particles and on the mass of the $\tilde{\chi}_1^0$ are quoted

Simplified model	Highest limit on directly produced SUSY particle mass (GeV)	Highest limit on $\tilde{\chi}_1^0$ mass (GeV)
Direct gluino pair production		
$\tilde{g} \to q\bar{q}\tilde{\chi}_1^0$	1970	1200
$\tilde{g} \to q\bar{q}Z\tilde{\chi}_1^0$ or $\tilde{g} \to q\bar{q}'W^{\pm}\tilde{\chi}_1^0$	2020	1090
$\tilde{g} \to b\bar{b}\tilde{\chi}_1^0$	2250	1525
$\tilde{g} \to t\bar{t}\tilde{\chi}_1^0$	2250	1250
Direct squark pair production		
Eight degenerate light squarks	1710	870
Single light squark	1250	525
Bottom squark	1240	700
Top squark	1200	580

racies in the fast simulation modeling of the signal acceptance.

6.1 Inclusive M_{T2} search

Figure 11 shows the exclusion limits at 95% CL for direct gluino pair production where the gluinos decay to light-flavor quarks under three different decay scenarios. Exclusion limits for direct gluino pair production where the gluinos decay to bottom and top quarks are shown in Fig. 12, and those for the direct production of squark pairs are shown in Fig. 13. Three alternate decay scenarios are also considered for the direct pair production of top squarks, and their exclusion limits are shown in Fig. 14.

Table 8 summarizes the limits on the masses of SUSY particles excluded for the simplified model scenarios considered. These results extend the constraints on gluino and squark masses by about 100–350 GeV and on the $\tilde{\chi}_1^0$ mass by 100–250 GeV with respect to the limits in Ref. [9].

Figure 15 shows the exclusion limits for the mono-ϕ model [35,36]. Based on the LO cross section calculation, we obtain mass limits as large as 1660 and 925 GeV on m_ϕ and on m_ψ, respectively. In this model, the analysis of Refs. [35,36] reports best fit parameters $(m_\phi, m_\psi) = (1250, 900)$ GeV and product of the cross section and branching fraction of about 0.3 pb. For this mass point, we find a modest (1.1 standard deviations) excess, and we set an upper limit on the product of the cross section and branching fraction of about 0.6 (0.4 expected) pb, equal to 4.7 (3.2) times the assumed LO theoretical cross section.

The LQ limits from the M_{T2} search are shown in Fig. 16, where only one LQ state is assumed to be within reach of the LHC, and where each LQ is assumed to decay to a neutrino and a single type of quark.

In Refs. [54,55], a model is proposed as a coherent explanation of the flavor physics anomalies. It is based on an LQ_V that can decay to $t\nu$ and to $b\tau$ final states, each with 50%
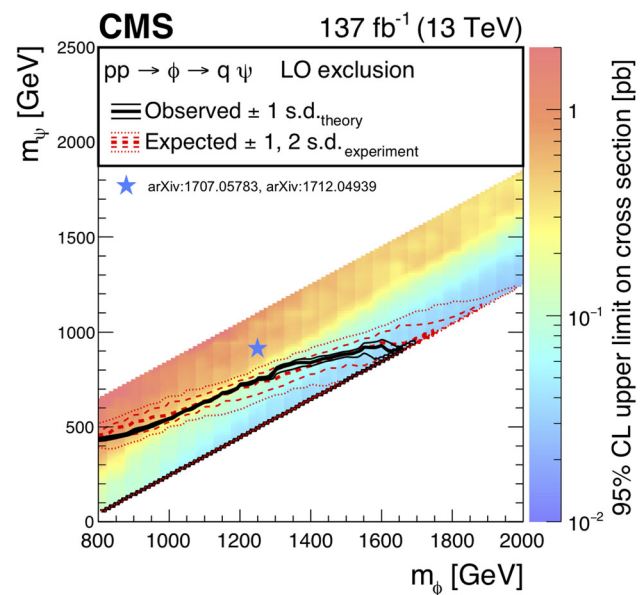

Fig. 15 Exclusion limit at 95% CL for the mono-ϕ model. We consider the mass range where such a model could be interesting based on a reinterpretation of previous analyses [35,36]. The area enclosed by the thick black curve represents the observed exclusion region, while the dashed red lines indicate the expected limits and their ± 1 and ± 2 standard deviation (s.d.) ranges. The thin black lines show the effect of the theoretical uncertainties in the signal cross section. The blue star at $(m_\phi, m_\psi) = (1250, 900)$ GeV indicates the best fit mass point reported in Refs. [35,36]. Signal cross sections are calculated at LO order in α_S

branching fraction. In our analysis, events are selected with a charged-lepton veto, including hadronically decaying τ leptons. Hence, only the 25% of events where both LQs decay to $t\nu$ are considered to set constraints on this model, and the theoretical prediction for this branching fraction is shown as a separate curve in Fig. 16 (lower).

Table 9 summarizes the limits on the masses of the LQs excluded for the considered scenarios. These results extend the constraints on LQ masses by up to about 200 GeV
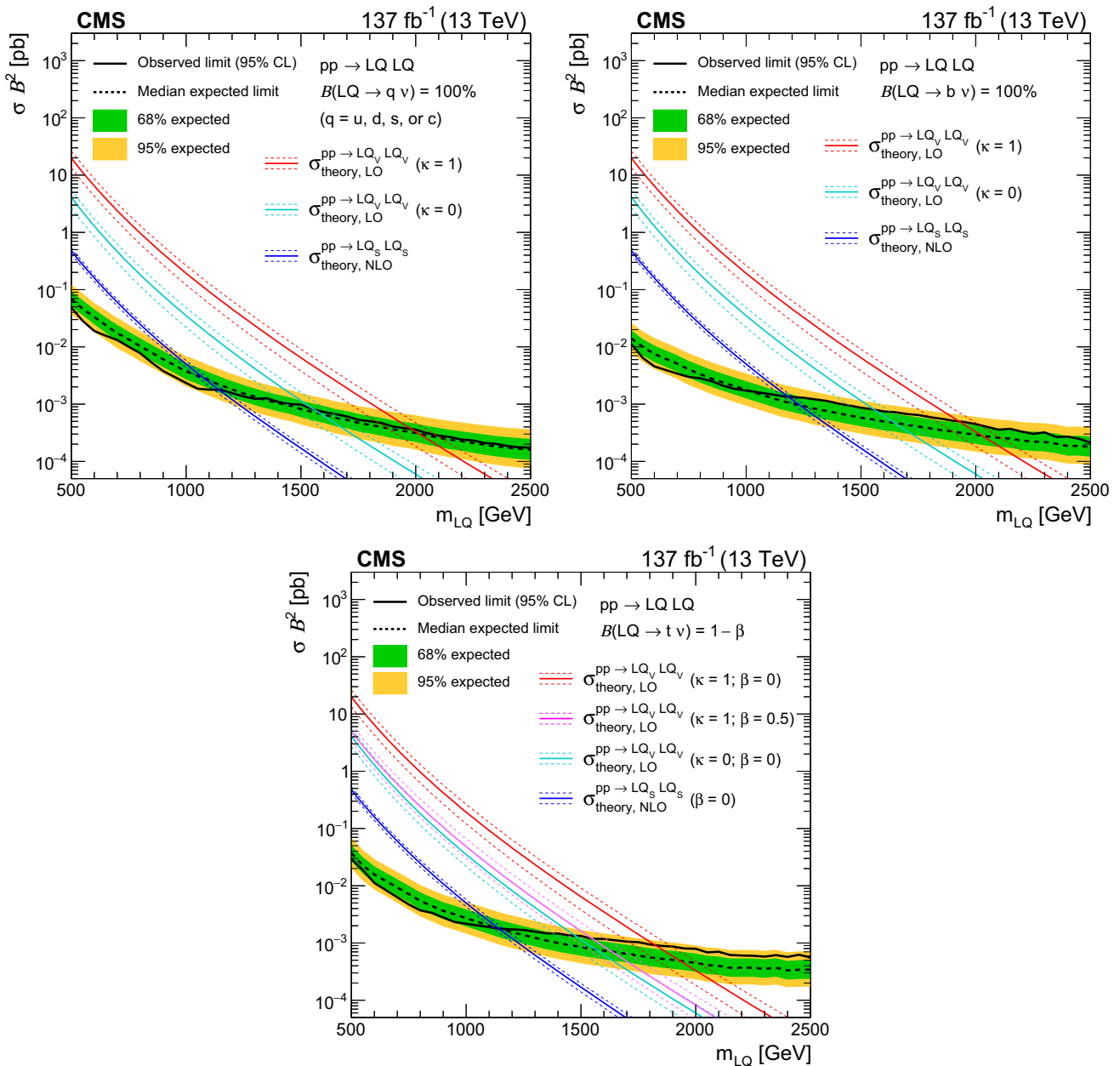
Fig. 16 The 95% CL upper limits on the production cross sections as a function of LQ mass for LQ pair production decaying with 100% branching fraction ($\mathcal{B}$) to a neutrino and (upper left) a light quark (one of u, d, s, or c), (upper right) a bottom quark, or (lower) a top quark. The solid (dashed) black line represents the observed (median expected) exclusion. The inner green (outer yellow) band indicates the region containing 68 (95)% of the distribution of limits expected under the background-only hypothesis. The dark blue lines show the theoretical cross section for LQ_S pair production with its uncertainty. The red (light blue) lines show the same for LQ_V pair production assuming $\kappa = 1$ (0). (Lower) Also shown in magenta is the product of the theoretical cross section and the square of the branching fraction ($\sigma\mathcal{B}^2$), for vector LQ pair production assuming $\kappa = 1$ and a 50% branching fraction to $t\nu_\tau$, with the remaining 50% to $b\tau$. Signal cross sections are calculated at NLO (LO) in α_S for scalar (vector) LQ pair production

Table 9 Summary of the observed 95% CL exclusion limits on the masses of LQs for the considered scenarios. The columns show scalar or vector LQ with the choice of κ, while the rows show the LQ decay channel. For mixed-decay scenarios, the assumed branching fractions ($\mathcal{B}$) are indicated

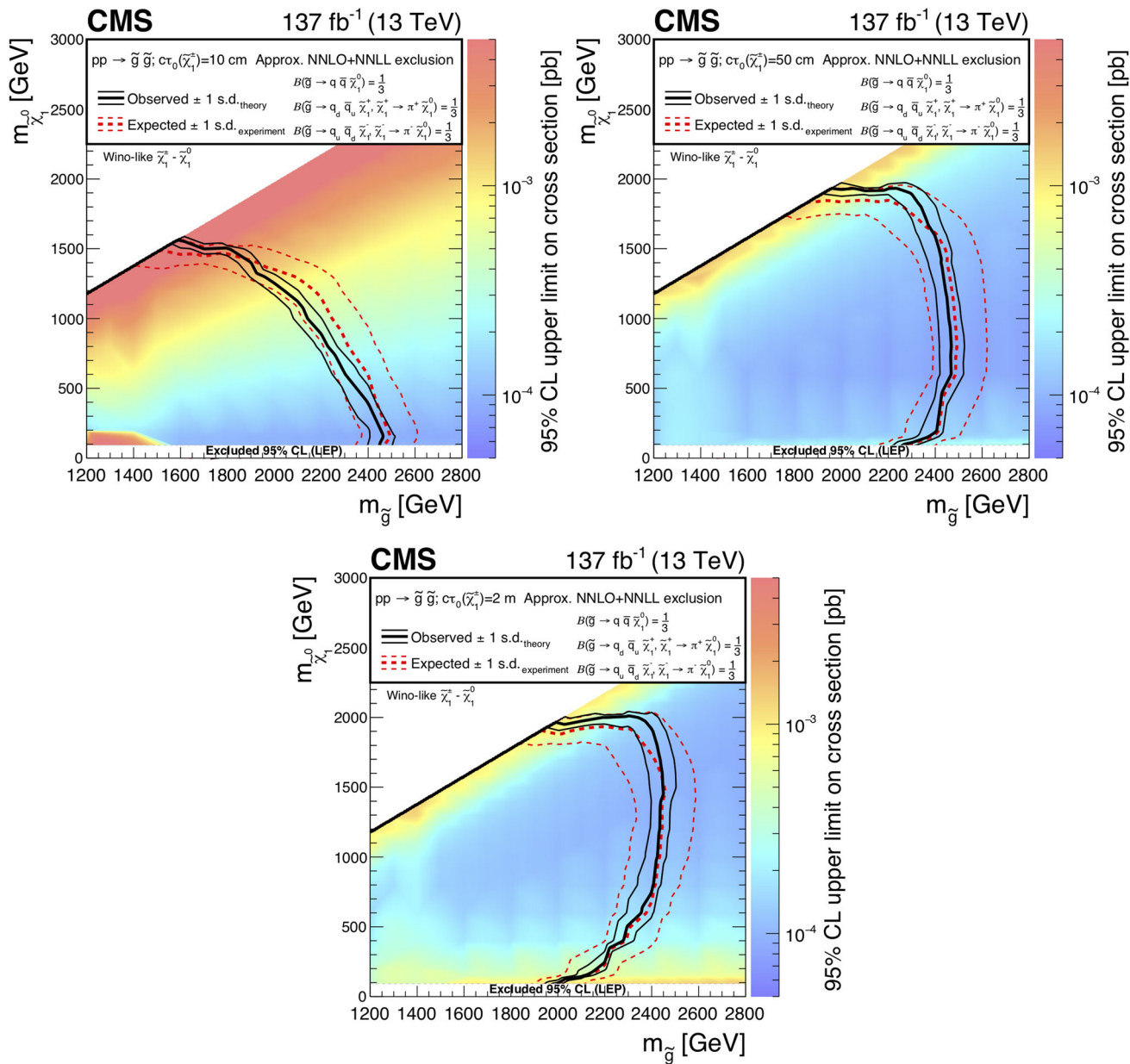|	LQ_S Mass (GeV)	LQ_V, $\kappa = 1$ Mass (GeV)	LQ_V, $\kappa = 0$ Mass (GeV)
$LQ \rightarrow q\nu$ (q = u, d, s, or c)	1140	1980	1560
$LQ \rightarrow b\nu$	1185	1925	1560
$LQ \rightarrow t\nu$	1140	1825	1475
$LQ \rightarrow \begin{cases} t\nu & (\mathcal{B} = 50\%) \\ b\tau & (\mathcal{B} = 50\%) \end{cases}$	–	1550	1225

Fig. 17 Exclusion limits at 95% CL for direct gluino pair production where the gluinos decay to light-flavor (u, d, s, c) quarks, with $c\tau_0(\tilde{\chi}_1^{\pm}) =$ (upper left) 10 cm, (upper right) 50 cm, and (lower) 200 cm. The area enclosed by the thick black curve represents the observed exclusion region, while the dashed red lines indicate the expected limits and their ±1 standard deviation (s.d.) ranges. The thin black lines show the effect of the theoretical uncertainties in the signal cross section. The white band for masses of the $\tilde{\chi}_1^0$ below 91.9 GeV represents the region of the mass plane excluded at the CERN LEP [151]. Signal cross sections are calculated at approximately NNLO+NNLL order in α_S [136–147], assuming decay branching fractions ($\mathcal{B}$) as indicated in the figure
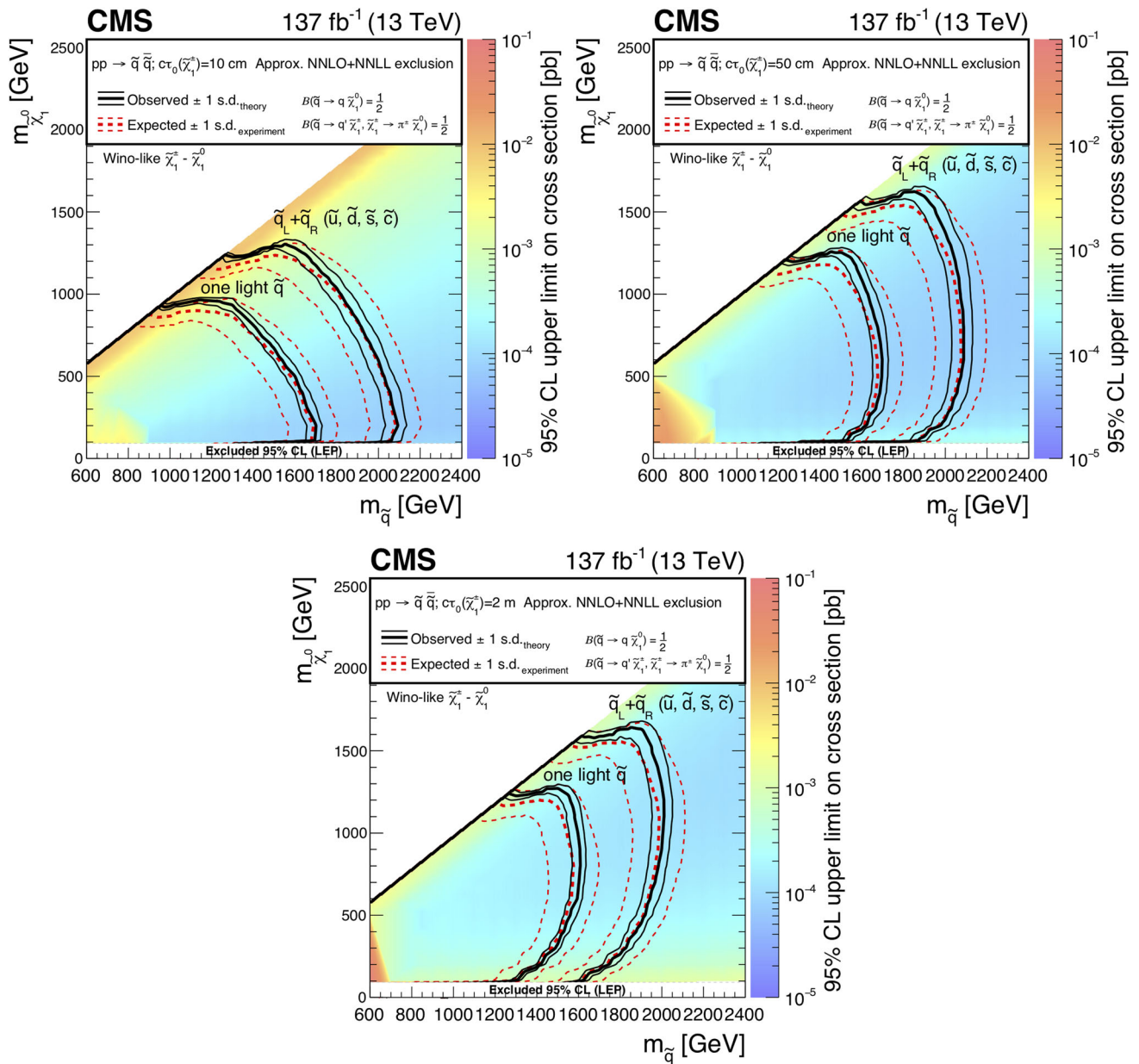
Fig. 18 Exclusion limits at 95% CL for light squark pair production with $c\tau_0(\tilde{\chi}_1^\pm) = $ (upper left) 10 cm, (upper right) 50 cm, and (lower) 200 cm. The area enclosed by the thick black curve represents the observed exclusion region, while the dashed red lines indicate the expected limits and their ± 1 standard deviation (s.d.) ranges. The thin black lines show the effect of the theoretical uncertainties in the signal cross section. The white band for masses of the $\tilde{\chi}_1^0$ below 91.9 GeV represents the region of the mass plane excluded at the CERN LEP [151]. Signal cross sections are calculated at approximately NNLO+NNLL order in α_S [136–147], assuming decay branching fractions ($\mathcal{B}$) as indicated in the figure
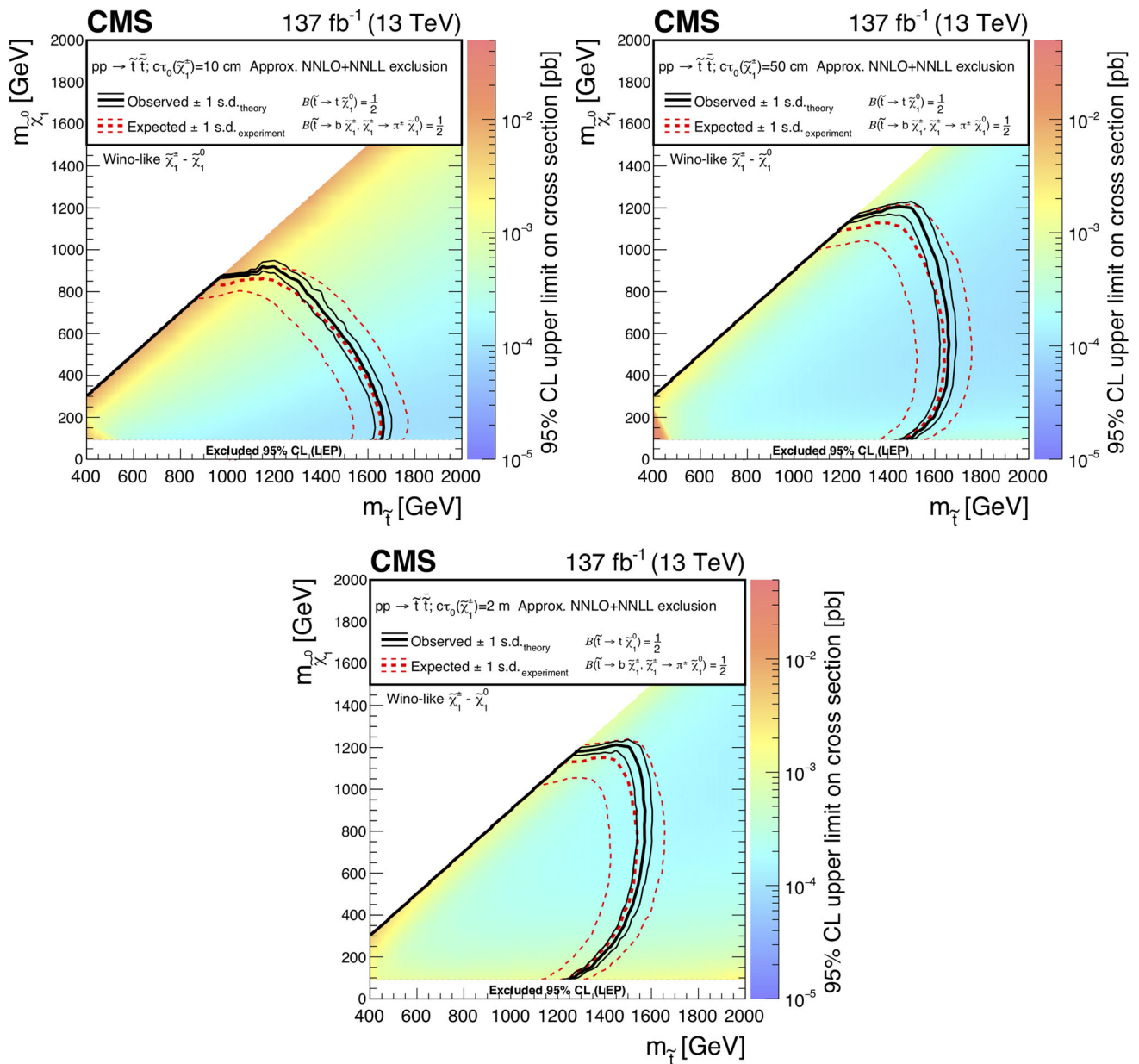
Fig. 19 Exclusion limits at 95% CL for top squark pair production with $c\tau_0(\tilde{\chi}_1^\pm) =$ (upper left) 10 cm, (upper right) 50 cm, and (lower) 200 cm. The area enclosed by the thick black curve represents the observed exclusion region, while the dashed red lines indicate the expected limits and their ± 1 standard deviation (s.d.) ranges. The thin black lines show the effect of the theoretical uncertainties in the signal cross sec-

tion. The white band for masses of the $\tilde{\chi}_1^0$ below 91.9 GeV represents the region of the mass plane excluded at the CERN LEP [151]. Signal cross sections are calculated at approximately NNLO+NNLL order in α_S [136–147], assuming decay branching fractions ($\mathcal{B}$) as indicated in the figure

Table 10 Summary of the observed 95% CL exclusion limits on the masses of SUSY particles for different simplified model scenarios, where the produced particles decay with equal probability to $\tilde{\chi}_1^+$, $\tilde{\chi}_1^-$, and $\tilde{\chi}_1^0$, and the $\tilde{\chi}_1^\pm$ are long lived. The highest limits on the mass of the directly produced particles and on the mass of the $\tilde{\chi}_1^0$ are quoted

Simplified model	Highest limit on directly produced SUSY particle mass (GeV)	Highest limit on $\tilde{\chi}_1^0$ mass (GeV)
Direct gluino pair production:		
$\tilde{g} \to q\bar{q}\tilde{\chi}_1^0$ or $\tilde{g} \to q\bar{q}'\tilde{\chi}_1^\pm$	2460	2000
Direct squark pair production:		
Eight degenerate light squarks	2090	1650
Single light squark	1700	1275
Top squark	1660	1210

with respect to the limits of Ref. [11], providing the most stringent constraint to date in models of LQ pair production.

The 95% CL upper limits on signal cross sections obtained using the most sensitive super signal regions of Table 6 are typically less stringent by a factor of $\sim 1.5-3$ compared to those obtained in the fully binned analysis. This difference in performance arises from the larger signal acceptance of the full analysis, as well as from the more favorable signal-to-background ratio achieved in its individual bins, compared to the super signal regions.

6.2 Search for disappearing tracks

Figure 17 shows the exclusion limits at 95% CL for direct gluino pair production where the gluinos decay to light-flavor (u, d, s, c) quarks, with $c\tau_0(\tilde{\chi}_1^\pm) = 10$, 50, and 200 cm. Exclusion limits for the direct production of light-flavor and top squark pairs are shown in Figs. 18 and 19, respectively, also for $c\tau_0(\tilde{\chi}_1^\pm) = 10$, 50, and 200 cm.

Exclusion limits from the disappearing track search tend to be strongest in longer $c\tau_0(\tilde{\chi}_1^\pm)$ models, when $m_{\tilde{\chi}_1^0}$ is near the mass of the gluino or squark, and in shorter $c\tau_0(\tilde{\chi}_1^\pm)$ models, when a large mass splitting generates a large boost for the $\tilde{\chi}_1^\pm$, and in models characterized by large jet multiplicities. Models with these properties tend to populate the background depleted disappearing track regions with high N_j and longer tracks. In the massless $\tilde{\chi}_1^\pm$ and $\tilde{\chi}_1^0$ limit, the $\tilde{\chi}_1^\pm$ receives a large Lorentz boost. Therefore, it tends not to decay inside the tracking detector, with a consequent reduction in the signal acceptance and in the analysis sensitivity.

When a $\tilde{\chi}_1^\pm$ decays within the volume of the tracking detector, it is not counted as a PF candidate and, being almost mass degenerate with the $\tilde{\chi}_1^0$, its decay products provide negligible visible energy in the detector. To a good approximation, as confirmed in simulation, the limits presented in Sect. 6.1 from the inclusive M_{T2} search should apply also to these models with an intermediate $\tilde{\chi}_1^\pm$.

For SUSY models with long-lived $\tilde{\chi}_1^\pm$, the search for disappearing tracks significantly extends the sensitivity of the inclusive M_{T2} search. Table 10 summarizes the limits on the masses of the SUSY particles excluded for the simplified model scenarios considered.

Two-dimensional constraints are also placed on the $\tilde{\chi}_1^\pm$ mass as a function of its proper decay length, as shown in Figs. 20 and 21, for the pair production of gluinos and light-flavor and top squarks, respectively. In particular, Figs. 20 and 21 show the excluded $\tilde{\chi}_1^\pm$ mass as a function of its proper decay length for representative gluino, light-flavor or top squark masses. For short $\tilde{\chi}_1^\pm$ lifetimes, the inclusive M_{T2} search is more sensitive than the dedicated search for disappearing tracks, based on expected exclusion limits. As already mentioned above, the inclusive M_{T2} search is not sensitive to the presence of an intermediate long-lived $\tilde{\chi}_1^\pm$ in the parent SUSY particle decay chain, especially when the $\tilde{\chi}_1^\pm$ lifetime is short, such that the $\tilde{\chi}_1^\pm$ cannot be reconstructed as a stable PF candidate. Furthermore, the signal acceptance of the inclusive M_{T2} search is not affected by the track reconstruction inefficiencies which may arise when the $\tilde{\chi}_1^\pm$ decays before the CMS tracker, for very short $\tilde{\chi}_1^\pm$ lifetimes.

Figure 22 shows exclusion limits on $\sigma/\sigma_{\text{theory}}$ as a function of $c\tau_0(\tilde{\chi}_1^\pm)$, for a choice of signal models where gluinos and squarks can decay via a long-lived $\tilde{\chi}_1^\pm$, as obtained from the search for disappearing tracks. Scenarios where the mass spectrum of SUSY particles is compressed are especially constrained across a wide range of $c\tau_0(\tilde{\chi}_1^\pm)$. The exclusion limits are typically stronger at intermediate $c\tau_0(\tilde{\chi}_1^\pm)$, as a larger fraction of $\tilde{\chi}_1^\pm$ decay within the CMS tracker and can therefore be identified as disappearing tracks.
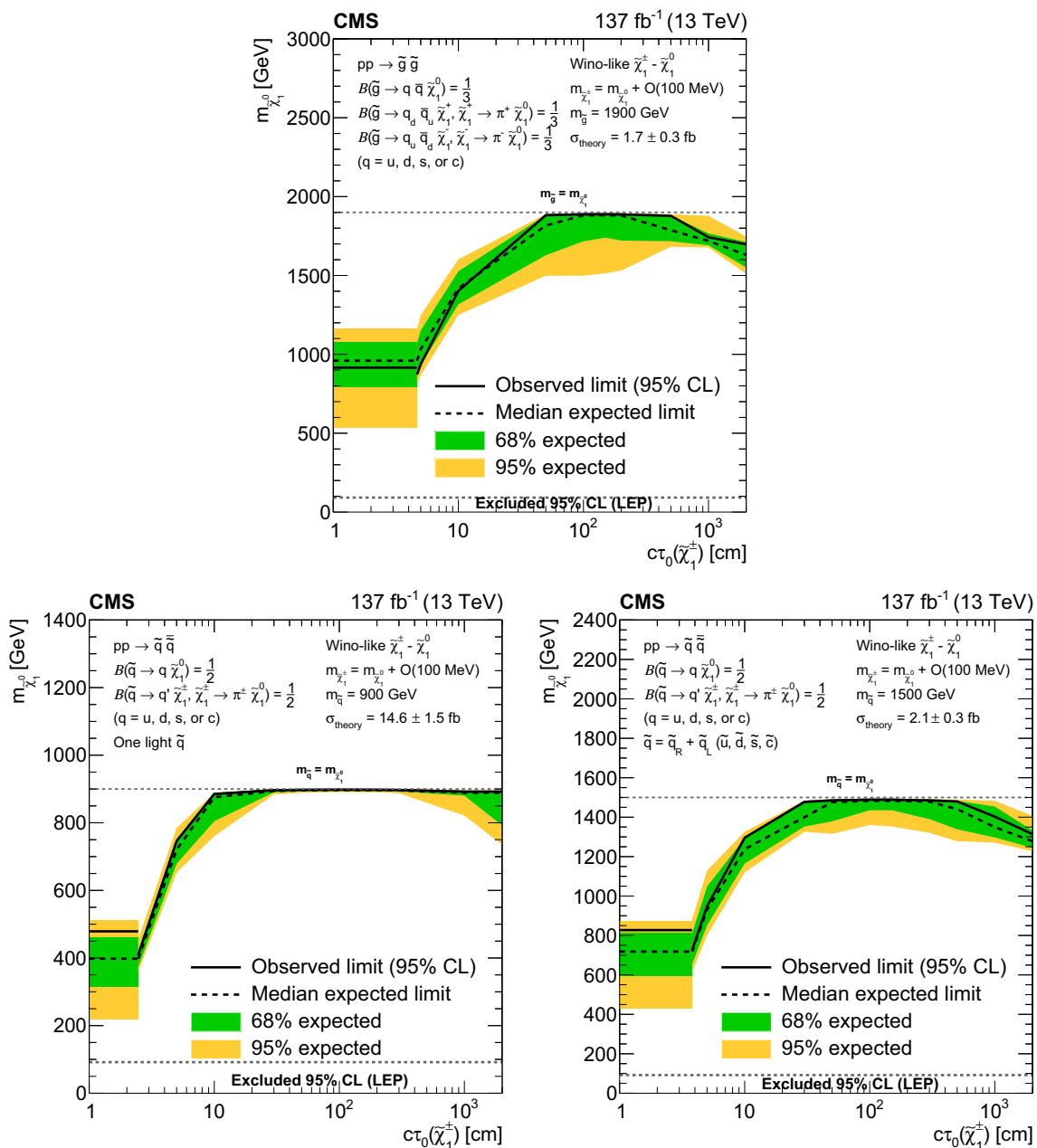
Fig. 20 Exclusion limits at 95% CL on the $\tilde{\chi}_1^0$ mass, with $m_{\tilde{\chi}_1^\pm} = m_{\tilde{\chi}_1^0} + \mathcal{O}(100\ \text{MeV})$, as a function of the $\tilde{\chi}_1^\pm$ proper decay length, for (upper) direct gluino and (lower) direct light-flavor (u, d, s, c) squark pair production, as obtained for representative gluino and squark masses. The gluinos decay to light-flavor quarks. For direct squark pair production, we assume either (lower left) one–fold or (lower right) eight–fold squark degeneracy. The area enclosed by the solid (dashed) black curve represents the observed (median expected) exclusion region, while the inner green (outer yellow) band indicates the region containing 68 (95)% of the distribution of limits expected under the background-only hypothesis. At short decay lengths, horizontal exclusion lines are obtained from the inclusive M_{T2} search, as this is not affected by track recon-struction inefficiencies, which may arise when the $\tilde{\chi}_1^\pm$ decays before the CMS tracker, and therefore shows better sensitivity to scenarios with very small $c\tau_0(\tilde{\chi}_1^\pm)$ compared to the disappearing track search, based on median expected limits. The horizontal dashed lines at (upper) $m_{\tilde{g}} = m_{\tilde{\chi}_1^0}$ and (lower) $m_{\tilde{q}} = m_{\tilde{\chi}_1^0}$ bound the mass range in which the decays are kinematically allowed. If all kinematically allowed $\tilde{\chi}_1^0$ masses ($m_{\tilde{\chi}_1^0} \leq m_{\tilde{g}}$, or $m_{\tilde{\chi}_1^0} \leq m_{\tilde{q}}$) are excluded, the curves, including 68 and 95% expected, tend to overlap. The band at masses of the $\tilde{\chi}_1^0$ below 91.9 GeV represents the region of the mass plane excluded at the CERN LEP [151]. Signal cross sections are calculated at approximately NNLO+NNLL order in α_S [136–147], assuming decay branching fractions ($\mathcal{B}$) as indicated in the figure
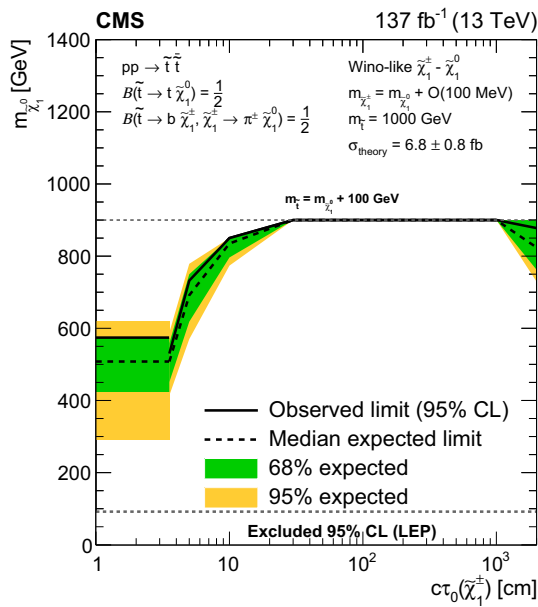
Fig. 21 Exclusion limits at 95% CL on the $\tilde{\chi}_1^0$ mass, with $m_{\tilde{\chi}_1^\pm} = m_{\tilde{\chi}_1^0} + \mathcal{O}(100\,\text{MeV})$, as a function of the $\tilde{\chi}_1^\pm$ proper decay length, for direct top squark pair production, as obtained for a representative top squark mass. The area enclosed by the solid (dashed) black curve represents the observed (median expected) exclusion region, while the inner green (outer yellow) band indicates the region containing 68 (95)% of the distribution of limits expected under the background-only hypothesis. At short decay lengths, horizontal exclusion lines are obtained from the inclusive M_{T2} search, as this is not affected by track reconstruction inefficiencies, which may arise when the $\tilde{\chi}_1^\pm$ decays before the CMS tracker, and therefore shows better sensitivity to scenarios with very small $c\tau_0(\tilde{\chi}_1^\pm)$ compared to the disappearing track search, based on median expected limits. The horizontal dashed line at $m_{\tilde{t}} = m_{\tilde{\chi}_1^0} + 100\,\text{GeV}$ indicates the minimum simulated mass difference between top squark and $\tilde{\chi}_1^0$, chosen such that the decay of top quarks to on-shell W bosons is allowed. If all kinematically allowed $\tilde{\chi}_1^0$ masses ($m_{\tilde{\chi}_1^0} \leq m_{\tilde{t}} - 100\,\text{GeV}$) are excluded, the curves, including 68 and 95% expected, tend to overlap. The band at masses of the $\tilde{\chi}_1^0$ below 91.9 GeV represents the region of the mass plane excluded at the CERN LEP [151]. Signal cross sections are calculated at approximately NNLO+NNLL order in α_S [136–147], assuming decay branching fractions ($\mathcal{B}$) as indicated in the figure

7 Summary

This paper presents the results of two related searches for phenomena beyond the standard model using events with jets and large values of the kinematic variable M_{T2}. The first is an inclusive search, while the second requires in addition disappearing tracks. The measurements are based on a data sample of proton–proton collisions at $\sqrt{s} = 13\,\text{TeV}$ collected in 2016–2018 with the CMS detector, and corresponding to an integrated luminosity of $137\,\text{fb}^{-1}$. No significant deviations from the standard model expectations are observed. Limits on pair-produced gluinos and squarks are established in the context of supersymmetry models conserving R-parity. The inclusive M_{T2} search probes gluino masses up to 2250 GeV and the lightest neutralino $\tilde{\chi}_1^0$ masses up to 1525 GeV, as well as light-flavor, bottom, and top squark masses up to 1710, 1240, and 1200 GeV, respectively, and $\tilde{\chi}_1^0$ masses up to 870, 700, and 580 GeV in each respective scenario. In models with a long-lived chargino $\tilde{\chi}_1^\pm$, where the gluinos and squarks decay with equal probability to $\tilde{\chi}_1^0$, $\tilde{\chi}_1^+$, and $\tilde{\chi}_1^-$, the search looking in addition for disappearing tracks probes gluino masses up to 2460 GeV and $\tilde{\chi}_1^0$ masses up to 2000 GeV, as well as light-flavor (top) squark masses up to 2090 (1660) GeV and $\tilde{\chi}_1^0$ masses up to 1650 (1210) GeV.

A resonantly produced colored scalar state ϕ decaying to a massive Dirac fermion ψ and a quark has recently been proposed as an explanation of an excess in data identified in regions with low jet multiplicities, based on previous results by the ATLAS and CMS Collaborations. From the inclusive M_{T2} search, mass limits as high as 1660 and 925 GeV are obtained for ϕ and ψ, respectively, and an upper limit on the product of the cross section and branching fraction of about 0.6 pb with a local significance of 1.1 standard deviations is observed for the previously reported best fit point $(m_\phi, m_\psi) = (1250, 900)$ GeV. The inclusive M_{T2} search is also used to constrain models of scalar and vector leptoquark (LQ) pair production with the LQ decaying to a neutrino and a top, bottom, or light-flavor quark. A vector LQ decaying with equal branching fraction to $t\nu$ and $b\tau$ has been proposed as part of an explanation of recent flavor anomalies. In such a model, LQ masses below 1550 GeV are excluded assuming the Yang–Mills case with coupling $\kappa = 1$, or 1225 GeV in the minimal coupling case $\kappa = 0$. The results presented in this paper extend the mass limits of the previous version of the CMS inclusive M_{T2} search, using a subset of the present data, by hundreds of GeV. In most of the cases, the results obtained are the most stringent constraints to date.
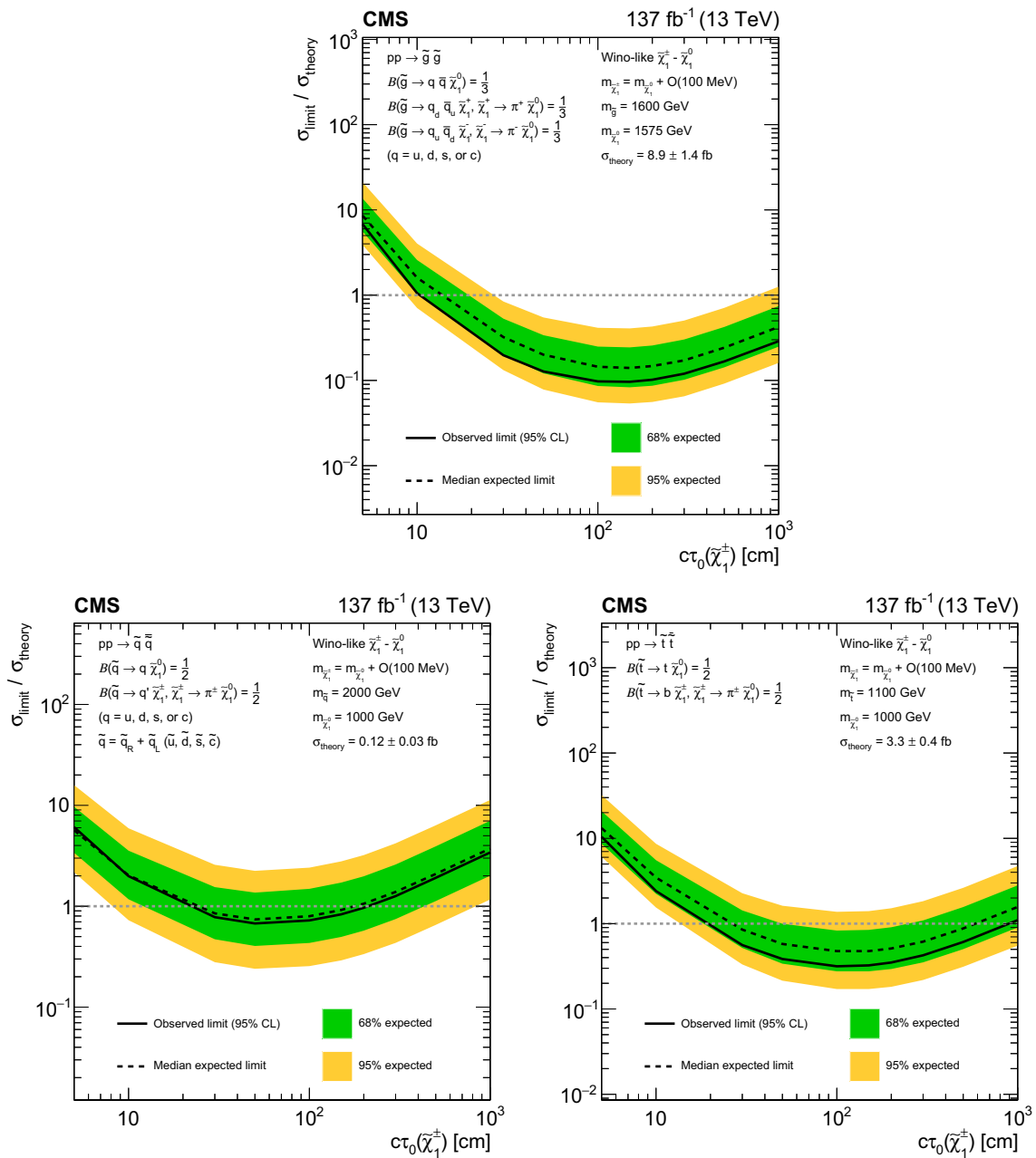
Fig. 22 Exclusion limits at 95% CL on $\sigma/\sigma_{\text{theory}}$ as a function of the $\tilde{\chi}_1^{\pm}$ decay length, for a choice of signal models of (upper) direct gluino pair production where the gluinos decay to light-flavor (u, d, s, c) quarks, (lower left) direct light-flavor squark pair production, and (lower right) direct top squark pair production, as obtained from the search for disappearing tracks. The area enclosed by the solid (dashed) black curve below the horizontal dashed line at $\sigma/\sigma_{\text{theory}} = 1$ represents the observed (median expected) exclusion region, while the inner green (outer yellow) band indicates the region containing 68 (95)% of the distribution of limits expected under the background-only hypothesis. Signal cross sections are calculated at approximately NNLO+NNLL order in α_S [136–147], assuming decay branching fractions ($\mathcal{B}$) as indicated in the figure

Acknowledgements We congratulate our colleagues in the CERN accelerator departments for the excellent performance of the LHC and thank the technical and administrative staffs at CERN and at other CMS institutes for their contributions to the success of the CMS effort. In addition, we gratefully acknowledge the computing centers and personnel of the Worldwide LHC Computing Grid for delivering so effectively the computing infrastructure essential to our analyses. Finally, we acknowledge the enduring support for the construction and operation of the LHC and the CMS detector provided by the following funding agencies: BMBWF and FWF (Austria); FNRS and FWO (Belgium); CNPq, CAPES, FAPERJ, FAPERGS, and FAPESP (Brazil); MES (Bulgaria); CERN; CAS, MoST, and NSFC (China); COLCIENCIAS (Colombia); MSES and CSF (Croatia); RPF (Cyprus); SENESCYT (Ecuador); MoER, ERC IUT, PUT and ERDF (Estonia); Academy of Finland, MEC, and HIP (Finland); CEA and CNRS/IN2P3 (France); BMBF, DFG, and HGF (Germany); GSRT (Greece); NKFIA (Hungary); DAE and DST (India); IPM (Iran); SFI (Ireland); INFN (Italy); MSIP and NRF (Republic of Korea); MES (Latvia); LAS (Lithuania); MOE and UM (Malaysia); BUAP, CINVESTAV, CONACYT, LNS, SEP, and UASLP-FAI (Mexico); MOS (Montenegro); MBIE (New Zealand); PAEC (Pakistan); MSHE and NSC (Poland); FCT (Portugal); JINR (Dubna); MON, RosAtom, RAS, RFBR, and NRC KI (Russia); MESTD (Serbia); SEIDI, CPAN, PCTI, and FEDER (Spain); MOSTR (Sri Lanka); Swiss Funding Agencies (Switzerland); MST (Taipei); ThEPCenter, IPST, STAR, and NSTDA (Thailand); TUBITAK and TAEK (Turkey); NASU and SFFR (Ukraine); STFC (United Kingdom); DOE and NSF (USA). Individuals have received support from the Marie-Curie program and the European Research Council and Horizon 2020 Grant, contract Nos. 675440, 752730, and 765710 (European Union); the Leventis Foundation; the A.P. Sloan Foundation; the Alexander von Humboldt Foundation; the Belgian Federal Science Policy Office; the Fonds pour la Formation à la Recherche dans l'Industrie et dans l'Agriculture (FRIA-Belgium); the Agentschap voor Innovatie door Wetenschap en Technologie (IWT-Belgium); the F.R.S.-FNRS and FWO (Belgium) under the "Excellence of Science – EOS" – be.h project n. 30820817; the Beijing Municipal Science & Technology Commission, No. Z181100004218003; the Ministry of Education, Youth and Sports (MEYS) of the Czech Republic; the Lendület ("Momentum") Program and the János Bolyai Research Scholarship of the Hungarian Academy of Sciences, the New National Excellence Program ÚNKP, the NKFIA research Grants 123842, 123959, 124845, 124850, 125105, 128713, 128786, and 129058 (Hungary); the Council of Science and Industrial Research, India; the HOMING PLUS program of the Foundation for Polish Science, cofinanced from European Union, Regional Development Fund, the Mobility Plus program of the Ministry of Science and Higher Education, the National Science Center (Poland), contracts Harmonia 2014/14/M/ST2/00428, Opus 2014/13/B/ST2/02543, 2014/15/B/ST2/03998, and 2015/19/B/ST2/02861, Sonata-bis 2012/07 /E/ST2/01406; the National Priorities Research Program by Qatar National Research Fund; the Ministry of Science and Education, Grant no. 3.2989.2017 (Russia); the Programa Estatal de Fomento de la Investigación Científica y Técnica de Excelencia María de Maeztu, Grant MDM-2015-0509 and the Programa Severo Ochoa del Principado de Asturias; the Thalis and Aristeia programs cofinanced by EU-ESF and the Greek NSRF; the Rachadapisek Sompot Fund for Postdoctoral Fellowship, Chulalongkorn University and the Chulalongkorn Academic into Its 2nd Century Project Advancement Project (Thailand); the Welch Foundation, contract C-1845; and the Weston Havens Foundation (USA).

Data Availability Statement This manuscript has no associated data or the data will not be deposited. [Authors' comment: Release and preservation of data used by the CMS Collaboration as the basis for publications is guided by the CMS policy as written in its document "CMS data preservation, re-use and open access policy" (https://cms-docdb.cern. ch/cgi-bin/PublicDocDB/RetrieveFile?docid=6032&filename=CMSD ataPolicyV1.2.pdf&version=2).]

A Disappearing track selection

The detailed selection of disappearing tracks (STs and STCs, as defined in Sect. 3.2.2) is summarized in Table 11.

B Definition of search regions and yields

B.1 Inclusive M_{T2} search: search regions and yields

The 282 exclusive search regions defined for the inclusive M_{T2} search, as described in Sect. 3.2.1, are summarized in Tables 12, 13, 14, 15, 16, 17, 18, 19, 20, 21, 22 and 23, together with the pre-fit background predictions and the observed yields.

B.2 Search for disappearing tracks: search regions and yields

The 68 search regions defined for the disappearing track search, as described in Sect. 3.2.2, are summarized in Tables 24, 25 and 26, together with the pre-fit background predictions and the observed yields.

C Detailed results

C.1 Inclusive M_{T2} search

Figures 23 and 24 show the background estimates and observed data yields in the regions $250 < H_T < 450$, $450 < H_T < 575$, $1200 < H_T < 1500$, and $H_T > 1500$ GeV. Each bin corresponds to a single M_{T2} bin, and vertical lines identify (H_T, N_j, N_b) topological regions.

Table 11 Selection requirements for STs and STCs. For the subset of medium (M) length tracks that have just four tracking layers with a measurement, the minimum required number of layers of the pixel tracking detector with a measurement is three (†). The selected tracks are required to not overlap with identified leptons. For this selection, all electrons and muons are considered, either identified as PF candidates or not. The selected tracks are as well required to not be identified as PF candidates, and to not overlap with other tracks with $p_T > 15$ GeV, even if those tracks are not associated with PF candidates. The factor by which the selection requirement is relaxed in order to select short track candidates is also reported. If no factor is reported, the requirement is not relaxed for the selection of short track candidates

Observable	Selection	Track length	STC factor
p_T (GeV)	>15	All	
$|\eta|$	< 2.4 and not $1.38 < |\eta| < 1.6$	All	
$\sigma(p_T) / p_T^2$ (GeV^{-1})	$< 0.2; < 0.02; < 0.005$	P; M; L	3
d_{xy} (from primary vertex) [cm]	< 0.02 (< 0.01)	P (M, L)	3
d_z (from primary vertex) [cm]	< 0.05	All	3
Neutral isolation ($\Delta R < 0.05$) (GeV)	< 10	All	6
Neutral isolation / p_T	< 0.1	All	6
Isolation ($\Delta R < 0.3$) (GeV)	< 10	All	6
Isolation / p_T	< 0.2	All	6
Number of pixel layers	≥ 3 (≥ 2)	P, M† (M, L)	
Number of tracker layers	$\geq 3; < 7; \geq 7$	P; M; L	
Number of lost inner hits	$=0$	All	
Number of lost outer hits	≥ 2	M, L	
Is a PF candidate?	No	All	
PF lepton veto ($\Delta R < 0.1$)	Yes	All	
Lepton veto ($\Delta R < 0.2$)	Yes	All	
Track veto ($\Delta R < 0.1$)	Yes	All	
Bad calorimeter module veto	Yes	All	
M_T (track, $\vec{p}_T^{\text{miss}}$) (GeV)	>100, if $p_T < 150$ GeV	L	

Table 12 Predictions and observations for the 12 search regions with $N_j = 1$. For each of the background predictions, the first uncertainty listed is statistical (from the limited size of data control samples and Monte Carlo samples), and the second is systematic

N_j, N_b	p_T^{jet} (GeV)	Lost lepton	$Z \to \nu\bar{\nu}$	Multijet	Total background	Data
1j, 0b	250–350	$70\,700 \pm 400 \pm 4100$	$167\,000 \pm 1000 \pm 11\,000$	$530 \pm 20 \pm 160$	$238\,000 \pm 1000 \pm 14\,000$	251 941
	350–450	$13\,440 \pm 130 \pm 790$	$40\,100 \pm 500 \pm 3100$	$55 \pm 5 \pm 16$	$53\,600 \pm 500 \pm 3700$	54 870
	450–575	$3050 \pm 50 \pm 180$	$10\,850^{+230}_{-220} \pm 690$	$5.6 \pm 1.1 \pm 1.6$	$13\,910 \pm 230 \pm 840$	14 473
	575–700	$603^{+20}_{-19} \pm 38$	$2590^{+110}_{-100} \pm 160$	$0.38 \pm 0.06 \pm 0.11$	$3200 \pm 110 \pm 190$	3432
	700–1000	$220 \pm 13 \pm 16$	$1076^{+70}_{-66} \pm 66$	$0.12 \pm 0.03 \pm 0.03$	$1295^{+71}_{-67} \pm 79$	1304
	1000–1200	$11.7^{+4.1}_{-3.2} \pm 0.9$	$86^{+23}_{-19} \pm 6$	< 0.01	$98^{+24}_{-19} \pm 7$	98
	≥ 1200	$2.8^{+2.7}_{-1.5} \pm 0.6$	$23^{+12}_{-8} \pm 2$	< 0.01	$26^{+13}_{-9} \pm 2$	30
1j, $\geq$ 1b	250–350	$4210 \pm 110 \pm 260$	$9030 \pm 230 \pm 630$	$58 \pm 10 \pm 17$	$13\,310^{+260}_{-250} \pm 820$	13 549
	350–450	$878 \pm 38 \pm 56$	$2180^{+110}_{-100} \pm 170$	$4.6 \pm 0.4 \pm 1.3$	$3060 \pm 110 \pm 220$	3078
	450–575	$211^{+16}_{-15} \pm 13$	$651^{+57}_{-53} \pm 44$	$0.63 \pm 0.18 \pm 0.18$	$863^{+59}_{-55} \pm 53$	810
	575–700	$40.3^{+6.0}_{-5.5} \pm 2.5$	$164^{+30}_{-26} \pm 11$	$0.04 \pm 0.02 \pm 0.02$	$205^{+31}_{-26} \pm 13$	184
	≥ 700	$19.2^{+5.7}_{-4.6} \pm 1.3$	$74^{+21}_{-16} \pm 7$	< 0.01	$94^{+21}_{-17} \pm 7$	83

Table 13 Predictions and observations for the 30 search regions with $250 \leq H_T < 450$ GeV. For each of the background predictions, the first uncertainty listed is statistical (from the limited size of data control samples and Monte Carlo samples), and the second is systematic

N_j, N_b	M_{T2} (GeV)	Lost lepton	$Z \to \nu\bar{\nu}$	Multijet	Total background	Data
$250 \leq H_T < 450$ GeV:						
2-3j, 0b	200–300	$73\,700 \pm 500 \pm 5000$	$156\,000 \pm 1000 \pm 12\,000$	$580 \pm 20 \pm 140$	$231\,000 \pm 1000 \pm 16\,000$	240 867
	300–400	$12\,030 \pm 200 \pm 820$	$31\,300 \pm 200 \pm 2500$	$50 \pm 5 \pm 10$	$43\,400 \pm 300 \pm 3200$	44 074
	≥ 400	$417^{+51}_{-47} \pm 28$	$1450 \pm 10 \pm 140$	$0.44 \pm 0.09 \pm 0.09$	$1870 \pm 50 \pm 160$	2022
2-3j, 1b	200–300	$12\,450 \pm 170 \pm 820$	$18\,700 \pm 300 \pm 1500$	$90 \pm 8 \pm 21$	$31\,300 \pm 300 \pm 2200$	32 120
	300–400	$2380 \pm 80 \pm 160$	$3750 \pm 60 \pm 310$	$6.9 \pm 1.0 \pm 1.5$	$6130 \pm 100 \pm 430$	6258
	≥ 400	$97 \pm 8 \pm 39$	$174 \pm 3 \pm 17$	$0.01 \pm 0.01 \pm 0.00$	$271^{+9}_{-8} \pm 45$	275
2-3j, 2b	200–300	$2240 \pm 70 \pm 150$	$2340^{+110}_{-100} \pm 200$	$9.7 \pm 1.1 \pm 2.3$	$4600^{+130}_{-120} \pm 320$	4709
	300–400	$398^{+34}_{-32} \pm 27$	$469^{+21}_{-20} \pm 39$	$0.68 \pm 0.17 \pm 0.15$	$868^{+40}_{-38} \pm 61$	984
	≥ 400	$13.3 \pm 2.3 \pm 5.4$	$21.7^{+1.0}_{-0.9} \pm 2.2$	< 0.01	$35.0 \pm 2.5 \pm 6.0$	30
2-6j, $\geq$ 3b	200–300	$507^{+32}_{-31} \pm 38$	$179^{+35}_{-30} \pm 27$	$1.77 \pm 0.46 \pm 0.46$	$688^{+47}_{-43} \pm 54$	699
	300–400	$69 \pm 6 \pm 15$	$40.0^{+7.8}_{-6.6} \pm 6.0$	$0.16 \pm 0.12 \pm 0.04$	$109^{+10}_{-9} \pm 16$	102
	≥ 400	$1.50 \pm 0.80 \pm 0.61$	$1.43^{+0.28}_{-0.24} \pm 0.25$	< 0.01	$2.92^{+0.85}_{-0.83} \pm 0.67$	0
4-6j, 0b	200–300	$12\,500 \pm 180 \pm 800$	$21\,600 \pm 300 \pm 1800$	$250 \pm 17 \pm 58$	$34\,400 \pm 400 \pm 2400$	35 187
	300–400	$2070 \pm 80 \pm 130$	$4660 \pm 70 \pm 410$	$18.2 \pm 3.6 \pm 3.8$	$6750 \pm 110 \pm 510$	6725
	≥ 400	$42 \pm 5 \pm 17$	$155 \pm 2 \pm 64$	$0.06 \pm 0.03 \pm 0.01$	$197 \pm 5 \pm 67$	170
4-6j, 1b	200–300	$5750 \pm 100 \pm 380$	$4300 \pm 150 \pm 360$	$61 \pm 7 \pm 15$	$10\,120 \pm 180 \pm 680$	10 564
	300–400	$784^{+43}_{-42} \pm 52$	$928^{+32}_{-31} \pm 84$	$2.07 \pm 0.29 \pm 0.45$	$1710 \pm 50 \pm 120$	1769
	≥ 400	$14.0 \pm 2.5 \pm 5.7$	$31 \pm 1 \pm 13$	$0.04 \pm 0.02 \pm 0.01$	$45 \pm 3 \pm 14$	40
4-6j, 2b	200–300	$2550^{+70}_{-60} \pm 170$	$921^{+68}_{-63} \pm 87$	$10.0 \pm 1.5 \pm 2.2$	$3480 \pm 90 \pm 230$	3621
	300–400	$220^{+23}_{-21} \pm 15$	$198^{+15}_{-14} \pm 20$	$0.47 \pm 0.15 \pm 0.11$	$419^{+27}_{-25} \pm 31$	496
	≥ 400	$3.2 \pm 0.8 \pm 1.3$	$6.6 \pm 0.5 \pm 2.7$	< 0.01	$9.8 \pm 0.9 \pm 3.1$	14
$\geq$ 7j, 0b	200–300	$55^{+15}_{-13} \pm 4$	$61^{+23}_{-17} \pm 26$	$2.64 \pm 0.39 \pm 0.57$	$119^{+28}_{-22} \pm 27$	108
	300–500	$3.8^{+2.1}_{-2.0} \pm 0.8$	$8.1^{+3.1}_{-2.3} \pm 4.3$	$0.08 \pm 0.04 \pm 0.02$	$12.0^{+3.7}_{-3.1} \pm 4.4$	30
	≥ 500	$0.0^{+3.2}_{-0.0} \pm 0.0$	$0.0^{+1.2}_{-0.0} \pm 0.0$	< 0.01	$0.0^{+3.4}_{-0.0} \pm 0.0$	0
$\geq$ 7j, 1b	200–300	$48.0^{+9.1}_{-8.2} \pm 3.5$	$19^{+19}_{-11} \pm 10$	$0.33 \pm 0.14 \pm 0.09$	$68^{+21}_{-13} \pm 11$	95
	≥ 300	$3.0 \pm 1.4 \pm 1.2$	$2.5^{+2.4}_{-1.3} \pm 1.7$	$0.03 \pm 0.02 \pm 0.01$	$5.6^{+2.8}_{-1.9} \pm 2.1$	12
$\geq$ 7j, 2b	200–300	$41.3^{+7.7}_{-7.0} \pm 3.1$	$6.0^{+5.8}_{-3.2} \pm 3.7$	$0.29 \pm 0.14 \pm 0.06$	$47.6^{+9.7}_{-7.7} \pm 5.0$	30
	≥ 300	$2.15^{+0.78}_{-0.76} \pm 0.87$	$0.74^{+0.72}_{-0.40} \pm 0.57$	< 0.01	$2.9^{+1.1}_{-0.9} \pm 1.1$	1
$\geq$ 7j, $\geq$ 3b	200–300	$7.3^{+1.7}_{-1.5} \pm 0.9$	$1.0^{+1.0}_{-0.6} \pm 1.1$	$0.04 \pm 0.04 \pm 0.01$	$8.4^{+1.9}_{-1.6} \pm 1.5$	17
	≥ 300	$0.47 \pm 0.35 \pm 0.20$	$0.12^{+0.11}_{-0.06} \pm 0.14$	< 0.01	$0.59^{+0.37}_{-0.35} \pm 0.24$	0

Table 14 Predictions and observations for the 28 search regions with $450 \leq H_T < 575$ GeV, and $2 \leq N_j \leq 3$, $2 \leq N_j \leq 6$ and $N_b \geq 3$, or $4 \leq N_j \leq 6$. For each of the background predictions, the first uncertainty listed is statistical (from the limited size of data control samples and Monte Carlo samples), and the second is systematic

N_j, N_b	M_{T2} (GeV)	Lost lepton	$Z \to \nu\bar{\nu}$	Multijet	Total background	Data
$450 \leq H_T < 575$ GeV:						
2-3j, 0b	200–300	$8860 \pm 110 \pm 640$	$20\,100 \pm 200 \pm 1300$	$69 \pm 13 \pm 16$	$29\,100 \pm 300 \pm 1900$	28 956
	300–400	$4230 \pm 80 \pm 300$	$11\,770 \pm 140 \pm 790$	$10.6 \pm 0.8 \pm 2.4$	$16\,000 \pm 200 \pm 1000$	15 876
	400–500	$1510 \pm 60 \pm 110$	$5020 \pm 60 \pm 360$	$2.86 \pm 0.62 \pm 0.60$	$6540 \pm 80 \pm 440$	6527
	≥ 500	$121^{+24}_{-21} \pm 9$	$580 \pm 7 \pm 63$	$0.07 \pm 0.03 \pm 0.02$	$701^{+25}_{-22} \pm 68$	740

Table 14 continued

N_j, N_b	M_{T2} (GeV)	Lost lepton	$Z \to \nu\bar{\nu}$	Multijet	Total background	Data
2-3j, 1b	200–300	$1326 \pm 43 \pm 88$	$2500 \pm 80 \pm 170$	$17.0 \pm 8.4 \pm 3.8$	$3840^{+100}_{-90} \pm 240$	3859
	300–400	$737 \pm 35 \pm 49$	$1464^{+49}_{-48} \pm 99$	$1.62 \pm 0.20 \pm 0.43$	$2200 \pm 60 \pm 140$	2065
	400–500	$259^{+25}_{-23} \pm 19$	$626^{+21}_{-20} \pm 45$	$0.49 \pm 0.10 \pm 0.12$	$885^{+32}_{-31} \pm 58$	907
	≥ 500	$19.1^{+2.8}_{-2.7} \pm 7.8$	$72.4 \pm 2.4 \pm 7.9$	$0.04 \pm 0.02 \pm 0.02$	$92 \pm 4 \pm 11$	79
2-3j, 2b	200–300	$201 \pm 15 \pm 13$	$322^{+31}_{-28} \pm 25$	$1.34 \pm 0.62 \pm 0.47$	$524^{+35}_{-32} \pm 35$	463
	300–400	$83.8^{+9.6}_{-9.1} \pm 9.1$	$188^{+18}_{-17} \pm 15$	$0.26 \pm 0.07 \pm 0.07$	$272^{+21}_{-19} \pm 20$	304
	400–500	$31.8^{+4.1}_{-4.0} \pm 6.7$	$80.4^{+7.7}_{-7.1} \pm 6.6$	$0.02 \pm 0.01 \pm 0.01$	$112^{+9}_{-8} \pm 10$	120
	≥ 500	$2.16^{+0.67}_{-0.66} \pm 0.88$	$9.3^{+0.9}_{-0.8} \pm 1.1$	< 0.01	$11.4 \pm 1.1 \pm 1.4$	15
2-6j, $\geq$ 3b	200–300	$232^{+17}_{-16} \pm 15$	$57^{+17}_{-13} \pm 7$	$2.20 \pm 0.70 \pm 0.80$	$291^{+24}_{-21} \pm 19$	297
	300–400	$81^{+12}_{-11} \pm 6$	$33.6^{+9.9}_{-7.8} \pm 4.3$	$0.26 \pm 0.08 \pm 0.08$	$115^{+16}_{-14} \pm 8$	76
	400–500	$10.7^{+2.1}_{-2.0} \pm 2.3$	$11.4^{+3.4}_{-2.7} \pm 1.5$	< 0.01	$22.1^{+4.0}_{-3.4} \pm 2.8$	24
	≥ 500	$1.08 \pm 0.58 \pm 0.44$	$1.03^{+0.30}_{-0.24} \pm 0.17$	< 0.01	$2.11^{+0.65}_{-0.62} \pm 0.48$	0
4-6j, 0b	200–300	$5660 \pm 90 \pm 370$	$8560 \pm 170 \pm 600$	$143 \pm 7 \pm 35$	$14\,360 \pm 190 \pm 890$	15 047
	300–400	$2250 \pm 60 \pm 150$	$4790^{+100}_{-90} \pm 350$	$24.3 \pm 2.6 \pm 6.2$	$7060 \pm 110 \pm 460$	6939
	400–500	$428^{+32}_{-30} \pm 28$	$1220 \pm 20 \pm 110$	$1.42 \pm 0.21 \pm 0.52$	$1650 \pm 40 \pm 130$	1817
	≥ 500	$14.8 \pm 2.2 \pm 6.0$	$86 \pm 2 \pm 35$	$0.04 \pm 0.02 \pm 0.01$	$101 \pm 3 \pm 36$	104
4-6j, 1b	200–300	$2810 \pm 60 \pm 190$	$1880 \pm 80 \pm 130$	$63 \pm 15 \pm 19$	$4750 \pm 100 \pm 300$	4736
	300–400	$937 \pm 36 \pm 63$	$1054^{+45}_{-43} \pm 78$	$5.4 \pm 0.4 \pm 1.4$	$2000 \pm 60 \pm 130$	2039
	400–500	$138^{+17}_{-16} \pm 10$	$269 \pm 11 \pm 25$	$0.36 \pm 0.10 \pm 0.10$	$407^{+20}_{-19} \pm 31$	403
	≥ 500	$7.5 \pm 2.2 \pm 3.0$	$19.1 \pm 0.8 \pm 7.9$	$0.01 \pm 0.01 \pm 0.00$	$26.5 \pm 2.3 \pm 8.5$	27
4-6j, 2b	200–300	$1343^{+38}_{-37} \pm 89$	$414^{+39}_{-35} \pm 33$	$11.5 \pm 1.0 \pm 3.3$	$1770 \pm 50 \pm 110$	1767
	300–400	$418^{+24}_{-23} \pm 29$	$232^{+22}_{-20} \pm 19$	$1.35 \pm 0.35 \pm 0.39$	$651^{+32}_{-31} \pm 43$	636
	400–500	$45.6^{+3.9}_{-3.8} \pm 9.6$	$59.1^{+5.5}_{-5.1} \pm 5.9$	$0.03 \pm 0.02 \pm 0.01$	$105^{+7}_{-6} \pm 12$	120
	≥ 500	$1.59 \pm 0.89 \pm 0.65$	$4.2 \pm 0.4 \pm 1.7$	< 0.01	$5.8 \pm 1.0 \pm 1.9$	7

Table 15 Predictions and observations for the 12 search regions with $450 \leq H_T < 575$ GeV and $N_j \geq 7$. For each of the background predictions, the first uncertainty listed is statistical (from the limited size of data control samples and Monte Carlo samples), and the second is systematic

N_j, N_b	M_{T2} (GeV)	Lost lepton	$Z \to \nu\bar{\nu}$	Multijet	Total background	Data
$450 \leq H_T < 575$ GeV:						
$\geq$ 7j, 0b	200–300	$149^{+17}_{-16} \pm 13$	$169^{+31}_{-27} \pm 34$	$11.5 \pm 0.8 \pm 3.0$	$329^{+36}_{-31} \pm 38$	354
	300–400	$38.9^{+5.8}_{-5.6} \pm 8.2$	$64^{+12}_{-10} \pm 17$	$1.24 \pm 0.42 \pm 0.32$	$104^{+13}_{-12} \pm 20$	110
	≥ 400	$1.28 \pm 0.82 \pm 0.52$	$8.8^{+1.6}_{-1.4} \pm 3.8$	$0.03 \pm 0.02 \pm 0.01$	$10.1^{+1.8}_{-1.6} \pm 3.8$	10
$\geq$ 7j, 1b	200–300	$191^{+13}_{-12} \pm 15$	$67^{+19}_{-15} \pm 15$	$4.4 \pm 0.5 \pm 1.2$	$262^{+23}_{-19} \pm 23$	268
	300–400	$37.8^{+3.4}_{-3.3} \pm 8.0$	$25.3^{+7.2}_{-5.7} \pm 7.3$	$0.30 \pm 0.07 \pm 0.08$	$63^{+8}_{-7} \pm 11$	65
	≥ 400	$2.31 \pm 0.69 \pm 0.94$	$3.5^{+1.0}_{-0.8} \pm 1.5$	$0.01 \pm 0.01 \pm 0.00$	$5.8^{+1.2}_{-1.0} \pm 1.8$	3
$\geq$ 7j, 2b	200–300	$173^{+12}_{-11} \pm 13$	$19.9^{+5.7}_{-4.5} \pm 5.2$	$1.24 \pm 0.18 \pm 0.33$	$194^{+13}_{-12} \pm 15$	197
	300–400	$26.8 \pm 2.6 \pm 5.7$	$7.6^{+2.2}_{-1.7} \pm 2.4$	$0.09 \pm 0.04 \pm 0.03$	$34.6^{+3.4}_{-3.1} \pm 6.3$	44
	≥ 400	$1.40 \pm 0.44 \pm 0.57$	$1.02^{+0.29}_{-0.23} \pm 0.46$	< 0.01	$2.42^{+0.53}_{-0.49} \pm 0.73$	3
$\geq$ 7j, $\geq$ 3b	200–300	$55.4^{+4.8}_{-4.7} \pm 7.3$	$2.3^{+0.7}_{-0.5} \pm 1.1$	$0.15 \pm 0.06 \pm 0.06$	$57.8^{+4.8}_{-4.7} \pm 7.4$	37
	300–400	$6.4 \pm 1.2 \pm 1.5$	$0.86^{+0.25}_{-0.20} \pm 0.46$	$0.01 \pm 0.01 \pm 0.00$	$7.3 \pm 1.2 \pm 1.6$	9
	≥ 400	$0.06 \pm 0.01 \pm 0.03$	$0.12 \pm 0.03 \pm 0.06$	< 0.01	$0.18^{+0.04}_{-0.03} \pm 0.07$	0

Table 16 Predictions and observations for the 21 search regions with $575 \leq H_T < 1200$ GeV and $2 \leq N_j \leq 3$. For each of the background predictions, the first uncertainty listed is statistical (from the limited size of data control samples and Monte Carlo samples), and the second is systematic

N_j, N_b	M_{T2} (GeV)	Lost lepton	$Z \to \nu\bar{\nu}$	Multijet	Total background	Data
$575 \leq H_T < 1200$ GeV:						
2-3j, 0b	200–300	$5270 \pm 60 \pm 370$	$11\,550 \pm 160 \pm 790$	$93 \pm 20 \pm 30$	$16\,900 \pm 200 \pm 1100$	17 256
	300–400	$2560 \pm 50 \pm 180$	$7770^{+110}_{-100} \pm 540$	$11.9 \pm 1.3 \pm 4.4$	$10\,340^{+120}_{-110} \pm 680$	10 145
	400–500	$1101^{+32}_{-31} \pm 77$	$3900 \pm 50 \pm 280$	$1.33 \pm 0.24 \pm 0.41$	$5000 \pm 60 \pm 340$	5021
	500–600	$502^{+24}_{-23} \pm 35$	$2250 \pm 30 \pm 170$	$0.37 \pm 0.07 \pm 0.12$	$2760 \pm 40 \pm 200$	2706
	600–700	$180^{+16}_{-15} \pm 13$	$746 \pm 10 \pm 73$	$0.09 \pm 0.03 \pm 0.03$	$926^{+19}_{-18} \pm 80$	1066
	700–800	$52.1^{+7.3}_{-6.5} \pm 5.5$	$256 \pm 3 \pm 36$	$0.01 \pm 0.01 \pm 0.00$	$308^{+8}_{-7} \pm 38$	347
	800–900	$17.7^{+2.6}_{-2.3} \pm 2.2$	$107 \pm 1 \pm 20$	< 0.01	$125 \pm 3 \pm 21$	111
	900–1000	$6.0 \pm 0.9 \pm 1.3$	$39.4 \pm 0.5 \pm 8.5$	$0.01 \pm 0.01 \pm 0.00$	$45.4^{+1.1}_{-1.0} \pm 8.7$	39
	1000–1100	$3.3^{+1.1}_{-1.0} \pm 1.0$	$13.3 \pm 0.2 \pm 3.9$	< 0.01	$16.6 \pm 1.1 \pm 4.1$	11
	≥ 1100	$0.31^{+0.09}_{-0.08} \pm 0.12$	$2.5 \pm 0.0 \pm 1.1$	< 0.01	$2.8 \pm 0.1 \pm 1.1$	2
2-3j, 1b	200–300	$826^{+27}_{-26} \pm 54$	$1480^{+60}_{-50} \pm 100$	$38 \pm 15 \pm 12$	$2340 \pm 60 \pm 140$	2499
	300–400	$426^{+21}_{-20} \pm 28$	$994^{+38}_{-37} \pm 69$	$2.33 \pm 0.26 \pm 0.84$	$1422^{+43}_{-42} \pm 90$	1366
	400–600	$282^{+18}_{-17} \pm 20$	$788^{+30}_{-29} \pm 55$	$0.27 \pm 0.06 \pm 0.10$	$1071^{+35}_{-34} \pm 69$	1057
	600–800	$43.5^{+3.2}_{-3.1} \pm 6.5$	$129 \pm 5 \pm 12$	< 0.01	$172 \pm 6 \pm 15$	225
	800–1000	$4.6 \pm 0.7 \pm 1.3$	$18.8 \pm 0.7 \pm 3.3$	< 0.01	$23.4 \pm 1.0 \pm 3.6$	22
	≥ 1000	$0.34 \pm 0.08 \pm 0.14$	$2.05 \pm 0.08 \pm 0.90$	< 0.01	$2.38 \pm 0.11 \pm 0.91$	1
2-3j, 2b	200–300	$105.1^{+9.2}_{-8.7} \pm 7.6$	$181^{+20}_{-18} \pm 15$	$3.8 \pm 0.5 \pm 1.3$	$290^{+22}_{-20} \pm 20$	316
	300–400	$55.0^{+6.7}_{-6.3} \pm 7.5$	$122^{+14}_{-12} \pm 10$	$0.27 \pm 0.06 \pm 0.10$	$177^{+15}_{-14} \pm 14$	159
	400–600	$36.5^{+4.6}_{-4.3} \pm 5.5$	$97^{+11}_{-10} \pm 8$	$0.08 \pm 0.03 \pm 0.03$	$133^{+12}_{-11} \pm 11$	107
	600–800	$4.7 \pm 0.8 \pm 1.3$	$15.8^{+1.8}_{-1.6} \pm 1.6$	< 0.01	$20.6^{+1.9}_{-1.8} \pm 2.2$	21
	≥ 800	$0.59 \pm 0.19 \pm 0.24$	$2.56^{+0.29}_{-0.26} \pm 0.45$	< 0.01	$3.14^{+0.35}_{-0.32} \pm 0.52$	1

Table 17 Predictions and observations for the 26 search regions with $575 \leq H_T < 1200$ GeV, and $2 \leq N_j \leq 6$ and $N_b \geq 3$, or $4 \leq N_j \leq 6$. For each of the background predictions, the first uncertainty listed is statistical (from the limited size of data control samples and Monte Carlo samples), and the second is systematic

N_j, N_b	M_{T2} (GeV)	Lost lepton	$Z \to \nu\bar{\nu}$	Multijet	Total background	Data
$575 \leq H_T < 1200$ GeV:						
2-6j, $\geq$ 3b	200–300	$299^{+17}_{-16} \pm 22$	$73^{+15}_{-13} \pm 10$	$6.2 \pm 0.4 \pm 2.1$	$379^{+22}_{-21} \pm 28$	345
	300–400	$100 \pm 10 \pm 7$	$43.5^{+8.8}_{-7.4} \pm 6.2$	$0.68 \pm 0.09 \pm 0.24$	$144^{+14}_{-12} \pm 11$	132
	400–600	$32.5^{+6.3}_{-5.6} \pm 2.5$	$31.2^{+6.3}_{-5.3} \pm 4.4$	$0.08 \pm 0.03 \pm 0.03$	$63.8^{+8.9}_{-7.7} \pm 5.8$	48
	600–800	$3.16^{+0.95}_{-0.90} \pm 0.68$	$5.4^{+1.1}_{-0.9} \pm 0.8$	< 0.01	$8.6^{+1.4}_{-1.3} \pm 1.1$	4
	≥ 800	$0.10 \pm 0.03 \pm 0.04$	$0.71^{+0.14}_{-0.12} \pm 0.15$	< 0.01	$0.81^{+0.15}_{-0.12} \pm 0.16$	0
4-6j, 0b	200–300	$6280 \pm 70 \pm 420$	$9470 \pm 160 \pm 650$	$360 \pm 20 \pm 110$	$16\,100 \pm 180 \pm 1000$	16 292
	300–400	$2700 \pm 50 \pm 180$	$5410 \pm 90 \pm 380$	$53 \pm 1 \pm 17$	$8160 \pm 100 \pm 520$	8330
	400–500	$927^{+28}_{-27} \pm 62$	$2420 \pm 40 \pm 180$	$7.7 \pm 0.4 \pm 2.4$	$3350 \pm 50 \pm 230$	3576
	500–600	$324^{+17}_{-16} \pm 22$	$1171^{+20}_{-19} \pm 100$	$1.46 \pm 0.12 \pm 0.46$	$1500 \pm 30 \pm 110$	1516
	600–700	$95.4^{+9.4}_{-8.7} \pm 6.4$	$413 \pm 7 \pm 47$	$0.33 \pm 0.06 \pm 0.10$	$509^{+12}_{-11} \pm 50$	543
	700–800	$35.6^{+5.0}_{-4.5} \pm 3.6$	$171 \pm 3 \pm 27$	$0.03 \pm 0.02 \pm 0.01$	$206^{+6}_{-5} \pm 27$	178
	800–900	$13.4^{+2.0}_{-1.8} \pm 1.6$	$64 \pm 1 \pm 11$	$0.02 \pm 0.01 \pm 0.01$	$77 \pm 2 \pm 11$	62

Table 17 continued

N_j, N_b	M_{T2} (GeV)	Lost lepton	$Z \to \nu\bar{\nu}$	Multijet	Total background	Data
	900–1000	$4.39^{+0.78}_{-0.73} \pm 0.93$	$23.6 \pm 0.4 \pm 5.3$	< 0.01	$28.0^{+0.9}_{-0.8} \pm 5.4$	20
	1000–1100	$0.64 \pm 0.16 \pm 0.20$	$6.3 \pm 0.1 \pm 2.0$	< 0.01	$6.9 \pm 0.2 \pm 2.0$	3
	≥ 1100	$0.78 \pm 0.58 \pm 0.32$	$0.89^{+0.02}_{-0.01} \pm 0.40$	< 0.01	$1.68 \pm 0.58 \pm 0.52$	1
4-6j, 1b	200–300	$2900 \pm 50 \pm 200$	$2220^{+80}_{-70} \pm 150$	$154 \pm 16 \pm 50$	$5270 \pm 90 \pm 330$	5335
	300–400	$1066 \pm 29 \pm 74$	$1267^{+44}_{-42} \pm 89$	$19.2 \pm 0.9 \pm 6.2$	$2350 \pm 50 \pm 150$	2547
	400–600	$504^{+22}_{-21} \pm 35$	$840^{+29}_{-28} \pm 61$	$2.98 \pm 0.21 \pm 0.93$	$1347^{+36}_{-35} \pm 88$	1284
	600–800	$35.3^{+5.9}_{-5.2} \pm 2.6$	$138 \pm 5 \pm 14$	$0.09 \pm 0.03 \pm 0.03$	$174^{+8}_{-7} \pm 16$	151
	800–1000	$3.89^{+0.83}_{-0.77} \pm 0.82$	$19.3^{+0.7}_{-0.6} \pm 4.3$	$0.01 \pm 0.01 \pm 0.00$	$23.2^{+1.1}_{-1.0} \pm 4.5$	18
	≥ 1000	$0.18 \pm 0.07 \pm 0.07$	$1.57 \pm 0.05 \pm 0.65$	< 0.01	$1.75 \pm 0.09 \pm 0.65$	1
4-6j, 2b	200–300	$1500 \pm 30 \pm 100$	$473^{+36}_{-33} \pm 36$	$42 \pm 2 \pm 13$	$2020 \pm 50 \pm 130$	1968
	300–400	$508 \pm 20 \pm 35$	$270^{+20}_{-19} \pm 21$	$4.9 \pm 0.3 \pm 1.6$	$783^{+29}_{-28} \pm 50$	788
	400–600	$167 \pm 12 \pm 12$	$179^{+14}_{-13} \pm 14$	$0.57 \pm 0.08 \pm 0.18$	$346^{+18}_{-17} \pm 23$	354
	600–800	$11.9^{+1.3}_{-1.2} \pm 2.5$	$29.5^{+2.2}_{-2.1} \pm 3.5$	$0.02 \pm 0.01 \pm 0.01$	$41.4^{+2.6}_{-2.4} \pm 4.6$	37
	≥ 800	$0.91 \pm 0.23 \pm 0.37$	$4.4 \pm 0.3 \pm 1.8$	< 0.01	$5.4 \pm 0.4 \pm 1.9$	7

Table 18 Predictions and observations for the 34 search regions with $575 \leq H_T < 1200$ GeV, and $7 \leq N_j \leq 9$, or $N_j \geq 10$. For each of the background predictions, the first uncertainty listed is statistical (from the limited size of data control samples and Monte Carlo samples), and the second is systematic

N_j, N_b	M_{T2} (GeV)	Lost lepton	$Z \to \nu\bar{\nu}$	Multijet	Total background	Data
$575 \leq H_T < 1200$ GeV:						
7-9j, 0b	200–300	$589^{+27}_{-26} \pm 39$	$573^{+47}_{-43} \pm 64$	$90 \pm 10 \pm 28$	$1252^{+55}_{-52} \pm 93$	1340
	300–400	$265^{+19}_{-18} \pm 18$	$279^{+23}_{-21} \pm 42$	$14.9 \pm 0.5 \pm 4.7$	$559^{+29}_{-28} \pm 51$	581
	400–600	$92^{+10}_{-9} \pm 6$	$159^{+13}_{-12} \pm 28$	$2.72 \pm 0.18 \pm 0.85$	$253^{+16}_{-15} \pm 30$	243
	600–800	$8.6 \pm 1.2 \pm 1.8$	$22.8^{+1.9}_{-1.7} \pm 6.4$	$0.10 \pm 0.03 \pm 0.03$	$31.6^{+2.2}_{-2.1} \pm 6.8$	32
	≥ 800	$0.51 \pm 0.16 \pm 0.21$	$3.0 \pm 0.2 \pm 1.3$	< 0.01	$3.5 \pm 0.3 \pm 1.3$	2
7-9j, 1b	200–300	$733 \pm 21 \pm 52$	$278^{+28}_{-25} \pm 33$	$48 \pm 3 \pm 16$	$1059^{+35}_{-33} \pm 73$	1052
	300–400	$252^{+13}_{-12} \pm 18$	$135^{+14}_{-12} \pm 21$	$7.7 \pm 0.4 \pm 2.5$	$395^{+19}_{-17} \pm 32$	387
	400–600	$71.3^{+6.9}_{-6.5} \pm 5.2$	$77^{+8}_{-7} \pm 14$	$1.36 \pm 0.13 \pm 0.45$	$150 \pm 10 \pm 16$	131
	600–800	$4.26^{+0.73}_{-0.71} \pm 0.90$	$11.0^{+1.1}_{-1.0} \pm 3.1$	$0.03 \pm 0.02 \pm 0.01$	$15.3^{+1.3}_{-1.2} \pm 3.3$	20
	≥ 800	$0.11 \pm 0.04 \pm 0.05$	$1.48^{+0.15}_{-0.13} \pm 0.63$	< 0.01	$1.60^{+0.15}_{-0.14} \pm 0.63$	1
7-9j, 2b	200–300	$675 \pm 20 \pm 51$	$82^{+8}_{-7} \pm 10$	$20.9 \pm 3.0 \pm 6.7$	$777^{+22}_{-21} \pm 56$	750
	300–400	$211 \pm 11 \pm 16$	$39.8^{+4.0}_{-3.6} \pm 6.4$	$2.42 \pm 0.19 \pm 0.79$	$253^{+12}_{-11} \pm 19$	259
	400–600	$55.4^{+5.5}_{-5.2} \pm 4.2$	$22.7^{+2.3}_{-2.1} \pm 4.2$	$0.50 \pm 0.07 \pm 0.16$	$78.6^{+5.9}_{-5.6} \pm 6.6$	72
	600–800	$3.00^{+0.63}_{-0.62} \pm 0.64$	$3.25^{+0.32}_{-0.30} \pm 0.93$	$0.01 \pm 0.01 \pm 0.01$	$6.3 \pm 0.7 \pm 1.2$	7
	≥ 800	$0.27 \pm 0.20 \pm 0.11$	$0.44 \pm 0.04 \pm 0.19$	< 0.01	$0.71 \pm 0.20 \pm 0.22$	1
7-9j, 3b	200–300	$185 \pm 8 \pm 18$	$11.3^{+1.1}_{-1.0} \pm 1.9$	$3.6 \pm 0.2 \pm 1.2$	$200 \pm 8 \pm 18$	184
	300–400	$52.0 \pm 3.8 \pm 5.0$	$5.5 \pm 0.5 \pm 1.2$	$0.72 \pm 0.12 \pm 0.26$	$58.3^{+3.9}_{-3.8} \pm 5.3$	59
	400–600	$13.6 \pm 1.8 \pm 1.3$	$3.13^{+0.31}_{-0.29} \pm 0.82$	$0.05 \pm 0.02 \pm 0.02$	$16.8 \pm 1.8 \pm 1.6$	14
	≥ 600	$0.49 \pm 0.21 \pm 0.20$	$0.51 \pm 0.05 \pm 0.21$	< 0.01	$1.00 \pm 0.21 \pm 0.29$	2

Table 18 continued

N_j, N_b	M_{T2} (GeV)	Lost lepton	$Z \to \nu\bar{\nu}$	Multijet	Total background	Data
7-9j, $\geq$ 4b	200–300	$38.8 \pm 3.1 \pm 7.4$	$2.01^{+0.20}_{-0.18} \pm 0.71$	$0.55 \pm 0.08 \pm 0.19$	$41.3^{+3.2}_{-3.1} \pm 7.4$	38
	300–400	$14.5^{+2.0}_{-1.9} \pm 2.8$	$0.98^{+0.10}_{-0.09} \pm 0.43$	$0.06 \pm 0.02 \pm 0.02$	$15.6^{+2.0}_{-1.9} \pm 2.8$	16
	$\geq$ 400	$3.75^{+0.98}_{-0.97} \pm 0.70$	$0.65 \pm 0.06 \pm 0.35$	< 0.01	$4.40^{+0.98}_{-0.97} \pm 0.79$	3
$\geq$ 10j, 0b	200–300	$11.5 \pm 1.6 \pm 1.0$	$4.4^{+0.4}_{-0.3} \pm 2.3$	$3.1 \pm 0.8 \pm 1.1$	$19.0 \pm 1.8 \pm 2.8$	27
	300–500	$5.6 \pm 1.0 \pm 0.5$	$3.0 \pm 0.2 \pm 1.7$	$0.55 \pm 0.08 \pm 0.20$	$9.1 \pm 1.0 \pm 1.8$	4
	$\geq$ 500	$0.30 \pm 0.11 \pm 0.12$	$0.44^{+0.04}_{-0.03} \pm 0.24$	$0.02 \pm 0.01 \pm 0.01$	$0.76 \pm 0.11 \pm 0.27$	3
$\geq$ 10j, 1b	200–300	$21.0 \pm 1.8 \pm 1.6$	$3.5 \pm 0.3 \pm 1.9$	$1.92 \pm 0.18 \pm 0.72$	$26.4 \pm 1.8 \pm 2.7$	32
	300–500	$7.7 \pm 1.0 \pm 0.6$	$2.4 \pm 0.2 \pm 1.4$	$0.45 \pm 0.07 \pm 0.17$	$10.5 \pm 1.1 \pm 1.6$	15
	$\geq$ 500	$0.83^{+0.42}_{-0.41} \pm 0.07$	$0.36^{+0.04}_{-0.03} \pm 0.20$	$0.02 \pm 0.01 \pm 0.01$	$1.20^{+0.42}_{-0.41} \pm 0.22$	0
$\geq$ 10j, 2b	200–300	$21.8 \pm 1.8 \pm 1.6$	$1.05 \pm 0.10 \pm 0.66$	$0.64 \pm 0.08 \pm 0.24$	$23.5 \pm 1.8 \pm 1.8$	26
	300–500	$8.8 \pm 1.2 \pm 0.6$	$0.69^{+0.07}_{-0.06} \pm 0.45$	$0.16 \pm 0.04 \pm 0.06$	$9.6^{+1.3}_{-1.2} \pm 0.8$	9
	$\geq$ 500	$0.22 \pm 0.13 \pm 0.02$	$0.10 \pm 0.01 \pm 0.06$	< 0.01	$0.32 \pm 0.13 \pm 0.07$	0
$\geq$ 10j, 3b	200–300	$9.9 \pm 1.3 \pm 1.2$	$0.25 \pm 0.02 \pm 0.20$	$0.29 \pm 0.05 \pm 0.12$	$10.4 \pm 1.3 \pm 1.2$	14
	$\geq$ 300	$1.59 \pm 0.50 \pm 0.18$	$0.19 \pm 0.02 \pm 0.16$	$0.02 \pm 0.01 \pm 0.01$	$1.80 \pm 0.50 \pm 0.25$	2
$\geq$ 10j, $\geq$ 4b	$\geq$ 200	$3.9 \pm 1.2 \pm 0.8$	$0.00^{+0.17}_{-0.00} \pm 0.00$	$0.05 \pm 0.02 \pm 0.02$	$4.0 \pm 1.2 \pm 0.8$	6

Table 19 Predictions and observations for the 17 search regions with $1200 \leq H_T < 1500$ GeV and $2 \leq N_j \leq 3$. For each of the background predictions, the first uncertainty listed is statistical (from the limited size of data control samples and Monte Carlo samples), and the second is systematic

N_j, N_b	M_{T2} (GeV)	Lost lepton	$Z \to \nu\bar{\nu}$	Multijet	Total background	Data
$1200 \leq H_T < 1500$ GeV:						
2-3j, 0b	200–400	$315 \pm 15 \pm 21$	$656^{+51}_{-47} \pm 73$	$39 \pm 16 \pm 12$	$1009^{+55}_{-52} \pm 85$	1128
	400–600	$43.0^{+5.2}_{-4.7} \pm 4.9$	$185^{+14}_{-13} \pm 30$	$0.03 \pm 0.02 \pm 0.01$	$228^{+15}_{-14} \pm 31$	207
	600–800	$14.1^{+2.1}_{-2.0} \pm 1.7$	$64 \pm 5 \pm 17$	< 0.01	$78 \pm 5 \pm 17$	83
	800–1000	$6.4^{+1.1}_{-1.0} \pm 1.3$	$32.5^{+2.5}_{-2.3} \pm 7.6$	< 0.01	$38.9^{+2.7}_{-2.5} \pm 7.8$	36
	1000–1200	$3.23^{+0.61}_{-0.59} \pm 0.99$	$17.5 \pm 1.3 \pm 5.2$	< 0.01	$20.7^{+1.5}_{-1.4} \pm 5.3$	19
	$\geq$ 1200	$0.87^{+0.14}_{-0.13} \pm 0.35$	$6.0^{+0.5}_{-0.4} \pm 2.6$	< 0.01	$6.9 \pm 0.5 \pm 2.6$	4
2-3j, 1b	200–400	$61.5^{+7.2}_{-6.5} \pm 4.2$	$78^{+19}_{-16} \pm 10$	$9.7 \pm 0.7 \pm 3.0$	$149^{+21}_{-17} \pm 12$	157
	400–600	$10.1 \pm 1.4 \pm 1.0$	$21.9^{+5.4}_{-4.4} \pm 3.8$	$0.03 \pm 0.02 \pm 0.01$	$32.0^{+5.6}_{-4.6} \pm 4.1$	27
	600–800	$2.36^{+0.36}_{-0.35} \pm 0.41$	$7.5^{+1.9}_{-1.5} \pm 2.0$	< 0.01	$9.8^{+1.9}_{-1.6} \pm 2.1$	9
	800–1000	$0.78^{+0.16}_{-0.15} \pm 0.19$	$3.84^{+0.95}_{-0.78} \pm 0.93$	< 0.01	$4.62^{+0.97}_{-0.79} \pm 0.96$	6
	1000–1200	$0.43 \pm 0.08 \pm 0.14$	$2.13^{+0.53}_{-0.43} \pm 0.64$	< 0.01	$2.56^{+0.54}_{-0.44} \pm 0.66$	2
	$\geq$ 1200	$0.14^{+0.05}_{-0.04} \pm 0.06$	$0.71^{+0.18}_{-0.14} \pm 0.31$	< 0.01	$0.86^{+0.18}_{-0.15} \pm 0.31$	0
2-3j, 2b	200–400	$4.8^{+2.0}_{-1.6} \pm 0.3$	$11^{+11}_{-6} \pm 2$	$1.38 \pm 0.13 \pm 0.43$	$18^{+11}_{-6} \pm 2$	18
	400–600	$0.61^{+0.30}_{-0.25} \pm 0.07$	$3.2^{+3.1}_{-1.7} \pm 0.7$	< 0.01	$3.8^{+3.1}_{-1.8} \pm 0.7$	5
	600–800	$0.21^{+0.11}_{-0.09} \pm 0.04$	$1.1^{+1.1}_{-0.6} \pm 0.4$	< 0.01	$1.3^{+1.1}_{-0.6} \pm 0.4$	2
	800–1000	$0.07^{+0.04}_{-0.03} \pm 0.02$	$0.56^{+0.55}_{-0.31} \pm 0.18$	< 0.01	$0.63^{+0.55}_{-0.31} \pm 0.18$	1
	$\geq$ 1000	$0.03 \pm 0.02 \pm 0.01$	$0.42^{+0.41}_{-0.23} \pm 0.18$	< 0.01	$0.46^{+0.41}_{-0.23} \pm 0.18$	1

Table 20 Predictions and observations for the 20 search regions with $1200 \leq H_T < 1500$ GeV, and $2 \leq N_j \leq 6$ and $N_b \geq 3$, or $4 \leq N_j \leq 6$. For each of the background predictions, the first uncertainty listed is sta-
tistical (from the limited size of data control samples and Monte Carlo samples), and the second is systematic

N_j, N_b	M_{T2} (GeV)	Lost lepton	$Z \to \nu\bar{\nu}$	Multijet	Total background	Data
$1200 \leq H_T < 1500$ GeV:						
2-6j, $\geq$ 3b	200–400	$22.6^{+4.7}_{-4.2} \pm 1.8$	$0.0^{+6.6}_{-0.0} \pm 0.0$	$4.4 \pm 0.2 \pm 1.5$	$27.0^{+8.1}_{-4.2} \pm 2.4$	25
	400–600	$1.58^{+0.51}_{-0.48} \pm 0.34$	$0.0^{+1.6}_{-0.0} \pm 0.0$	$0.02 \pm 0.01 \pm 0.01$	$1.6^{+1.7}_{-0.5} \pm 0.3$	3
	$\geq$ 600	$0.47^{+0.27}_{-0.26} \pm 0.19$	$0.00^{+0.94}_{-0.00} \pm 0.00$	< 0.01	$0.47^{+0.98}_{-0.26} \pm 0.19$	4
4-6j, 0b	200–400	$606^{+21}_{-20} \pm 41$	$909^{+63}_{-59} \pm 90$	$208 \pm 12 \pm 64$	$1720^{+70}_{-60} \pm 130$	1768
	400–600	$84.3^{+7.4}_{-6.9} \pm 5.8$	$234^{+16}_{-15} \pm 34$	$0.88 \pm 0.09 \pm 0.27$	$319^{+18}_{-17} \pm 36$	301
	600–800	$21.1^{+3.2}_{-2.9} \pm 2.3$	$75 \pm 5 \pm 17$	$0.06 \pm 0.02 \pm 0.02$	$96 \pm 6 \pm 17$	99
	800–1000	$7.6^{+1.2}_{-1.1} \pm 1.1$	$35.2^{+2.4}_{-2.3} \pm 8.0$	$0.01 \pm 0.01 \pm 0.00$	$42.7^{+2.7}_{-2.3} \pm 8.2$	41
	1000–1200	$2.23^{+0.36}_{-0.33} \pm 0.61$	$14.1^{+1.0}_{-0.9} \pm 4.2$	< 0.01	$16.3 \pm 1.0 \pm 4.2$	15
	$\geq$ 1200	$0.47^{+0.10}_{-0.09} \pm 0.19$	$3.0 \pm 0.2 \pm 1.3$	< 0.01	$3.5 \pm 0.2 \pm 1.3$	5
4-6j, 1b	200–400	$278^{+15}_{-14} \pm 20$	$254^{+33}_{-30} \pm 28$	$97 \pm 2 \pm 30$	$629^{+36}_{-33} \pm 50$	579
	400–600	$30.3^{+4.0}_{-3.7} \pm 2.7$	$65^{+9}_{-8} \pm 10$	$0.33 \pm 0.06 \pm 0.10$	$96^{+9}_{-8} \pm 11$	79
	600–800	$8.2^{+1.4}_{-1.3} \pm 1.0$	$21.0^{+2.8}_{-2.5} \pm 4.8$	$0.02 \pm 0.01 \pm 0.01$	$29.2^{+3.1}_{-2.8} \pm 5.0$	16
	800–1000	$2.36^{+0.56}_{-0.54} \pm 0.50$	$9.8^{+1.3}_{-1.1} \pm 2.3$	$0.01 \pm 0.01 \pm 0.00$	$12.2^{+1.4}_{-1.3} \pm 2.4$	9
	1000–1200	$1.00 \pm 0.24 \pm 0.31$	$4.0 \pm 0.5 \pm 1.2$	< 0.01	$5.0^{+0.6}_{-0.5} \pm 1.2$	6
	$\geq$ 1200	$0.07 \pm 0.02 \pm 0.03$	$0.86^{+0.11}_{-0.10} \pm 0.37$	< 0.01	$0.92^{+0.11}_{-0.10} \pm 0.37$	1
4-6j, 2b	200–400	$120.4^{+9.1}_{-8.7} \pm 9.8$	$45^{+18}_{-13} \pm 5$	$26.0 \pm 0.6 \pm 8.1$	$191^{+20}_{-16} \pm 15$	194
	400–600	$11.9 \pm 1.4 \pm 1.5$	$11.5^{+4.6}_{-3.4} \pm 1.8$	$0.11 \pm 0.03 \pm 0.04$	$23.4^{+4.8}_{-3.7} \pm 2.6$	27
	600–800	$3.49 \pm 0.83 \pm 0.75$	$3.7^{+1.5}_{-1.1} \pm 1.0$	< 0.01	$7.2^{+1.7}_{-1.4} \pm 1.3$	7
	800–1000	$0.66 \pm 0.16 \pm 0.20$	$1.73^{+0.69}_{-0.51} \pm 0.48$	< 0.01	$2.38^{+0.71}_{-0.54} \pm 0.53$	3
	$\geq$ 1000	$0.15 \pm 0.04 \pm 0.06$	$0.84^{+0.34}_{-0.25} \pm 0.36$	< 0.01	$1.00^{+0.34}_{-0.25} \pm 0.36$	0

Table 21 Predictions and observations for the 31 search regions with $1200 \leq H_T < 1500$ GeV, and $7 \leq N_j \leq 9$, or $N_j \geq 10$. For each of the background predictions, the first uncertainty listed is statistical (from
the limited size of data control samples and Monte Carlo samples), and the second is systematic

N_j, N_b	M_{T2} (GeV)	Lost lepton	$Z \to \nu\bar{\nu}$	Multijet	Total background	Data
$1200 \leq H_T < 1500$ GeV:						
7-9j, 0b	200–400	$120.4^{+9.8}_{-9.2} \pm 9.0$	$108^{+26}_{-21} \pm 21$	$91 \pm 3 \pm 29$	$319^{+28}_{-24} \pm 38$	379
	400–600	$16.5^{+1.9}_{-1.8} \pm 2.0$	$25.8^{+6.3}_{-5.1} \pm 5.7$	$0.80 \pm 0.09 \pm 0.25$	$43.1^{+6.5}_{-5.4} \pm 6.3$	45
	600–800	$2.94 \pm 0.42 \pm 0.63$	$8.6^{+2.1}_{-1.7} \pm 2.1$	$0.06 \pm 0.02 \pm 0.02$	$11.6^{+2.1}_{-1.8} \pm 2.2$	17
	800–1000	$0.77^{+0.14}_{-0.13} \pm 0.24$	$2.90^{+0.70}_{-0.58} \pm 1.00$	$0.01 \pm 0.01 \pm 0.00$	$3.7^{+0.7}_{-0.6} \pm 1.0$	3
	$\geq$ 1000	$0.11 \pm 0.03 \pm 0.05$	$1.09^{+0.26}_{-0.22} \pm 0.50$	< 0.01	$1.21^{+0.27}_{-0.22} \pm 0.50$	0
7-9j, 1b	200–400	$133.8^{+8.0}_{-7.7} \pm 9.8$	$36^{+13}_{-10} \pm 8$	$58 \pm 2 \pm 18$	$228^{+15}_{-13} \pm 23$	247
	400–600	$16.6^{+2.9}_{-2.7} \pm 1.3$	$8.7^{+3.2}_{-2.4} \pm 2.1$	$0.46 \pm 0.07 \pm 0.14$	$25.8^{+4.3}_{-3.6} \pm 2.7$	23
	600–800	$1.83^{+0.43}_{-0.41} \pm 0.28$	$2.9^{+1.1}_{-0.8} \pm 0.8$	$0.03 \pm 0.02 \pm 0.01$	$4.8^{+1.1}_{-0.9} \pm 0.8$	7
	800–1000	$0.65^{+0.24}_{-0.23} \pm 0.18$	$0.95^{+0.34}_{-0.26} \pm 0.34$	$0.02 \pm 0.01 \pm 0.01$	$1.62^{+0.42}_{-0.35} \pm 0.39$	2
	$\geq$ 1000	$0.22 \pm 0.19 \pm 0.09$	$0.36^{+0.13}_{-0.10} \pm 0.17$	< 0.01	$0.58^{+0.23}_{-0.21} \pm 0.19$	0
7-9j, 2b	200–400	$124.0^{+7.6}_{-7.4} \pm 9.1$	$9.9^{+3.6}_{-2.7} \pm 2.5$	$21.4 \pm 0.5 \pm 6.9$	$155 \pm 8 \pm 12$	162
	400–600	$15.0^{+2.8}_{-2.6} \pm 1.3$	$2.41^{+0.87}_{-0.66} \pm 0.67$	$0.12 \pm 0.03 \pm 0.04$	$17.5^{+3.0}_{-2.7} \pm 1.5$	18
	600–800	$2.47^{+0.78}_{-0.76} \pm 0.53$	$0.81^{+0.29}_{-0.22} \pm 0.26$	$0.01 \pm 0.01 \pm 0.00$	$3.29^{+0.83}_{-0.79} \pm 0.60$	1
	$\geq$ 800	$0.24 \pm 0.11 \pm 0.10$	$0.36^{+0.13}_{-0.10} \pm 0.16$	< 0.01	$0.60^{+0.17}_{-0.15} \pm 0.19$	1

Table 21 continued

N_j, N_b	M_{T2} (GeV)	Lost lepton	$Z \to \nu\bar{\nu}$	Multijet	Total background	Data
7-9j, 3b	200–400	$30.0 \pm 2.6 \pm 3.2$	$1.89^{+0.68}_{-0.52} \pm 0.64$	$5.0 \pm 0.3 \pm 1.8$	$36.9^{+2.7}_{-2.6} \pm 3.8$	46
	400–600	$4.1^{+1.1}_{-1.0} \pm 0.6$	$0.45^{+0.16}_{-0.12} \pm 0.18$	$0.02 \pm 0.01 \pm 0.01$	$4.6^{+1.1}_{-1.0} \pm 0.6$	2
	≥ 600	$0.92^{+0.50}_{-0.49} \pm 0.38$	$0.23^{+0.08}_{-0.06} \pm 0.11$	< 0.01	$1.15 \pm 0.50 \pm 0.40$	1
7-9j, ≥ 4b	200–400	$9.1 \pm 1.6 \pm 1.8$	$0.26^{+0.10}_{-0.07} \pm 0.23$	$0.88 \pm 0.10 \pm 0.32$	$10.3 \pm 1.6 \pm 1.9$	9
	≥ 400	$0.44^{+0.24}_{-0.23} \pm 0.08$	$0.10^{+0.04}_{-0.03} \pm 0.09$	< 0.01	$0.53 \pm 0.24 \pm 0.12$	0
≥ 10j, 0b	200–400	$7.7^{+1.2}_{-1.1} \pm 0.8$	$2.7^{+0.6}_{-0.5} \pm 2.8$	$8.3 \pm 0.9 \pm 3.0$	$18.7^{+1.6}_{-1.5} \pm 4.1$	17
	400–600	$1.00 \pm 0.32 \pm 0.22$	$0.56^{+0.13}_{-0.11} \pm 0.62$	$0.11 \pm 0.03 \pm 0.04$	$1.66^{+0.35}_{-0.34} \pm 0.66$	1
	≥ 600	$0.10^{+0.35}_{-0.04} \pm 0.04$	$0.14^{+0.08}_{-0.03} \pm 0.14$	$0.01 \pm 0.01 \pm 0.00$	$0.24^{+0.36}_{-0.05} \pm 0.15$	0
≥ 10j, 1b	200–400	$15.2 \pm 1.8 \pm 1.4$	$1.1^{+0.4}_{-0.3} \pm 1.2$	$5.3 \pm 0.2 \pm 1.9$	$21.6^{+1.9}_{-1.8} \pm 2.7$	22
	400–600	$1.27^{+0.38}_{-0.36} \pm 0.11$	$0.22^{+0.08}_{-0.06} \pm 0.26$	$0.05 \pm 0.02 \pm 0.02$	$1.55^{+0.39}_{-0.37} \pm 0.29$	6
	≥ 600	$0.03 \pm 0.02 \pm 0.01$	$0.05^{+0.10}_{-0.01} \pm 0.05$	< 0.01	$0.07^{+0.11}_{-0.02} \pm 0.05$	0
≥ 10j, 2b	200–400	$16.9 \pm 1.8 \pm 1.5$	$0.44^{+0.16}_{-0.12} \pm 0.50$	$2.7 \pm 0.2 \pm 1.0$	$20.1 \pm 1.8 \pm 1.9$	16
	400–600	$2.62^{+0.71}_{-0.68} \pm 0.30$	$0.09 \pm 0.03 \pm 0.11$	$0.01 \pm 0.01 \pm 0.00$	$2.73^{+0.71}_{-0.68} \pm 0.32$	2
	≥ 600	$0.23 \pm 0.15 \pm 0.10$	$0.02^{+0.08}_{-0.01} \pm 0.02$	< 0.01	$0.25^{+0.17}_{-0.15} \pm 0.10$	0
≥ 10j, 3b	200–400	$5.58^{+0.86}_{-0.85} \pm 0.61$	$0.12^{+0.11}_{-0.03} \pm 0.16$	$1.04 \pm 0.10 \pm 0.42$	$6.74^{+0.87}_{-0.86} \pm 0.76$	6
	≥ 400	$0.51 \pm 0.22 \pm 0.06$	$0.03^{+0.11}_{-0.01} \pm 0.04$	< 0.01	$0.54^{+0.25}_{-0.22} \pm 0.08$	0
≥ 10j, ≥ 4b	≥ 200	$2.59 \pm 0.82 \pm 0.62$	$0.10^{+0.13}_{-0.03} \pm 0.13$	$0.31 \pm 0.06 \pm 0.13$	$3.00^{+0.83}_{-0.82} \pm 0.65$	7

Table 22 Predictions and observations for the 30 search regions with $H_T \geq 1500$ GeV, and $2 \leq N_j \leq 3$, $2 \leq N_j \leq 6$ and $N_b \geq 3$, or $4 \leq N_j \leq 6$. For each of the background predictions, the first uncertainty listed is statistical (from the limited size of data control samples and Monte Carlo samples), and the second is systematic

N_j, N_b	M_{T2} (GeV)	Lost lepton	$Z \to \nu\bar{\nu}$	Multijet	Total background	Data
$H_T \geq 1500$ GeV:						
2-3j, 0b	400–600	$27.2^{+4.4}_{-3.9} \pm 2.5$	$150^{+14}_{-13} \pm 19$	$0.16 \pm 0.04 \pm 0.05$	$177^{+15}_{-13} \pm 20$	125
	600–800	$7.8^{+1.4}_{-1.2} \pm 0.8$	$38.7^{+3.6}_{-3.3} \pm 8.4$	< 0.01	$46.5^{+3.9}_{-3.6} \pm 8.6$	37
	800–1000	$2.29^{+0.39}_{-0.34} \pm 0.35$	$17.2^{+1.6}_{-1.5} \pm 3.4$	< 0.01	$19.5^{+1.7}_{-1.5} \pm 3.4$	19
	1000–1200	$1.20^{+0.21}_{-0.19} \pm 0.26$	$9.0 \pm 0.8 \pm 1.8$	< 0.01	$10.2^{+0.9}_{-0.8} \pm 1.9$	14
	1200–1400	$0.80^{+0.16}_{-0.14} \pm 0.22$	$4.9^{+0.5}_{-0.4} \pm 1.3$	< 0.01	$5.7^{+0.5}_{-0.4} \pm 1.4$	4
	1400–1800	$0.43^{+0.09}_{-0.08} \pm 0.15$	$2.80^{+0.26}_{-0.24} \pm 0.98$	< 0.01	$3.23^{+0.28}_{-0.26} \pm 0.99$	3
	≥ 1800	$0.05 \pm 0.02 \pm 0.02$	$0.41^{+0.04}_{-0.03} \pm 0.19$	< 0.01	$0.46 \pm 0.04 \pm 0.19$	0
2-3j, 1b	400–600	$5.2^{+1.1}_{-1.0} \pm 0.6$	$13.4^{+4.9}_{-3.7} \pm 1.9$	$0.09 \pm 0.03 \pm 0.03$	$18.7^{+5.0}_{-3.8} \pm 2.1$	23
	600–800	$1.52^{+0.43}_{-0.41} \pm 0.27$	$3.5^{+1.3}_{-1.0} \pm 1.0$	< 0.01	$5.0^{+1.3}_{-1.0} \pm 1.0$	3
	800–1000	$0.38 \pm 0.09 \pm 0.10$	$1.53^{+0.55}_{-0.42} \pm 0.35$	< 0.01	$1.90^{+0.56}_{-0.43} \pm 0.37$	3
	1000–1200	$0.10 \pm 0.03 \pm 0.03$	$0.81^{+0.29}_{-0.22} \pm 0.24$	< 0.01	$0.91^{+0.29}_{-0.22} \pm 0.24$	4
	≥ 1200	$0.19 \pm 0.06 \pm 0.08$	$0.73^{+0.26}_{-0.20} \pm 0.31$	< 0.01	$0.92^{+0.27}_{-0.21} \pm 0.32$	0
2-3j, 2b	≥ 400	$0.63^{+0.49}_{-0.36} \pm 0.26$	$0.0^{+3.0}_{-0.0} \pm 0.0$	< 0.01	$0.6^{+3.0}_{-0.4} \pm 0.3$	2
2-6j, ≥ 3b	400–600	$1.72^{+0.73}_{-0.68} \pm 0.42$	$1.1^{+2.4}_{-0.9} \pm 0.3$	$0.03 \pm 0.02 \pm 0.01$	$2.8^{+2.5}_{-1.1} \pm 0.6$	1
	≥ 600	$0.37^{+0.19}_{-0.18} \pm 0.16$	$0.5^{+1.2}_{-0.4} \pm 0.2$	< 0.01	$0.9^{+1.2}_{-0.5} \pm 0.2$	0

Table 22 continued

N_j, N_b	M_{T2} (GeV)	Lost lepton	$Z \to \nu\bar{\nu}$	Multijet	Total background	Data
4-6j, 0b	400–600	$46.4^{+5.6}_{-5.1} \pm 3.6$	$176^{+15}_{-14} \pm 23$	$1.62 \pm 0.13 \pm 0.46$	$224^{+16}_{-15} \pm 24$	207
	600–800	$10.6^{+2.3}_{-1.9} \pm 1.2$	$45.5^{+4.0}_{-3.7} \pm 9.9$	$0.07 \pm 0.03 \pm 0.02$	$56^{+5}_{-4} \pm 10$	62
	800–1000	$4.5^{+1.1}_{-1.0} \pm 0.5$	$20.3^{+1.8}_{-1.6} \pm 3.9$	< 0.01	$24.8^{+2.1}_{-1.9} \pm 4.1$	31
	1000–1200	$1.35^{+0.30}_{-0.26} \pm 0.24$	$10.6 \pm 0.9 \pm 2.1$	< 0.01	$11.9^{+1.0}_{-0.9} \pm 2.2$	12
	1200–1400	$0.89^{+0.27}_{-0.25} \pm 0.23$	$5.7 \pm 0.5 \pm 1.5$	< 0.01	$6.6^{+0.6}_{-0.5} \pm 1.6$	9
	1400–1600	$0.20 \pm 0.05 \pm 0.07$	$2.64^{+0.23}_{-0.21} \pm 0.92$	< 0.01	$2.84^{+0.24}_{-0.22} \pm 0.92$	3
	≥ 1600	$0.09 \pm 0.03 \pm 0.04$	$1.18 \pm 0.10 \pm 0.51$	< 0.01	$1.27^{+0.11}_{-0.10} \pm 0.51$	2
4-6j, 1b	400–600	$21.0^{+3.7}_{-3.3} \pm 2.0$	$32.6^{+7.0}_{-5.8} \pm 5.5$	$0.81 \pm 0.09 \pm 0.23$	$54.5^{+7.9}_{-6.7} \pm 6.3$	72
	600–800	$4.79^{+0.91}_{-0.83} \pm 0.62$	$8.4^{+1.8}_{-1.5} \pm 2.3$	$0.02 \pm 0.01 \pm 0.01$	$13.2^{+2.0}_{-1.7} \pm 2.5$	20
	800–1000	$1.27^{+0.26}_{-0.24} \pm 0.27$	$3.71^{+0.79}_{-0.66} \pm 0.92$	$0.03 \pm 0.02 \pm 0.01$	$5.01^{+0.84}_{-0.71} \pm 0.97$	8
	1000–1400	$0.89^{+0.21}_{-0.20} \pm 0.28$	$3.00^{+0.64}_{-0.54} \pm 0.93$	< 0.01	$3.89^{+0.68}_{-0.57} \pm 0.98$	6
	≥ 1400	$0.40^{+0.34}_{-0.33} \pm 0.16$	$0.72^{+0.15}_{-0.13} \pm 0.31$	< 0.01	$1.12^{+0.37}_{-0.36} \pm 0.36$	3
4-6j, 2b	400–600	$7.2^{+1.2}_{-1.1} \pm 1.1$	$4.3^{+2.9}_{-1.9} \pm 1.4$	$0.17 \pm 0.04 \pm 0.05$	$11.7^{+3.2}_{-2.2} \pm 1.9$	11
	600–800	$1.66^{+0.41}_{-0.40} \pm 0.46$	$1.12^{+0.76}_{-0.48} \pm 0.55$	$0.01 \pm 0.01 \pm 0.00$	$2.79^{+0.86}_{-0.63} \pm 0.73$	3
	≥ 800	$0.32 \pm 0.13 \pm 0.13$	$0.99^{+0.67}_{-0.43} \pm 0.52$	< 0.01	$1.31^{+0.68}_{-0.45} \pm 0.54$	4

Table 23 Predictions and observations for the 21 search regions with $H_T \geq 1500$ GeV, and $7 \leq N_j \leq 9$, or $N_j \geq 10$. For each of the background predictions, the first uncertainty listed is statistical (from the limited size of data control samples and Monte Carlo samples), and the second is systematic

N_j, N_b	M_{T2} (GeV)	Lost lepton	$Z \to \nu\bar{\nu}$	Multijet	Total background	*Data*
$H_T \geq 1500$ GeV:						
7-9j, 0b	400–600	$14.3^{+1.8}_{-1.7} \pm 1.7$	$32.3^{+7.5}_{-6.2} \pm 4.3$	$1.50 \pm 0.13 \pm 0.44$	$48.1^{+7.7}_{-6.4} \pm 5.0$	36
	600–800	$3.77^{+0.56}_{-0.55} \pm 0.69$	$8.3^{+1.9}_{-1.6} \pm 2.2$	$0.18 \pm 0.04 \pm 0.05$	$12.3^{+2.0}_{-1.7} \pm 2.3$	9
	800–1000	$1.16^{+0.18}_{-0.17} \pm 0.30$	$3.70^{+0.86}_{-0.71} \pm 0.83$	$0.01 \pm 0.01 \pm 0.00$	$4.86^{+0.88}_{-0.73} \pm 0.90$	6
	1000–1400	$0.58 \pm 0.11 \pm 0.19$	$2.96^{+0.69}_{-0.57} \pm 0.86$	$0.01 \pm 0.01 \pm 0.00$	$3.55^{+0.69}_{-0.58} \pm 0.89$	4
	≥ 1400	$0.05 \pm 0.01 \pm 0.02$	$0.71^{+0.17}_{-0.14} \pm 0.30$	< 0.01	$0.76^{+0.17}_{-0.14} \pm 0.30$	2
7-9j, 1b	400–600	$12.8^{+2.5}_{-2.3} \pm 1.6$	$9.2^{+4.2}_{-3.0} \pm 1.4$	$0.82 \pm 0.09 \pm 0.24$	$22.9^{+4.9}_{-3.8} \pm 2.3$	25
	600–800	$3.49^{+0.94}_{-0.89} \pm 0.76$	$2.4^{+1.1}_{-0.8} \pm 1.0$	$0.06 \pm 0.02 \pm 0.02$	$5.9^{+1.4}_{-1.2} \pm 1.2$	7
	≥ 800	$1.09^{+0.34}_{-0.32} \pm 0.45$	$2.10^{+0.96}_{-0.69} \pm 0.93$	< 0.01	$3.2^{+1.0}_{-0.8} \pm 1.0$	2
7-9j, 2b	400–600	$8.1^{+1.8}_{-1.6} \pm 1.0$	$2.4^{+1.1}_{-0.8} \pm 0.4$	$0.35 \pm 0.06 \pm 0.10$	$10.9^{+2.1}_{-1.8} \pm 1.2$	10
	600–800	$1.78^{+0.54}_{-0.52} \pm 0.40$	$0.62^{+0.28}_{-0.20} \pm 0.25$	$0.02 \pm 0.01 \pm 0.01$	$2.41^{+0.61}_{-0.56} \pm 0.49$	5
	≥ 800	$0.40^{+0.19}_{-0.18} \pm 0.17$	$0.55^{+0.25}_{-0.18} \pm 0.25$	$0.01 \pm 0.01 \pm 0.00$	$0.96^{+0.31}_{-0.26} \pm 0.30$	0
7-9j, 3b	400–800	$2.40^{+0.74}_{-0.72} \pm 0.29$	$0.32^{+0.15}_{-0.10} \pm 0.12$	$0.10 \pm 0.03 \pm 0.03$	$2.82^{+0.76}_{-0.72} \pm 0.32$	2
	≥ 800	$0.16 \pm 0.09 \pm 0.07$	$0.08^{+0.04}_{-0.03} \pm 0.04$	< 0.01	$0.24 \pm 0.09 \pm 0.08$	0
7-9j, $\geq 4b$	≥ 400	$0.52^{+0.23}_{-0.22} \pm 0.08$	$0.07^{+0.03}_{-0.02} \pm 0.06$	$0.02 \pm 0.01 \pm 0.01$	$0.61^{+0.23}_{-0.22} \pm 0.10$	1
$\geq 10j$, 0b	400–800	$1.41 \pm 0.38 \pm 0.33$	$1.52^{+0.35}_{-0.29} \pm 0.34$	$0.23 \pm 0.05 \pm 0.08$	$3.17^{+0.52}_{-0.48} \pm 0.49$	11
	≥ 800	$0.05 \pm 0.02 \pm 0.02$	$0.37^{+0.09}_{-0.07} \pm 0.17$	$0.01 \pm 0.01 \pm 0.00$	$0.43^{+0.09}_{-0.08} \pm 0.17$	0
$\geq 10j$, 1b	400–800	$2.16^{+0.71}_{-0.69} \pm 0.25$	$0.56^{+0.25}_{-0.18} \pm 0.16$	$0.14 \pm 0.04 \pm 0.05$	$2.85^{+0.76}_{-0.71} \pm 0.31$	3
	≥ 800	$0.55 \pm 0.30 \pm 0.22$	$0.13^{+0.06}_{-0.04} \pm 0.07$	< 0.01	$0.68^{+0.31}_{-0.30} \pm 0.23$	0
$\geq 10j$, 2b	≥ 400	$1.98^{+0.69}_{-0.67} \pm 0.24$	$0.30^{+0.14}_{-0.10} \pm 0.12$	$0.05 \pm 0.02 \pm 0.02$	$2.33^{+0.70}_{-0.68} \pm 0.28$	0
$\geq 10j$, 3b	≥ 400	$0.77 \pm 0.35 \pm 0.09$	$0.00^{+0.45}_{-0.00} \pm 0.00$	$0.05 \pm 0.03 \pm 0.02$	$0.82^{+0.57}_{-0.35} \pm 0.09$	1
$\geq 10j$, $\geq 4b$	≥ 400	$0.09 \pm 0.05 \pm 0.01$	$0.00^{+0.45}_{-0.00} \pm 0.00$	< 0.01	$0.09^{+0.45}_{-0.05} \pm 0.01$	0

Table 24 Summary of the 28 signal regions of the search for disappearing tracks, for the 2016 data set, together with the corresponding background predictions and observations. For the background predic-
tions, the first uncertainty listed is statistical (from the limited size of control samples), and the second is systematic. The systematic uncertainty is not shown when it is negligible

Track length	N_j	H_T range (GeV)	Track p_T (GeV)	Label	Background	Data
P	2–3	[250, 450)	[15, 50)	P LL lo	$15.5^{+3.0}_{-2.7} \pm 3.2$	16
			[50, ∞)	P LL hi	$9.8^{+2.6}_{-2.2} \pm 2.5$	3
		[450, 1200)	[15, 50)	P LM lo	$4.2^{+1.0}_{-0.9} \pm 1.2$	2
			[50, ∞)	P LM hi	$2.02^{+0.66}_{-0.55} \pm 0.63$	1
		[1200, ∞)	[15, 50)	P LH lo	$0.19^{+0.26}_{-0.13} \pm 0.13$	0
			[50, ∞)	P LH hi	$0.06^{+0.14}_{-0.05} \pm 0.03$	0
	≥ 4	[250, 450)	[15, 50)	P HL lo	$3.3^{+0.7}_{-0.6} \pm 1.4$	1
			[50, ∞)	P HL hi	$1.98^{+0.43}_{-0.38} \pm 0.57$	1
		[450, 1200)	[15, 50)	P HM lo	$4.7^{+0.8}_{-0.7} \pm 1.9$	6
			[50, ∞)	P HM hi	$2.37^{+0.50}_{-0.44} \pm 0.55$	1
		[1200, ∞)	[15, 50)	P HH lo	$0.43^{+0.24}_{-0.17} \pm 0.27$	0
			[50, ∞)	P HH hi	$0.17^{+0.10}_{-0.07} \pm 0.04$	0
M	2–3	[250, 450)	[15, 50)	M LL lo	$3.9^{+1.5}_{-1.2} \pm 1.3$	3
			[50, ∞)	M LL hi	$14^{+3.7}_{-3.2} \pm 4.0$	8
		[450, 1200)	[15, 50)	M LM lo	$2.1^{+0.89}_{-0.71} \pm 1.1$	3
			[50, ∞)	M LM hi	$0.68^{+0.90}_{-0.45} \pm 0.35$	4
		[1200, ∞)	[15, 50)	M LH lo	$0.0^{+0.25}_{-0.0} \pm 0.0$	0
			[50, ∞)	M LH hi	$0.0^{+0.7}_{-0.0}$	0
	≥ 4	[250, 450)	[15, 50)	M HL lo	$1.8^{+0.6}_{-0.5} \pm 0.9$	0
			[50, ∞)	M HL hi	$2.1^{+0.8}_{-0.6}\ ^{+2.3}_{-2.1}$	2
		[450, 1200)	[15, 50)	M HM lo	$2.2^{+0.7}_{-0.6} \pm 1.3$	1
			[50, ∞)	M HM hi	$2.9^{+0.9}_{-0.8} \pm 2.3$	0
		[1200, ∞)	[15, 50)	M HH lo	$0.23^{+0.23}_{-0.13} \pm 0.11$	0
			[50, ∞)	M HH hi	$0.30^{+0.40}_{-0.20} \pm 0.29$	1
L	2–3	[250, 1200)	[15, ∞)	L LLM	$0.046^{+0.050}_{-0.034}\ ^{+0.057}_{-0.046}$	0
		[1200, ∞)	[15, ∞)	L LH	$0.015^{+0.036}_{-0.015}\ ^{+0.022}_{-0.015}$	0
	≥ 4	[250, 1200)	[15, ∞)	L HLM	$0.092^{+0.136}_{-0.085}\ ^{+0.130}_{-0.092}$	0
		[1200, ∞)	[15, ∞)	L HH	$0.0^{+0.1}_{-0.0}$	0

Table 25 Summary of the 24 signal regions of the search for disappearing tracks for pixel tracks, for the 2017–2018 data set, together with the corresponding background predictions and observations. For
the background predictions, the first uncertainty listed is statistical (from the limited size of control samples), and the second is systematic. The systematic uncertainty is not shown when it is negligible

Track length	N_j	H_T range (GeV)	Track p_T (GeV)	Label	Background	Data
P3	2–3	[250, 450)	[15, 50)	P3 LL lo	$78^{+9}_{-9} \pm 34$	73
			[50, ∞)	P3 LL hi	$43.9^{+6.7}_{-6.2} \pm 8.1$	41
		[450, 1200)	[15, 50)	P3 LM lo	$30^{+5}_{-5} \pm 16$	21
			[50, ∞)	P3 LM hi	$13^{+3}_{-3} \pm 13$	16
		[1200, ∞)	[15, 50)	P3 LH lo	$0.0^{+1.0}_{-0.0}$	1

Table 25 continued

Track length	N_j	H_T range (GeV)	Track p_T (GeV)	Label	Background	Data
			$[\,50, \infty\,)$	P3 LH hi	$0.43^{+0.98}_{-0.36} \pm 0.34$	0
	≥ 4	$[\,250, 450\,)$	$[\,15, 50\,)$	P3 HL lo	$25.8^{+3.8}_{-3.4} \pm 7.9$	17
			$[\,50, \infty\,)$	P3 HL hi	$10.8^{+2.1}_{-1.8} \pm 3.5$	7
		$[\,450, 1200\,)$	$[\,15, 50\,)$	P3 HM lo	$28.9^{+4.0}_{-3.7} \pm 5.7$	37
			$[\,50, \infty\,)$	P3 HM hi	$12.3^{+2.2}_{-1.9} \pm 6.8$	11
		$[\,1200, \infty\,)$	$[\,15, 50\,)$	P3 HH lo	$3.1^{+1.5}_{-1.1} \pm 0.5$	5
			$[\,50, \infty\,)$	P3 HH hi	$0.49^{+0.65}_{-0.32} \pm 0.12$	3
P4	2–3	$[\,250, 450\,)$	$[\,15, 50\,)$	P4 LL lo	$24^{+5}_{-5} \pm 11$	10
			$[\,50, \infty\,)$	P4 LL hi	$4.1^{+1.9}_{-1.5} \pm 3.7$	0
		$[\,450, 1200\,)$	$[\,15, 50\,)$	P4 LM lo	$8.7^{+2.7}_{-2.2} \pm 4.6$	8
			$[\,50, \infty\,)$	P4 LM hi	$1.1^{+0.7}_{-0.5}{}^{+1.4}_{-1.1}$	0
		$[\,1200, \infty\,)$	$[\,15, 50\,)$	P4 LH lo	$0.40^{+0.91}_{-0.33} \pm 0.40$	0
			$[\,50, \infty\,)$	P4 LH hi	$0.0^{+0.39}_{-0.0}$	0
	≥ 4	$[\,250, 450\,)$	$[\,15, 50\,)$	P4 HL lo	$6.3^{+1.6}_{-1.3} \pm 2.2$	7
			$[\,50, \infty\,)$	P4 HL hi	$0.62^{+0.35}_{-0.25} \pm 0.43$	0
		$[\,450, 1200\,)$	$[\,15, 50\,)$	P4 HM lo	$6.9^{+1.6}_{-1.4} \pm 6.2$	2
			$[\,50, \infty\,)$	P4 HM hi	$1.32^{+0.54}_{-0.43} \pm 0.63$	2
		$[\,1200, \infty\,)$	$[\,15, 50\,)$	P4 HH lo	$0.42^{+0.56}_{-0.28} \pm 0.12$	0
			$[\,50, \infty\,)$	P4 HH hi	$0.08^{+0.18}_{-0.07} \pm 0.03$	0

Table 26 Summary of the 16 signal regions of the search for disappearing tracks for medium (M) length and long (L) tracks, for the 2017–2018 data set, together with the corresponding background predictions and observations. For the background predictions, the first uncertainty listed is statistical (from the limited size of control samples), and the second is systematic. The systematic uncertainty is not shown when it is negligible

Track length	N_j	H_T range (GeV)	Track p_T (GeV)	Label	Background	Data
M	2–3	$[\,250, 450\,)$	$[\,15, 50\,)$	M LL lo	$8.4^{+2.4}_{-2.0} \pm 3.4$	8
			$[\,50, \infty\,)$	M LL hi	$5.4^{+2.2}_{-1.8} \pm 2.6$	2
		$[\,450, 1200\,)$	$[\,15, 50\,)$	M LM lo	$1.90^{+0.85}_{-0.66} \pm 0.92$	6
			$[\,50, \infty\,)$	M LM hi	$1.12^{+0.77}_{-0.54} \pm 0.97$	1
		$[\,1200, \infty\,)$	$[\,15, 50\,)$	M LH lo	$0.00^{+0.36}_{-0}$	0
			$[\,50, \infty\,)$	M LH hi	$0.00^{+0.46}_{-0}$	0
	≥ 4	$[\,250, 450\,)$	$[\,15, 50\,)$	M HL lo	$1.6^{+0.6}_{-0.5}{}^{+3.0}_{-1.6}$	3
			$[\,50, \infty\,)$	M HL hi	$1.11^{+0.57}_{-0.42} \pm 0.58$	1
		$[\,450, 1200\,)$	$[\,15, 50\,)$	M HM lo	$1.9^{+0.6}_{-0.5}{}^{+3.5}_{-1.9}$	3
			$[\,50, \infty\,)$	M HM hi	$1.5^{+0.7}_{-0.5} \pm 1.1$	0
		$[\,1200, \infty\,)$	$[\,15, 50\,)$	M HH lo	$0.38^{+0.31}_{-0.19}{}^{+0.70}_{-0.38}$	1
			$[\,50, \infty\,)$	M HH hi	$0.12^{+0.29}_{-0.10} \pm 0.04$	0
L	2–3	$[\,250, 1200\,)$	$[\,15, \infty\,)$	L LLM	$0.46^{+0.26}_{-0.20}{}^{+0.53}_{-0.46}$	0
		$[\,1200, \infty\,)$	$[\,15, \infty\,)$	L LH	$0.00^{+0.14}_{-0}$	0
	≥ 4	$[\,250, 1200\,)$	$[\,15, \infty\,)$	L HLM	$0.013^{+0.015}_{-0.014}{}^{+0.018}_{-0.013}$	0
		$[\,1200, \infty\,)$	$[\,15, \infty\,)$	L HH	$0.000^{+0.008}_{-0}$	0

Fig. 23 (Upper) Comparison of the estimated background and observed data events in each signal bin in the very-low-H_T region. The hatched bands represent the full uncertainty in the background estimate.

The notations j, b indicate N_j, N_b labeling. (Lower) Same for the low-H_T region. On the x axis, the M_{T2} binning is shown in units of GeV

Fig. 24 (Upper) Comparison of the estimated background and observed data events in each signal bin in the high-H_T region. The hatched bands represent the full uncertainty in the background esti-

mate. The notations j, b indicate N_j, N_b labeling. (Lower) Same for the extreme-H_T region. On the x axis, the M_{T2} binning is shown in units of GeV

References

1. C.G. Lester, D.J. Summers, Measuring masses of semiinvisibly decaying particles pair produced at hadron colliders. Phys. Lett. B **463**, 99 (1999). https://doi.org/10.1016/S0370-2693(99)00945-4. arXiv:hep-ph/9906349

2. ATLAS Collaboration, Search for new phenomena with large jet multiplicities and missing transverse momentum using large-radius jets and flavour-tagging at ATLAS in 13 TeV pp collisions. JHEP **12**, 034 (2017). https://doi.org/10.1007/JHEP12(2017)034. arXiv:1708.02794

3. ATLAS Collaboration, Search for supersymmetry in events with b-tagged jets and missing transverse momentum in pp collisions at $\sqrt{s}$ = 13 TeV with the ATLAS detector. JHEP **11**, 195 (2017). https://doi.org/10.1007/JHEP11(2017)195. arXiv:1708.09266

4. ATLAS Collaboration, Search for a scalar partner of the top quark in the jets plus missing transverse momentum final state at $\sqrt{s}$ = 13 TeV with the ATLAS detector. JHEP **12**, 085 (2017). https://doi.org/10.1007/JHEP12(2017)085. arXiv:1709.04183

5. ATLAS Collaboration, Search for supersymmetry in final states with missing transverse momentum and multiple b-jets in proton-proton collisions at $\sqrt{s}$ = 13 TeV with the ATLAS detector. JHEP **06**, 107 (2018). https://doi.org/10.1007/JHEP06(2018)107. arXiv:1711.01901

6. ATLAS Collaboration, Search for dark matter and other new phenomena in events with an energetic jet and large missing transverse momentum using the ATLAS detector. JHEP **01**, 126 (2018). https://doi.org/10.1007/JHEP01(2018)126. arXiv:1711.03301

7. ATLAS Collaboration, Search for squarks and gluinos in final states with jets and missing transverse momentum using 36 fb^{-1} of $\sqrt{s}$ = 13 TeV pp collision data with the ATLAS detector. Phys. Rev. D **97**, 112001 (2018). https://doi.org/10.1103/PhysRevD.97.112001. arXiv:1712.02332

8. CMS Collaboration, Search for supersymmetry in multijet events with missing transverse momentum in proton-proton collisions at 13 TeV. Phys. Rev. D **96**, 032003 (2017). https://doi.org/10.1103/PhysRevD.96.032003, arXiv:1704.07781

9. CMS Collaboration, Search for new phenomena with the M_{T2} variable in the all-hadronic final state produced in proton–proton collisions at $\sqrt{s}$ = 13 TeV. Eur. Phys. J. C **77**, 710 (2017). https://doi.org/10.1140/epjc/s10052-017-5267-x. arXiv:1705.04650

10. CMS Collaboration, Search for natural and split supersymmetry in proton–proton collisions at $\sqrt{s}$ = 13 TeV in final states with jets and missing transverse momentum. JHEP **05**, 025 (2018). https://doi.org/10.1007/JHEP05(2018)025. arXiv:1802.02110

11. CMS Collaboration, Constraints on models of scalar and vector leptoquarks decaying to a quark and a neutrino at $\sqrt{s}$ = 13 TeV. Phys. Rev. D **98**, 032005 (2018). https://doi.org/10.1103/PhysRevD.98.032005. arXiv:1805.10228

12. CMS Collaboration, Inclusive search for supersymmetry in pp collisions at $\sqrt{s}$ = 13 TeV using razor variables and boosted object identification in zero and one lepton final states. JHEP **03**, 031 (2019). https://doi.org/10.1007/JHEP03(2019)031. arXiv:1812.06302

13. G.F. Giudice, M.A. Luty, H. Murayama, R. Rattazzi, Gaugino mass without singlets. JHEP **12**, 027 (1998). https://doi.org/10.1088/1126-6708/1998/12/027. arXiv:hep-ph/9810442

14. L. Randall, R. Sundrum, Out of this world supersymmetry breaking. Nucl. Phys. B **557**, 79 (1999). https://doi.org/10.1016/S0550-3213(99)00359-4. arXiv:hep-th/9810155

15. ATLAS Collaboration, Search for charginos nearly mass degenerate with the lightest neutralino based on a disappearing-track signature in pp collisions at $\sqrt{s}$ = 8 TeV with the ATLAS detector. Phys. Rev. D **88**, 112006 (2013) https://doi.org/10.1103/PhysRevD.88.112006, arXiv:1310.3675

16. ATLAS Collaboration, Search for long-lived charginos based on a disappearing-track signature in pp collisions at $\sqrt{s}$ = 13 TeV with the ATLAS detector, JHEP **06**, 022 (2018). https://doi.org/10.1007/JHEP06(2018)022, arXiv:1712.02118

17. CMS Collaboration, Search for disappearing tracks in proton-proton collisions at $\sqrt{s}$ = 8 TeV. JHEP **01**, 096 (2015). https://doi.org/10.1007/JHEP01(2015)096. arXiv:1411.6006

18. CMS Collaboration, Constraints on the pMSSM, AMSB model and on other models from the search for long-lived charged particles in proton-proton collisions at $\sqrt{s}$ = 8 TeV. Eur. Phys. J. C **75**, 325 (2015). https://doi.org/10.1140/epjc/s10052-015-3533-3. arXiv:1502.02522

19. CMS Collaboration, Search for disappearing tracks as a signature of new long-lived particles in proton-proton collisions at $\sqrt{s}$ = 13 TeV. JHEP **08**, 016 (2018). https://doi.org/10.1007/JHEP08(2018)016. arXiv:1804.07321

20. CMS Collaboration, Search for long-lived charged particles in proton-proton collisions at $\sqrt{s}$ = 13 TeV. Phys. Rev. D **94**, 112004 (2016). https://doi.org/10.1103/PhysRevD.94.112004. arXiv:1609.08382

21. N. Arkani-Hamed et al., MARMOSET: The path from LHC data to the new standard model via on-shell effective theories, (2007). arXiv:hep-ph/0703088

22. J. Alwall, P. Schuster, N. Toro, Simplified models for a first characterization of new physics at the LHC. Phys. Rev. D **79**, 075020 (2009). https://doi.org/10.1103/PhysRevD.79.075020. arXiv:0810.3921

23. J. Alwall, M.-P. Le, M. Lisanti, J.G. Wacker, Model-independent jets plus missing energy searches. Phys. Rev. D **79**, 015005 (2009). https://doi.org/10.1103/PhysRevD.79.015005. arXiv:0809.3264

24. LHC New Physics Working Group Collaboration, Simplified models for LHC new physics searches. J. Phys. G **39**, 105005 (2012). https://doi.org/10.1088/0954-3899/39/10/105005. arXiv:1105.2838

25. C.M.S. Collaboration, Interpretation of searches for supersymmetry with simplified models. Phys. Rev. D **88**, 052017 (2013). https://doi.org/10.1103/PhysRevD.88.052017. arXiv:1301.2175

26. G.R. Farrar, P. Fayet, Phenomenology of the production, decay, and detection of new hadronic states associated with supersymmetry. Phys. Lett. B **76**, 575 (1978). https://doi.org/10.1016/0370-2693(78)90858-4

27. P. Ramond, Dual theory for free fermions. Phys. Rev. D **3**, 2415 (1971). https://doi.org/10.1103/PhysRevD.3.2415

28. Y.A. Golfand, E.P. Likhtman, Extension of the algebra of Poincaré group generators and violation of P invariance. JETP Lett. **13**, 323 (1971)

29. A. Neveu, J.H. Schwarz, Factorizable dual model of pions. Nucl. Phys. B **31**, 86 (1971). https://doi.org/10.1016/0550-3213(71)90448-2

30. D.V. Volkov, V.P. Akulov, Possible universal neutrino interaction. JETP Lett. **16**, 438 (1972)

31. J. Wess, B. Zumino, A Lagrangian model invariant under supergauge transformations. Phys. Lett. B **49**, 52 (1974). https://doi.org/10.1016/0370-2693(74)90578-4

32. J. Wess, B. Zumino, Supergauge transformations in four dimensions. Nucl. Phys. B **70**, 39 (1974). https://doi.org/10.1016/0550-3213(74)90355-1

33. P. Fayet, Supergauge invariant extension of the Higgs mechanism and a model for the electron and its neutrino. Nucl. Phys. B **90**, 104 (1975). https://doi.org/10.1016/0550-3213(75)90636-7

34. H.P. Nilles, Supersymmetry, supergravity and particle physics. Phys. Rep. **110**, 1 (1984). https://doi.org/10.1016/0370-1573(84)90008-5

35. P. Asadi et al., Digging deeper for new physics in the LHC data. JHEP **11**, 194 (2017). https://doi.org/10.1007/JHEP11(2017)194. arXiv:1707.05783

36. P. Asadi et al., An update on the LHC monojet excess. JHEP **03**, 130 (2018). https://doi.org/10.1007/JHEP03(2018)130. arXiv:1712.04939

37. CMS Collaboration, Search for new physics in final states with an energetic jet or a hadronically decaying W or Z boson and transverse momentum imbalance at $\sqrt{s} = 13$ TeV. Phys. Rev. D **97**, 092005 (2018). https://doi.org/10.1103/PhysRevD.97.092005. arXiv:1712.02345

38. J.C. Pati, A. Salam, Unified lepton-hadron symmetry and a gauge theory of the basic interactions. Phys. Rev. D **8**, 1240 (1973). https://doi.org/10.1103/PhysRevD.8.1240

39. J.C. Pati, A. Salam, Lepton number as the fourth color. Phys. Rev. D **10**, 275 (1974). https://doi.org/10.1103/PhysRevD.10.275. **(Erratum: 10.1103/PhysRevD.11.703.2)**

40. H. Georgi, S.L. Glashow, Unity of all elementary particle forces. Phys. Rev. Lett. **32**, 438 (1974). https://doi.org/10.1103/PhysRevLett.32.438

41. H. Fritzsch, P. Minkowski, Unified interactions of leptons and hadrons. Annals Phys. **93**, 193 (1975). https://doi.org/10.1016/0003-4916(75)90211-0

42. S. Dimopoulos, L. Susskind, Mass without scalars. Nucl. Phys. B **155**, 237 (1979). https://doi.org/10.1016/0550-3213(79)90364-X. [2,930(1979)]

43. S. Dimopoulos, Technicolored signatures. Nucl. Phys. B **168**, 69 (1980). https://doi.org/10.1016/0550-3213(80)90277-1

44. E. Farhi, L. Susskind, Technicolor. Phys. Rept. **74**, 277 (1981). https://doi.org/10.1016/0370-1573(81)90173-3

45. K.D. Lane, M.V. Ramana, Walking technicolor signatures at hadron colliders. Phys. Rev. D **44**, 2678 (1991). https://doi.org/10.1103/PhysRevD.44.2678

46. B. Schrempp, F. Schrempp, Light leptoquarks. Phys. Lett. B **153**, 101 (1985). https://doi.org/10.1016/0370-2693(85)91450-9

47. B. Gripaios, Composite leptoquarks at the LHC. JHEP **02**, 045 (2010). https://doi.org/10.1007/JHEP02(2010)045. arXiv:0910.1789

48. R. Barbier et al., R-parity violating supersymmetry. Phys. Rept. **420**, 1 (2005). https://doi.org/10.1016/j.physrep.2005.08.006. arXiv:hep-ph/0406039

49. M. Tanaka, R. Watanabe, New physics in the weak interaction of $\bar{B} \to D^{(*)}\tau\bar{\nu}$. Phys. Rev. D **87**, 034028 (2013). https://doi.org/10.1103/PhysRevD.87.034028. arXiv:1212.1878

50. Y. Sakaki, M. Tanaka, A. Tayduganov, R. Watanabe, Testing leptoquark models in $\bar{B} \to D^{(*)}\tau\bar{\nu}$. Phys. Rev. D **88**, 094012 (2013). https://doi.org/10.1103/PhysRevD.88.094012. arXiv:1309.0301

51. I. Doršner, S. Fajfer, N. Košnik, I. Nišandžić, Minimally flavored colored scalar in $\bar{B} \to D^{(*)}\tau\bar{\nu}$ and the mass matrices constraints. JHEP **11**, 084 (2013). https://doi.org/10.1007/JHEP11(2013)084. arXiv:1306.6493

52. B. Gripaios, M. Nardecchia, S.A. Renner, Composite leptoquarks and anomalies in B-meson decays. JHEP **05**, 006 (2015). https://doi.org/10.1007/JHEP05(2015)006. arXiv:1412.1791

53. M. Bauer, M. Neubert, Minimal leptoquark explanation for the $R_{D^{(*)}}$, R_K, and $(g - 2)_g$ anomalies. Phys. Rev. Lett. **116**, 141802 (2016). https://doi.org/10.1103/PhysRevLett.116.141802. arXiv:1511.01900

54. D. Buttazzo, A. Greljo, G. Isidori, D. Marzocca, B-physics anomalies: a guide to combined explanations. JHEP **11**, 044 (2017). https://doi.org/10.1007/JHEP11(2017)044. arXiv:1706.07808

55. I. Doršner, A. Greljo, Leptoquark toolbox for precision collider studies. JHEP **05**, 126 (2018). https://doi.org/10.1007/JHEP05(2018)126. arXiv:1801.07641

56. BaBar Collaboration, Evidence for an excess of $\bar{B} \to D^{(*)}\tau^-\bar{\nu}_\tau$ decays. Phys. Rev. Lett. **109**, 101802 (2012). https://doi.org/10.1103/PhysRevLett.109.101802. arXiv:1205.5442

57. BaBar Collaboration, Measurement of an excess of $\bar{B} \to D^{(*)}\tau^-\bar{\nu}_\tau$ decays and implications for charged Higgs bosons.

Phys. Rev. D **88**, 072012 (2013). https://doi.org/10.1103/PhysRevD.88.072012. arXiv:1303.0571

58. Belle Collaboration, Observation of $B^0 \to D^{*-}\tau^+\nu_\tau$ decay at Belle. Phys. Rev. Lett. **99**, 191807 (2007). https://doi.org/10.1103/PhysRevLett.99.191807. arXiv:0706.4429

59. Belle Collaboration, Observation of $B^+ \to \bar{D}^{*0}\tau^+\nu_\tau$ and evidence for $B^+ \to \bar{D}^0\tau^+\nu_\tau$ at Belle. Phys. Rev. D **82**, 072005 (2010). https://doi.org/10.1103/PhysRevD.82.072005. arXiv:1005.2302

60. Belle Collaboration, Measurement of the branching ratio of $\bar{B} \to D^{(*)}\tau^-\bar{\nu}_\tau$ relative to $\bar{B} \to D^{(*)}\ell^-\bar{\nu}_\ell$ decays with hadronic tagging at Belle. Phys. Rev. D **92**, 072014 (2015). https://doi.org/10.1103/PhysRevD.92.072014. arXiv:1507.03233

61. Belle Collaboration, Measurement of the τ lepton polarization and $R(D^*)$ in the decay $\bar{B} \to D^*\tau^-\bar{\nu}_\tau$. Phys. Rev. Lett. **118**, 211801 (2017). https://doi.org/10.1103/PhysRevLett.118.211801. arXiv:1612.00529

62. Belle Collaboration, Test of lepton flavor universality in $B \to K^*\ell^+\ell^-$ decays at Belle, (2019). arXiv:1904.02440

63. LHCb Collaboration, Measurement of form-factor-independent observables in the decay $B^0 \to K^{*0}\mu^+\mu^-$, Phys. Rev. Lett. **111**, 191801 (2013) https://doi.org/10.1103/PhysRevLett.111.191801, arXiv:1308.1707

64. LHCb Collaboration, Test of lepton universality using $B^+ \to K^+\ell^+\ell^-$ decays, Phys. Rev. Lett. **113**, 151601 (2014) https://doi.org/10.1103/PhysRevLett.113.151601, arXiv:1406.6482

65. LHCb Collaboration, Measurement of the ratio of branching fractions $\mathcal{B}(\bar{B}^0 \to D^{*+}\tau^-\bar{\nu}_\tau)/\mathcal{B}(\bar{B}^0 \to D^{*+}\mu^-\bar{\nu}_\mu)$. Phys. Rev. Lett. **115**, 111803 (2015). https://doi.org/10.1103/PhysRevLett.115.111803, arXiv:1506.08614. [Erratum: https://doi.org/10.1103/PhysRevLett.115.159901]

66. LHCb Collaboration, Angular analysis of the $B^0 \to K^{*0}\mu^+\mu^-$ decay using 3 fb^{-1} of integrated luminosity. JHEP **02**, 104 (2016). https://doi.org/10.1007/JHEP02(2016)104, arXiv:1512.04442

67. LHCb Collaboration, Test of lepton universality with $B^0 \to K^{*0}\ell^+\ell^-$ decays. JHEP **08**, 055 (2017). https://doi.org/10.1007/JHEP08(2017)055, arXiv:1705.05802

68. LHCb Collaboration, Search for lepton-universality violation in $B^+ \to K^+\ell^+\ell^-$ decays, Phys. Rev. Lett. **122** 191801 (2019). https://doi.org/10.1103/PhysRevLett.122.191801, arXiv:1903.09252

69. B. Diaz, M. Schmaltz, Y.-M. Zhong, The leptoquark hunter's guide: Pair production. JHEP **10**, 097 (2017). https://doi.org/10.1007/JHEP10(2017)097. arXiv:1706.05033

70. ATLAS Collaboration, Searches for scalar leptoquarks in pp collisions at $\sqrt{s} = 8$ TeV with the ATLAS detector. Eur. Phys. J. C **76**, 5 (2016). https://doi.org/10.1140/epjc/s10052-015-3823-9, arXiv:1508.04735

71. ATLAS Collaboration, Searches for scalar leptoquarks and differential cross-section measurements in dilepton-dijet events in proton-proton collisions at a centre-of-mass energy of $\sqrt{s} = 13$ TeV with the ATLAS experiment (2019). arXiv:1902.00377 **(Submitted to: Eur. Phys. J. C)**

72. ATLAS Collaboration, Searches for third-generation scalar leptoquarks in $\sqrt{s} = 13$ TeV pp collisions with the ATLAS detector. JHEP **06** 144 (2019). https://doi.org/10.1007/JHEP06(2019)144, arXiv:1902.08103

73. CMS Collaboration, Search for third-generation scalar leptoquarks decaying to a top quark and a τ lepton at $\sqrt{s} = 13$ TeV. Eur. Phys. J. C **78**, 707 (2018). https://doi.org/10.1140/epjc/s10052-018-6143-z. arXiv:1803.02864

74. CMS Collaboration, Search for pair production of first and second generation leptoquarks in proton-proton collisions at $\sqrt{s} = 8$ TeV. Phys. Rev. D **93**, 032004 (2016). https://doi.org/10.1103/PhysRevD.93.032004. arXiv:1509.03744

75. CMS Collaboration, Search for pair production of third-generation scalar leptoquarks and top squarks in proton-proton collisions at $\sqrt{s} = 8$ TeV. Phys. Lett. B **739**, 229 (2014). https://doi.org/10.1016/j.physletb.2014.10.063. arXiv:1408.0806

76. CMS Collaboration, Search for pair production of second-generation leptoquarks at $\sqrt{s} = 13$ TeV. Phys. Rev. D **99**, 032014 (2019). https://doi.org/10.1103/PhysRevD.99.032014. arXiv:1808.05082

77. CMS Collaboration, Search for pair production of first-generation scalar leptoquarks at $\sqrt{s} = 13$ TeV. Phys. Rev. D **99**, 052002 (2019). https://doi.org/10.1103/PhysRevD.99.052002. arXiv:1811.01197

78. CDF Collaboration, Search for first-generation scalar leptoquarks in p$\bar{\text{p}}$ collisions at $\sqrt{s} = 1.96$ TeV, Phys. Rev. D **72** 051107 (2005). https://doi.org/10.1103/PhysRevD.72.051107, arXiv:hep-ex/0506074

79. CDF Collaboration, Search for second-generation scalar leptoquarks in p$\bar{\text{p}}$ collisions at $\sqrt{s} = 1.96$ TeV. Phys. Rev. D **73** 051102 (2006). https://doi.org/10.1103/PhysRevD.73.051102, arXiv:hep-ex/0512055

80. CDF Collaboration, Search for new physics with a dijet plus missing transverse energy signature in p$\bar{\text{p}}$ collisions at $\sqrt{s} = 1.96$ TeV. Phys. Rev. Lett. **105** 131801 (2010). https://doi.org/10.1103/PhysRevLett.105.131801, arXiv:0912.4691

81. D0 Collaboration, Search for scalar leptoquarks and T-odd quarks in the acoplanar jet topology using 2.5 fb^{-1} of p$\bar{\text{p}}$ collision data at $\sqrt{s} = 1.96$ TeV. Phys. Lett. B **668**, 357 (2008). https://doi.org/10.1016/j.physletb.2008.09.014, arXiv:0808.0446

82. D0 Collaboration, Search for pair production of second generation scalar leptoquarks. Phys. Lett. B **671**, 224 (2009). https://doi.org/10.1016/j.physletb.2008.12.017. arXiv:0808.4023

83. D0 Collaboration, Search for first generation leptoquark pair production in the electron + missing energy + jets final state. Phys. Rev. D **84**, 071104 (2011). https://doi.org/10.1103/PhysRevD.84.071104. arXiv:1107.1849

84. H1 Collaboration, Search for first generation leptoquarks in ep collisions at HERA. Phys. Lett. B **704**, 388 (2011). https://doi.org/10.1016/j.physletb.2011.09.017. arXiv:1107.3716

85. ZEUS Collaboration, Search for first-generation leptoquarks at HERA. Phys. Rev. D **86**, 012005 (2012). https://doi.org/10.1103/PhysRevD.86.012005. arXiv:1205.5179

86. ATLAS Collaboration, Search for third generation scalar leptoquarks in pp collisions at $\sqrt{s} = 7$ TeV with the ATLAS detector. JHEP **06**, 033 (2013). https://doi.org/10.1007/JHEP06(2013)033, arXiv:1303.0526

87. CMS Collaboration, Search for third-generation scalar leptoquarks and heavy right-handed neutrinos in final states with two tau leptons and two jets in proton–proton collisions at $\sqrt{s} = 13$ TeV. JHEP **07**, 121 (2017). https://doi.org/10.1007/JHEP07(2017)121. arXiv:1703.03995

88. CMS Collaboration, Search for heavy neutrinos and third-generation leptoquarks in hadronic states of two τ leptons and two jets in proton-proton collisions at $\sqrt{s} = 13$ TeV. JHEP **03**, 170 (2019). https://doi.org/10.1007/JHEP03(2019)170. arXiv:1811.00806

89. CDF Collaboration, Search for third generation vector leptoquarks in p$\bar{\text{p}}$ collisions at $\sqrt{s} = 1.96$ TeV, Phys. Rev. D **77**, 091105 (2008) https://doi.org/10.1103/PhysRevD.77.091105, arXiv:0706.2832

90. CDF Collaboration, Search for pair production of scalar top quarks decaying to a τ lepton and a b quark in p$\bar{\text{p}}$ collisions at $\sqrt{s} = 1.96$ TeV, Phys. Rev. Lett. **101**, 071802 (2008) https://doi.org/10.1103/PhysRevLett.101.071802, arXiv:0802.3887

91. D0 Collaboration, Search for third generation scalar leptoquarks decaying into τb. Phys. Rev. Lett. **101**, 241802 (2008). https://doi.org/10.1103/PhysRevLett.101.241802. arXiv:0806.3527

92. CMS Collaboration, The CMS experiment at the CERN LHC. JINST **3**, S08004 (2008). https://doi.org/10.1088/1748-0221/3/08/S08004

93. CMS Collaboration, The CMS trigger system. JINST **12**, P01020 (2017). https://doi.org/10.1088/1748-0221/12/01/P01020. arXiv:1609.02366

94. CMS Collaboration, CMS technical design report for the pixel detector upgrade, Technical Report CERN-LHCC-2012-016, CMS-TDR-011, 2012. https://doi.org/10.2172/1151650

95. CMS Collaboration, Particle-flow reconstruction and global event description with the CMS detector. JINST **12**, P10003 (2017). https://doi.org/10.1088/1748-0221/12/10/P10003. arXiv:1706.04965

96. CMS Collaboration, Search for new physics with the M_{T2} variable in all-jets final states produced in pp collisions at $\sqrt{s} = 13$ TeV. JHEP **10**, 006 (2016). https://doi.org/10.1007/JHEP10(2016)006. arXiv:1603.04053

97. M. Cacciari, G.P. Salam, G. Soyez, The anti-k^T jet clustering algorithm. JHEP **04**, 063 (2008). https://doi.org/10.1088/1126-6708/2008/04/063. arXiv:0802.1189

98. M. Cacciari, G.P. Salam, G. Soyez, FastJet user manual. Eur. Phys. J. C **72**, 1896 (2012). https://doi.org/10.1140/epjc/s10052-012-1896-2. arXiv:1111.6097

99. M. Cacciari, G.P. Salam, Pileup subtraction using jet areas. Phys. Lett. B **659**, 119 (2008). https://doi.org/10.1016/j.physletb.2007.09.077. arXiv:0707.1378

100. CMS Collaboration, Jet energy scale and resolution in the CMS experiment in pp collisions at 8 TeV. JINST **12**, P02014 (2017). https://doi.org/10.1088/1748-0221/12/02/P02014. arXiv:1607.03663

101. CMS Collaboration, Jet energy scale and resolution performance with 13 TeV data collected by CMS in 2016, Detector Performance Report CMS-DP-2018-028, (2018). http://cds.cern.ch/record/2622157

102. CMS Collaboration, Identification of heavy-flavour jets with the CMS detector in pp collisions at 13 TeV. JINST **13**, P05011 (2018). https://doi.org/10.1088/1748-0221/13/05/P05011. arXiv:1712.07158

103. CMS Collaboration, Missing transverse energy performance of the CMS detector. JINST **6**, P09001 (2011). https://doi.org/10.1088/1748-0221/6/09/P09001. arXiv:1106.5048

104. CMS Collaboration, Performance of missing transverse momentum reconstruction in proton–proton collisions at $\sqrt{s} = 13$ TeV using the CMS detector. JINST **14**, P07004 (2019). https://doi.org/10.1088/1748-0221/14/07/P07004. arXiv:1903.06078

105. T. Sjöstrand, The Lund Monte Carlo for e^+e^- jet physics. Comput. Phys. Commun. **28**, 229 (1983). https://doi.org/10.1016/0010-4655(83)90041-3

106. T. Sjöstrand, S. Mrenna, P. Skands, PYTHIA 6.4 physics and manual. JHEP **05**, 026 (2006). https://doi.org/10.1088/1126-6708/2006/05/026. arXiv:hep-ph/0603175

107. UA1 Collaboration, Experimental observation of isolated large transverse energy electrons with associated missing energy at $\sqrt{s} = 540$ GeV. Phys. Lett. B **122**, 103 (1983). https://doi.org/10.1016/0370-2693(83)91177-2

108. CMS Collaboration, Searches for supersymmetry using the M_{T2} variable in hadronic events produced in pp collisions at 8 TeV. JHEP **05**, 078 (2015). https://doi.org/10.1007/JHEP05(2015)078. arXiv:1502.04358

109. CMS Collaboration, Search for supersymmetry in hadronic final states using M_{T2} in pp collisions at $\sqrt{s} = 7$ TeV. JHEP **10**, 018 (2012). https://doi.org/10.1007/JHEP10(2012)018. arXiv:1207.1798

110. J. Alwall et al., The automated computation of tree-level and next-to-leading order differential cross sections, and their matching to

parton shower simulations. JHEP **07**, 079 (2014). https://doi.org/10.1007/JHEP07(2014)079. arXiv:1405.0301

111. P. Nason, A new method for combining NLO QCD with shower Monte Carlo algorithms. JHEP **11**, 040 (2004). https://doi.org/10.1088/1126-6708/2004/11/040. arXiv:hep-ph/0409146

112. S. Frixione, P. Nason, C. Oleari, Matching NLO QCD computations with parton shower simulations: the POWHEG method. JHEP **11**, 070 (2007). https://doi.org/10.1088/1126-6708/2007/11/070. arXiv:0709.2092

113. S. Alioli, P. Nason, C. Oleari, E. Re, NLO single-top production matched with shower in POWHEG: *s*- and *t*-channel contributions. JHEP **09**, 111 (2009). https://doi.org/10.1088/1126-6708/2009/09/111. arXiv:0907.4076. [Erratum: 10.1007/JHEP02(2010) 011]

114. S. Alioli, P. Nason, C. Oleari, E. Re, A general framework for implementing NLO calculations in shower Monte Carlo programs: the POWHEG BOX. JHEP **06**, 043 (2010). https://doi.org/10.1007/JHEP06(2010)043. arXiv:1002.2581

115. E. Re, Single-top *Wt*-channel production matched with parton showers using the POWHEG method. Eur. Phys. J. C **71**, 1547 (2011). https://doi.org/10.1140/epjc/s10052-011-1547-z. arXiv:1009.2450

116. R. Gavin, Y. Li, F. Petriello, S. Quackenbush, FEWZ 2.0: A code for hadronic Z production at next-to-next-to-leading order. Comput. Phys. Commun. **182**, 2388 (2011). https://doi.org/10.1016/j.cpc.2011.06.008. arXiv:1011.3540

117. R. Gavin, Y. Li, F. Petriello, S. Quackenbush, W physics at the LHC with FEWZ 2.1. Comput. Phys. Commun. **184**, 208 (2013). https://doi.org/10.1016/j.cpc.2012.09.005. arXiv:1201.5896

118. M. Czakon, A. Mitov, Top++: a program for the calculation of the top-pair cross-section at hadron colliders. Comput. Phys. Commun. **185**, 2930 (2014). https://doi.org/10.1016/j.cpc.2014.06.021. arXiv:1112.5675

119. C. Borschensky et al., Squark and gluino production cross sections in pp collisions at $\sqrt{s} = 13, 14, 33$ and 100 TeV. Eur. Phys. J. C **74**, 3174 (2014). https://doi.org/10.1140/epjc/s10052-014-3174-y. arXiv:1407.5066

120. GEANT4 Collaboration, GEANT4—a simulation toolkit. Nucl. Instrum. Meth. A **506**, 250 (2003) https://doi.org/10.1016/S0168-9002(03)01368-8

121. S. Abdullin et al., The fast simulation of the CMS detector at LHC. J. Phys. Conf. Ser. **331**, 032049 (2011). https://doi.org/10.1088/1742-6596/331/3/032049

122. A. Giammanco, The fast simulation of the CMS experiment. J. Phys. Conf. Ser. **513**, 022012 (2014). https://doi.org/10.1088/1742-6596/513/2/022012

123. T. Sjöstrand et al., An Introduction to PYTHIA 8.2. Comput. Phys. Commun. **191**, 159 (2015). https://doi.org/10.1016/j.cpc.2015.01.024. arXiv:1410.3012

124. J. Alwall et al., Comparative study of various algorithms for the merging of parton showers and matrix elements in hadronic collisions. Eur. Phys. J. C **53**, 473 (2008). https://doi.org/10.1140/epjc/s10052-007-0490-5. arXiv:0706.2569

125. R. Frederix, S. Frixione, Merging meets matching in MC@NLO. JHEP **12**, 061 (2012). https://doi.org/10.1007/JHEP12(2012)061. arXiv:1209.6215

126. C.M.S. Collaboration, Event generator tunes obtained from underlying event and multiparton scattering measurements. Eur. Phys. J. C **76**, 155 (2016). https://doi.org/10.1140/epjc/s10052-016-3988-x. arXiv:1512.00815

127. CMS Collaboration, Extraction and validation of a new set of CMS PYTHIA8 tunes from underlying-event measurements, (2019). arXiv:1903.12179 **(Submitted to: Eur. Phys. J. C)**

128. NNPDF Collaboration, Parton distributions with QED corrections. Nucl. Phys. B **877**, 290 (2013). https://doi.org/10.1016/j.nuclphysb.2013.10.010, arXiv:1308.0598

129. NNPDF Collaboration, Parton distributions from high-precision collider data. Eur. Phys. J. C **77**, 663 (2017) https://doi.org/10.1140/epjc/s10052-017-5199-5, arXiv:1706.00428

130. CMS Collaboration, Measurements of t$\bar{\text{t}}$ cross sections in association with b jets and inclusive jets and their ratio using dilepton final states in pp collisions at $\sqrt{s} = 13$ TeV. Phys. Lett. B **776**, 355 (2018). https://doi.org/10.1016/j.physletb.2017.11.043. arXiv:1705.10141

131. CMS Collaboration, Jet algorithms performance in 13 TeV data. CMS Physics Analysis Summary CMS-PAS-JME-16-003 (2017) http://cds.cern.ch/record/2656875

132. T. Junk, Confidence level computation for combining searches with small statistics. Nucl. Instrum. Meth. A **434**, 435 (1999). https://doi.org/10.1016/S0168-9002(99)00498-2. arXiv:hep-ex/9902006

133. A.L. Read, Presentation of search results: the CL_s technique. J. Phys. G **28**, 2693 (2002). https://doi.org/10.1088/0954-3899/28/10/313

134. G. Cowan, K. Cranmer, E. Gross, O. Vitells, Asymptotic formulae for likelihood-based tests of new physics. Eur. Phys. J. C **71**, 1554 (2011). https://doi.org/10.1140/epjc/s10052-011-1554-0. arXiv:1007.1727 [Erratum: 10.1140/epjc/s10052-013-2501-z]

135. ATLAS and CMS Collaborations, Procedure for the LHC Higgs boson search combination in summer 2011, ATLAS/CMS joint note ATL-PHYS-PUB-2011-011, CMS-NOTE-2011-005, (2011). http://cds.cern.ch/record/1379837

136. W. Beenakker, R. Höpker, M. Spira, P.M. Zerwas, Squark and gluino production at hadron colliders. Nucl. Phys. B **492**, 51 (1997). https://doi.org/10.1016/S0550-3213(97)00084-9. arXiv:hep-ph/9610490

137. W. Beenakker et al., Stop production at hadron colliders. Nucl. Phys. B **515**, 3 (1998). https://doi.org/10.1016/S0550-3213(98)00014-5. arXiv:hep-ph/9710451

138. A. Kulesza, L. Motyka, Threshold resummation for squark-antisquark and gluino-pair production at the LHC. Phys. Rev. Lett. **102**, 111802 (2009). https://doi.org/10.1103/PhysRevLett.102.111802. arXiv:0807.2405

139. A. Kulesza, L. Motyka, Soft gluon resummation for the production of gluino–gluino and squark–antisquark pairs at the LHC. Phys. Rev. D **80**, 095004 (2009). https://doi.org/10.1103/PhysRevD.80.095004. arXiv:0905.4749

140. W. Beenakker et al., Soft-gluon resummation for squark and gluino hadroproduction. JHEP **12**, 041 (2009). https://doi.org/10.1088/1126-6708/2009/12/041. arXiv:0909.4418

141. W. Beenakker et al., Supersymmetric top and bottom squark production at hadron colliders. JHEP **08**, 098 (2010). https://doi.org/10.1007/JHEP08(2010)098. arXiv:1006.4771

142. W. Beenakker et al., Squark and gluino hadroproduction. Int. J. Mod. Phys. A **26**, 2637 (2011). https://doi.org/10.1142/S0217751X11053560. arXiv:1105.1110

143. W. Beenakker et al., NNLL resummation for squark–antisquark pair production at the LHC. JHEP **01**, 076 (2012). https://doi.org/10.1007/JHEP01(2012)076. arXiv:1110.2446

144. W. Beenakker et al., Towards NNLL resummation: hard matching coefficients for squark and gluino hadroproduction. JHEP **10**, 120 (2013). https://doi.org/10.1007/JHEP10(2013)120. arXiv:1304.6354

145. W. Beenakker et al., NNLL resummation for squark and gluino production at the LHC. JHEP **12**, 023 (2014). https://doi.org/10.1007/JHEP12(2014)023. arXiv:1404.3134

146. W. Beenakker et al., NNLL resummation for stop pair-production at the LHC. JHEP **05**, 153 (2016). https://doi.org/10.1007/JHEP05(2016)153. arXiv:1601.02954

147. W. Beenakker et al., NNLL-fast: predictions for coloured supersymmetric particle production at the LHC with threshold and Coulomb resummation. JHEP **12**, 133 (2016). https://doi.org/10.1007/JHEP12(2016)133. arXiv:1607.07741

148. CMS Collaboration, CMS luminosity measurements for the 2016 data-taking period. CMS Physics Analysis Summary CMS-PAS-LUM-17-001 (2017). https://cds.cern.ch/record/2257069

149. CMS Collaboration, CMS luminosity measurement for the 2017 data-taking period at $\sqrt{s}$ = 13 TeV. CMS Physics Analysis Summary CMS-PAS-LUM-17-004, (2018). https://cds.cern.ch/record/2621960

150. CMS Collaboration, CMS luminosity measurement for the 2018 data-taking period at $\sqrt{s}$ = 13 TeV. CMS Physics Analysis Summary CMS-PAS-LUM-18-002, (2019). https://cds.cern.ch/record/2676164

151. LEP2 SUSY Working Group, ALEPH, DELPHI, L3 and OPAL experiments, Combined LEP chargino results, up to 208 GeV for low Δm (2002). http://lepsusy.web.cern.ch/lepsusy/www/inoslowdmsummer02/charginolowdm_pub.html

CMS Collaboration

Yerevan Physics Institute, Yerevan, Armenia
A. M. Sirunyan[†], A. Tumasyan

Institut für Hochenergiephysik, Wien, Austria
W. Adam, F. Ambrogi, T. Bergauer, J. Brandstetter, M. Dragicevic, J. Erö, A. Escalante Del Valle, M. Flechl, R. Frühwirth[1], M. Jeitler[1], N. Krammer, I. Krätschmer, D. Liko, T. Madlener, I. Mikulec, N. Rad, J. Schieck[1], R. Schöfbeck, M. Spanring, D. Spitzbart, W. Waltenberger, C.-E. Wulz[1], M. Zarucki

Institute for Nuclear Problems, Minsk, Belarus
V. Drugakov, V. Mossolov, J. Suarez Gonzalez

Universiteit Antwerpen, Antwerpen, Belgium
M. R. Darwish, E. A. De Wolf, D. Di Croce, X. Janssen, A. Lelek, M. Pieters, H. Rejeb Sfar, H. Van Haevermaet, P. Van Mechelen, S. Van Putte, N. Van Remortel

Vrije Universiteit Brussel, Brussel, Belgium
F. Blekman, E. S. Bols, S. S. Chhibra, J. D'Hondt, J. De Clercq, D. Lontkovskyi, S. Lowette, I. Marchesini, S. Moortgat, Q. Python, K. Skovpen, S. Tavernier, W. Van Doninck, P. Van Mulders

Université Libre de Bruxelles, Bruxelles, Belgium
D. Beghin, B. Bilin, H. Brun, B. Clerbaux, G. De Lentdecker, H. Delannoy, B. Dorney, L. Favart, A. Grebenyuk, A. K. Kalsi, A. Popov, N. Postiau, E. Starling, L. Thomas, C. Vander Velde, P. Vanlaer, D. Vannerom

Ghent University, Ghent, Belgium
T. Cornelis, D. Dobur, I. Khvastunov[2], M. Niedziela, C. Roskas, D. Trocino, M. Tytgat, W. Verbeke, B. Vermassen, M. Vit

Université Catholique de Louvain, Louvain-la-Neuve, Belgium
O. Bondu, G. Bruno, C. Caputo, P. David, C. Delaere, M. Delcourt, A. Giammanco, V. Lemaitre, J. Prisciandaro, A. Saggio, M. Vidal Marono, P. Vischia, J. Zobec

Centro Brasileiro de Pesquisas Fisicas, Rio de Janeiro, Brazil
F. L. Alves, G. A. Alves, G. Correia Silva, C. Hensel, A. Moraes, P. Rebello Teles

Universidade do Estado do Rio de Janeiro, Rio de Janeiro, Brazil
E. Belchior Batista Das Chagas, W. Carvalho, J. Chinellato[3], E. Coelho, E. M. Da Costa, G. G. Da Silveira[4], D. De Jesus Damiao, C. De Oliveira Martins, S. Fonseca De Souza, L. M. Huertas Guativa, H. Malbouisson, J. Martins[5], D. Matos Figueiredo, M. Medina Jaime[6], M. Melo De Almeida, C. Mora Herrera, L. Mundim, H. Nogima, W. L. Prado Da Silva, L. J. Sanchez Rosas, A. Santoro, A. Sznajder, M. Thiel, E. J. Tonelli Manganote[3], F. Torres Da Silva De Araujo, A. Vilela Pereira

Universidade Estadual Paulista[a], Universidade Federal do ABC[b], São Paulo, Brazil
C. A. Bernardes[a], L. Calligaris[a], T. R. Fernandez Perez Tomei[a], E. M. Gregores[b], D. S. Lemos, P. G. Mercadante[b], S. F. Novaes[a], SandraS. Padula[a]

Institute for Nuclear Research and Nuclear Energy, Bulgarian Academy of Sciences, Sofia, Bulgaria
A. Aleksandrov, G. Antchev, R. Hadjiiska, P. Iaydjiev, M. Misheva, M. Rodozov, M. Shopova, G. Sultanov

University of Sofia, Sofia, Bulgaria
M. Bonchev, A. Dimitrov, T. Ivanov, L. Litov, B. Pavlov, P. Petkov

Beihang University, Beijing, China
W. Fang[7], X. Gao[7], L. Yuan

Institute of High Energy Physics, Beijing, China
G. M. Chen, H. S. Chen, M. Chen, C. H. Jiang, D. Leggat, H. Liao, Z. Liu, A. Spiezia, J. Tao, E. Yazgan, H. Zhang, S. Zhang[8], J. Zhao

State Key Laboratory of Nuclear Physics and Technology, Peking University, Beijing, China
A. Agapitos, Y. Ban, G. Chen, A. Levin, J. Li, L. Li, Q. Li, Y. Mao, S. J. Qian, D. Wang, Q. Wang

Tsinghua University, Beijing, China
M. Ahmad, Z. Hu, Y. Wang

Zhejiang University, Hangzhou, China
M. Xiao

Universidad de Los Andes, Bogota, Colombia
C. Avila, A. Cabrera, C. Florez, C. F. González Hernández, M. A. Segura Delgado

Universidad de Antioquia, Medellin, Colombia
J. Mejia Guisao, J. D. Ruiz Alvarez, C. A. Salazar González, N. Vanegas Arbelaez

University of Split, Faculty of Electrical Engineering, Mechanical Engineering and Naval Architecture, Split, Croatia
D. Giljanović, N. Godinovic, D. Lelas, I. Puljak, T. Sculac

University of Split, Faculty of Science, Split, Croatia
Z. Antunovic, M. Kovac

Institute Rudjer Boskovic, Zagreb, Croatia
V. Brigljevic, D. Ferencek, K. Kadija, B. Mesic, M. Roguljic, A. Starodumov[9], T. Susa

University of Cyprus, Nicosia, Cyprus
M. W. Ather, A. Attikis, E. Erodotou, A. Ioannou, M. Kolosova, S. Konstantinou, G. Mavromanolakis, J. Mousa, C. Nicolaou, F. Ptochos, P. A. Razis, H. Rykaczewski, D. Tsiakkouri

Charles University, Prague, Czech Republic
M. Finger[10], M. Finger Jr.[10], A. Kveton, J. Tomsa

Escuela Politecnica Nacional, Quito, Ecuador
E. Ayala

Universidad San Francisco de Quito, Quito, Ecuador
E. Carrera Jarrin

Academy of Scientific Research and Technology of the Arab Republic of Egypt, Egyptian Network of High Energy Physics, Cairo, Egypt
Y. Assran[11,12], S. Elgammal[12]

National Institute of Chemical Physics and Biophysics, Tallinn, Estonia
S. Bhowmik, A. Carvalho Antunes De Oliveira, R. K. Dewanjee, K. Ehataht, M. Kadastik, M. Raidal, C. Veelken

Department of Physics, University of Helsinki, Helsinki, Finland
P. Eerola, L. Forthomme, H. Kirschenmann, K. Osterberg, M. Voutilainen

Helsinki Institute of Physics, Helsinki, Finland
F. Garcia, J. Havukainen, J. K. Heikkilä, V. Karimäki, M. S. Kim, R. Kinnunen, T. Lampén, K. Lassila-Perini, S. Laurila, S. Lehti, T. Lindén, P. Luukka, T. Mäenpää, H. Siikonen, E. Tuominen, J. Tuominiemi

Lappeenranta University of Technology, Lappeenranta, Finland
T. Tuuva

IRFU, CEA, Université Paris-Saclay, Gif-sur-Yvette, France

M. Besancon, F. Couderc, M. Dejardin, D. Denegri, B. Fabbro, J. L. Faure, F. Ferri, S. Ganjour, A. Givernaud, P. Gras, G. Hamel de Monchenault, P. Jarry, C. Leloup, E. Locci, J. Malcles, J. Rander, A. Rosowsky, M. Ö. Sahin, A. Savoy-Navarro[13], M. Titov

Laboratoire Leprince-Ringuet, Ecole polytechnique, CNRS/IN2P3, Université Paris-Saclay, Palaiseau, France

S. Ahuja, C. Amendola, F. Beaudette, P. Busson, C. Charlot, B. Diab, G. Falmagne, R. Granier de Cassagnac, I. Kucher, A. Lobanov, C. Martin Perez, M. Nguyen, C. Ochando, P. Paganini, J. Rembser, R. Salerno, J. B. Sauvan, Y. Sirois, A. Zabi, A. Zghiche

Université de Strasbourg, CNRS, IPHC UMR 7178, Strasbourg, France

J.-L. Agram[14], J. Andrea, D. Bloch, G. Bourgatte, J.-M. Brom, E. C. Chabert, C. Collard, E. Conte[14], J.-C. Fontaine[14], D. Gelé, U. Goerlach, M. Jansová, A.-C. Le Bihan, N. Tonon, P. Van Hove

Centre de Calcul de l'Institut National de Physique Nucleaire et de Physique des Particules, CNRS/IN2P3, Villeurbanne, France

S. Gadrat

Université de Lyon, Université Claude Bernard Lyon 1, CNRS-IN2P3, Institut de Physique Nucléaire de Lyon, Villeurbanne, France

S. Beauceron, C. Bernet, G. Boudoul, C. Camen, A. Carle, N. Chanon, R. Chierici, D. Contardo, P. Depasse, H. El Mamouni, J. Fay, S. Gascon, M. Gouzevitch, B. Ille, Sa. Jain, F. Lagarde, I. B. Laktineh, H. Lattaud, A. Lesauvage, M. Lethuillier, L. Mirabito, S. Perries, V. Sordini, L. Torterotot, G. Touquet, M. Vander Donckt, S. Viret

Georgian Technical University, Tbilisi, Georgia

A. Khvedelidze[10]

Tbilisi State University, Tbilisi, Georgia

Z. Tsamalaidze[10]

RWTH Aachen University, I. Physikalisches Institut, Aachen, Germany

C. Autermann, L. Feld, M. K. Kiesel, K. Klein, M. Lipinski, D. Meuser, A. Pauls, M. Preuten, M. P. Rauch, J. Schulz, M. Teroerde, B. Wittmer

RWTH Aachen University, III. Physikalisches Institut A, Aachen, Germany

M. Erdmann, B. Fischer, S. Ghosh, T. Hebbeker, K. Hoepfner, H. Keller, L. Mastrolorenzo, M. Merschmeyer, A. Meyer, P. Millet, G. Mocellin, S. Mondal, S. Mukherjee, D. Noll, A. Novak, T. Pook, A. Pozdnyakov, T. Quast, M. Radziej, Y. Rath, H. Reithler, J. Roemer, A. Schmidt, S. C. Schuler, A. Sharma, S. Wiedenbeck, S. Zaleski

RWTH Aachen University, III. Physikalisches Institut B, Aachen, Germany

G. Flügge, W. Haj Ahmad[15], O. Hlushchenko, T. Kress, T. Müller, A. Nowack, C. Pistone, O. Pooth, D. Roy, H. Sert, A. Stahl[16]

Deutsches Elektronen-Synchrotron, Hamburg, Germany

M. Aldaya Martin, P. Asmuss, I. Babounikau, H. Bakhshiansohi, K. Beernaert, O. Behnke, A. Bermúdez Martínez, D. Bertsche, A. A. Bin Anuar, K. Borras[17], V. Botta, A. Campbell, A. Cardini, P. Connor, S. Consuegra Rodríguez, C. Contreras-Campana, V. Danilov, A. De Wit, M. M. Defranchis, C. Diez Pardos, D. Domínguez Damiani, G. Eckerlin, D. Eckstein, T. Eichhorn, A. Elwood, E. Eren, E. Gallo[18], A. Geiser, A. Grohsjean, M. Guthoff, M. Haranko, A. Harb, A. Jafari, N. Z. Jomhari, H. Jung, A. Kasem[17], M. Kasemann, H. Kaveh, J. Keaveney, C. Kleinwort, J. Knolle, D. Krücker, W. Lange, T. Lenz, J. Lidrych, K. Lipka, W. Lohmann[19], R. Mankel, I.-A. Melzer-Pellmann, A. B. Meyer, M. Meyer, M. Missiroli, G. Mittag, J. Mnich, A. Mussgiller, V. Myronenko, D. Pérez Adán, S. K. Pflitsch, D. Pitzl, A. Raspereza, A. Saibel, M. Savitskyi, V. Scheurer, P. Schütze, C. Schwanenberger, R. Shevchenko, A. Singh, H. Tholen, O. Turkot, A. Vagnerini, M. Van De Klundert, R. Walsh, Y. Wen, K. Wichmann, C. Wissing, O. Zenaiev, R. Zlebcik

University of Hamburg, Hamburg, Germany

R. Aggleton, S. Bein, L. Benato, A. Benecke, V. Blobel, T. Dreyer, A. Ebrahimi, F. Feindt, A. Fröhlich, C. Garbers, E. Garutti, D. Gonzalez, P. Gunnellini, J. Haller, A. Hinzmann, A. Karavdina, G. Kasieczka, R. Klanner, R. Kogler, N. Kovalchuk, S. Kurz, V. Kutzner, J. Lange, T. Lange, A. Malara, J. Multhaup, C. E. N. Niemeyer, A. Perieanu,

A. Reimers, O. Rieger, C. Scharf, P. Schleper, S. Schumann, J. Schwandt, J. Sonneveld, H. Stadie, G. Steinbrück, F. M. Stober, B. Vormwald, I. Zoi

Karlsruher Institut fuer Technologie, Karlsruhe, Germany
M. Akbiyik, C. Barth, M. Baselga, S. Baur, T. Berger, E. Butz, R. Caspart, T. Chwalek, W. De Boer, A. Dierlamm, K. El Morabit, N. Faltermann, M. Giffels, P. Goldenzweig, A. Gottmann, M. A. Harrendorf, F. Hartmann[16], U. Husemann, I. Katkov[14], S. Kudella, S. Mitra, M. U. Mozer, D. Müller, Th. Müller, M. Musich, A. Nürnberg, G. Quast, K. Rabbertz, M. Schröder, I. Shvetsov, H. J. Simonis, R. Ulrich, M. Wassmer, M. Weber, C. Wöhrmann, R. Wolf

Institute of Nuclear and Particle Physics (INPP), NCSR Demokritos, Aghia Paraskevi, Greece
G. Anagnostou, P. Asenov, G. Daskalakis, T. Geralis, A. Kyriakis, D. Loukas, G. Paspalaki

National and Kapodistrian University of Athens, Athens, Greece
M. Diamantopoulou, G. Karathanasis, P. Kontaxakis, A. Manousakis-katsikakis, A. Panagiotou, I. Papavergou, N. Saoulidou, A. Stakia, K. Theofilatos, K. Vellidis, E. Vourliotis

National Technical University of Athens, Athens, Greece
G. Bakas, K. Kousouris, I. Papakrivopoulos, G. Tsipolitis

University of Ioánnina, Ioánnina, Greece
I. Evangelou, C. Foudas, P. Gianneios, P. Katsoulis, P. Kokkas, S. Mallios, K. Manitara, N. Manthos, I. Papadopoulos, J. Strologas, F. A. Triantis, D. Tsitsonis

MTA-ELTE Lendület CMS Particle and Nuclear Physics Group, Eötvös Loránd University, Budapest, Hungary
M. Bartók[20], R. Chudasama, M. Csanad, P. Major, K. Mandal, A. Mehta, M. I. Nagy, G. Pasztor, O. Surányi, G. I. Veres

Wigner Research Centre for Physics, Budapest, Hungary
G. Bencze, C. Hajdu, D. Horvath[21], F. Sikler, T. Vámi, V. Veszpremi, G. Vesztergombi[†]

Institute of Nuclear Research ATOMKI, Debrecen, Hungary
N. Beni, S. Czellar, J. Karancsi[20], A. Makovec, J. Molnar, Z. Szillasi

Institute of Physics, University of Debrecen, Debrecen, Hungary
P. Raics, D. Teyssier, Z. L. Trocsanyi, B. Ujvari

Eszterhazy Karoly University, Karoly Robert Campus, Gyongyos, Hungary
T. Csorgo, W. J. Metzger, F. Nemes, T. Novak

Indian Institute of Science (IISc), Bangalore, India
S. Choudhury, J. R. Komaragiri, P. C. Tiwari

National Institute of Science Education and Research, HBNI, Bhubaneswar, India
S. Bahinipati[23], C. Kar, G. Kole, P. Mal, V. K. Muraleedharan Nair Bindhu, A. Nayak[24], D. K. Sahoo[23], S. K. Swain

Panjab University, Chandigarh, India
S. Bansal, S. B. Beri, V. Bhatnagar, S. Chauhan, R. Chawla, N. Dhingra, R. Gupta, A. Kaur, M. Kaur, S. Kaur, P. Kumari, M. Lohan, M. Meena, K. Sandeep, S. Sharma, J. B. Singh, A. K. Virdi, G. Walia

University of Delhi, Delhi, India
A. Bhardwaj, B. C. Choudhary, R. B. Garg, M. Gola, S. Keshri, Ashok Kumar, M. Naimuddin, P. Priyanka, K. Ranjan, Aashaq Shah, R. Sharma

Saha Institute of Nuclear Physics, HBNI, Kolkata, India
R. Bhardwaj[25], M. Bharti[25], R. Bhattacharya, S. Bhattacharya, U. Bhawandeep[25], D. Bhowmik, S. Dutta, S. Ghosh, M. Maity[26], K. Mondal, S. Nandan, A. Purohit, P. K. Rout, G. Saha, S. Sarkar, T. Sarkar[26], M. Sharan, B. Singh[25], S. Thakur[25]

Indian Institute of Technology Madras, Madras, India
P. K. Behera, P. Kalbhor, A. Muhammad, P. R. Pujahari, A. Sharma, A. K. Sikdar

Bhabha Atomic Research Centre, Mumbai, India
D. Dutta, V. Jha, V. Kumar, D. K. Mishra, P. K. Netrakanti, L. M. Pant, P. Shukla

Tata Institute of Fundamental Research-A, Mumbai, India
T. Aziz, M. A. Bhat, S. Dugad, G. B. Mohanty, N. Sur, RavindraKumar Verma

Tata Institute of Fundamental Research-B, Mumbai, India
S. Banerjee, S. Bhattacharya, S. Chatterjee, P. Das, M. Guchait, S. Karmakar, S. Kumar, G. Majumder, K. Mazumdar,
N. Sahoo, S. Sawant

Indian Institute of Science Education and Research (IISER), Pune, India
S. Dube, V. Hegde, B. Kansal, A. Kapoor, K. Kothekar, S. Pandey, A. Rane, A. Rastogi, S. Sharma

Institute for Research in Fundamental Sciences (IPM), Tehran, Iran
S. Chenarani[27], E. Eskandari Tadavani, S. M. Etesami[27], M. Khakzad, M. Mohammadi Najafabadi, M. Naseri,
F. Rezaei Hosseinabadi

University College Dublin, Dublin, Ireland
M. Felcini, M. Grunewald

INFN Sezione di Bari[a], Università di Bari[b], Politecnico di Bari[c], Bari, Italy
M. Abbrescia[a,b], R. Aly[a,b,28], C. Calabria[a,b], A. Colaleo[a], D. Creanza[a,c], L. Cristella[a,b], N. De Filippis[a,c],
M. De Palma[a,b], A. Di Florio[a,b], W. Elmetenawee[a,b], L. Fiore[a], A. Gelmi[a,b], G. Iaselli[a,c], M. Ince[a,b], S. Lezki[a,b],
G. Maggi[a,c], M. Maggi[a], G. Miniello[a,b], S. My[a,b], S. Nuzzo[a,b], A. Pompili[a,b], G. Pugliese[a,c], R. Radogna[a], A. Ranieri[a],
G. Selvaggi[a,b], L. Silvestris[a], F. M. Simone[a,b], R. Venditti[a], P. Verwilligen[a]

INFN Sezione di Bologna[a], Università di Bologna[b], Bologna, Italy
G. Abbiendi[a], C. Battilana[a,b], D. Bonacorsi[a,b], L. Borgonovi[a,b], S. Braibant-Giacomelli[a,b], R. Campanini[a,b],
P. Capiluppi[a,b], A. Castro[a,b], F. R. Cavallo[a], C. Ciocca[a], G. Codispoti[a,b], M. Cuffiani[a,b], G. M. Dallavalle[a], F. Fabbri[a],
A. Fanfani[a,b], E. Fontanesi[a,b], P. Giacomelli[a], C. Grandi[a], L. Guiducci[a,b], F. Iemmi[a,b], S. Lo Meo[a,29], S. Marcellini[a],
G. Masetti[a], F. L. Navarria[a,b], A. Perrotta[a], F. Primavera[a,b], A. M. Rossi[a,b], T. Rovelli[a,b], G. P. Siroli[a,b], N. Tosi[a]

INFN Sezione di Catania[a], Università di Catania[b], Catania, Italy
S. Albergo[a,b,30], S. Costa[a,b], A. Di Mattia[a], R. Potenza[a,b], A. Tricomi[a,b,30], C. Tuve[a,b]

INFN Sezione di Firenze[a], Università di Firenze[b], Firenze, Italy
G. Barbagli[a], A. Cassese, R. Ceccarelli, V. Ciulli[a,b], C. Civinini[a], R. D'Alessandro[a,b], E. Focardi[a,b], G. Latino[a,b],
P. Lenzi[a,b], M. Meschini[a], S. Paoletti[a], G. Sguazzoni, L. Viliani[a]

INFN Laboratori Nazionali di Frascati, Frascati, Italy
L. Benussi, S. Bianco, D. Piccolo

INFN Sezione di Genova[a], Università di Genova[b], Genova, Italy
M. Bozzo[a,b], F. Ferro[a], R. Mulargia[a,b], E. Robutti[a], S. Tosi[a,b]

INFN Sezione di Milano-Bicocca[a], Università di Milano-Bicocca[b], Milano, Italy
A. Benaglia[a], A. Beschi[a,b], F. Brivio[a,b], V. Ciriolo[a,b,16], S. Di Guida[a,b,16], M. E. Dinardo[a,b], P. Dini[a], S. Gennai[a],
A. Ghezzi[a,b], P. Govoni[a,b], L. Guzzi[a,b], M. Malberti[a], S. Malvezzi[a], D. Menasce[a], F. Monti[a,b], L. Moroni[a],
M. Paganoni[a,b], D. Pedrini[a], S. Ragazzi[a,b], T. Tabarelli de Fatis[a,b], D. Zuolo[a,b]

INFN Sezione di Napoli[a], Università di Napoli 'Federico II' [b], Napoli, Italy, Università della Basilicata[c], Potenza, Italy, Università G. Marconi[d], Roma, Italy
S. Buontempo[a], N. Cavallo[a,c], A. De Iorio[a,b], A. Di Crescenzo[a,b], F. Fabozzi[a,c], F. Fienga[a], G. Galati[a], A. O. M. Iorio[a,b],
L. Lista[a,b], S. Meola[a,d,16], P. Paolucci[a,16], B. Rossi[a], C. Sciacca[a,b], E. Voevodina[a,b]

INFN Sezione di Padova[a], Università di Padova[b], Padova, Italy, Università di Trento[c], Trento, Italy
P. Azzi[a], N. Bacchetta[a], D. Bisello[a,b], A. Boletti[a,b], A. Bragagnolo[a,b], R. Carlin[a,b], P. Checchia[a], P. De Castro Manzano[a],
T. Dorigo[a], U. Dosselli[a], F. Gasparini[a,b], U. Gasparini[a,b], A. Gozzelino[a], S. Y. Hoh[a,b], P. Lujan[a], M. Margoni[a,b],
A. T. Meneguzzo[a,b], J. Pazzini[a,b], M. Presilla[b], P. Ronchese[a,b], R. Rossin[a,b], F. Simonetto[a,b], A. Tiko, M. Tosi[a,b],
M. Zanetti[a,b], P. Zotto[a,b], G. Zumerle[a,b]

INFN Sezione di Pavia[a], Università di Pavia[b], Pavia, Italy

A. Braghieri[a], D. Fiorina[a,b], P. Montagna[a,b], S. P. Ratti[a,b], V. Re[a], M. Ressegotti[a,b], C. Riccardi[a,b], P. Salvini[a], I. Vai[a], P. Vitulo[a,b]

INFN Sezione di Perugia[a], Università di Perugia[b], Perugia, Italy

M. Biasini[a,b], G. M. Bilei[a], D. Ciangottini[a,b], L. Fanò[a,b], P. Lariccia[a,b], R. Leonardi[a,b], E. Manoni[a], G. Mantovani[a,b], V. Mariani[a,b], M. Menichelli[a], A. Rossi[a,b], A. Santocchia[a,b], D. Spiga[a]

INFN Sezione di Pisa[a], Università di Pisa[b], Scuola Normale Superiore di Pisa[c], Pisa, Italy

K. Androsov[a], P. Azzurri[a], G. Bagliesi[a], V. Bertacchi[a,c], L. Bianchini[a], T. Boccali[a], R. Castaldi[a], M. A. Ciocci[a,b], R. Dell'Orso[a], G. Fedi[a], L. Giannini[a,c], A. Giassi[a], M. T. Grippo[a], F. Ligabue[a,c], E. Manca[a,c], G. Mandorli[a,c], A. Messineo[a,b], F. Palla[a], A. Rizzi[a,b], G. Rolandi[31], S. Roy Chowdhury, A. Scribano[a], P. Spagnolo[a], R. Tenchini[a], G. Tonelli[a,b], N. Turini, A. Venturi[a], P. G. Verdini[a]

INFN Sezione di Roma[a], Sapienza Università di Roma[b], Rome, Italy

F. Cavallari[a], M. Cipriani[a,b], D. Del Re[a,b], E. Di Marco[a,b], M. Diemoz[a], E. Longo[a,b], P. Meridiani[a], G. Organtini[a,b], F. Pandolfi[a], R. Paramatti[a,b], C. Quaranta[a,b], S. Rahatlou[a,b], C. Rovelli[a], F. Santanastasio[a,b], L. Soffi[a,b]

INFN Sezione di Torino[a], Università di Torino[b], Torino, Italy, Università del Piemonte Orientale[c], Novara, Italy

N. Amapane[a,b], R. Arcidiacono[a,c], S. Argiro[a,b], M. Arneodo[a,c], N. Bartosik[a], R. Bellan[a,b], A. Bellora, C. Biino[a], A. Cappati[a,b], N. Cartiglia[a], S. Cometti[a], M. Costa[a,b], R. Covarelli[a,b], N. Demaria[a], B. Kiani[a,b], C. Mariotti[a], S. Maselli[a], E. Migliore[a,b], V. Monaco[a,b], E. Monteil[a,b], M. Monteno[a], M. M. Obertino[a,b], G. Ortona[a,b], L. Pacher[a,b], N. Pastrone[a], M. Pelliccioni[a], G. L. Pinna Angioni[a,b], A. Romero[a,b], M. Ruspa[a,c], R. Salvatico[a,b], V. Sola[a], A. Solano[a,b], D. Soldi[a,b], A. Staiano[a]

INFN Sezione di Trieste[a], Università di Trieste[b], Trieste, Italy

S. Belforte[a], V. Candelise[a,b], M. Casarsa[a], F. Cossutti[a], A. Da Rold[a,b], G. Della Ricca[a,b], F. Vazzoler[a,b], A. Zanetti[a]

Kyungpook National University, Daegu, Korea

B. Kim, D. H. Kim, G. N. Kim, J. Lee, S. W. Lee, C. S. Moon, Y. D. Oh, S. I. Pak, S. Sekmen, D. C. Son, Y. C. Yang

Chonnam National University, Institute for Universe and Elementary Particles, Kwangju, Korea

H. Kim, D. H. Moon, G. Oh

Hanyang University, Seoul, Korea

B. Francois, T. J. Kim, J. Park

Korea University, Seoul, Korea

S. Cho, S. Choi, Y. Go, S. Ha, B. Hong, K. Lee, K. S. Lee, J. Lim, J. Park, S. K. Park, Y. Roh, J. Yoo

Department of Physics, Kyung Hee University, Seoul, South Korea

J. Goh

Sejong University, Seoul, Korea

H. S. Kim

Seoul National University, Seoul, Korea

J. Almond, J. H. Bhyun, J. Choi, S. Jeon, J. Kim, J. S. Kim, H. Lee, K. Lee, S. Lee, K. Nam, M. Oh, S. B. Oh, B. C. Radburn-Smith, U. K. Yang, H. D. Yoo, I. Yoon, G. B. Yu

University of Seoul, Seoul, Korea

D. Jeon, H. Kim, J. H. Kim, J. S. H. Lee, I. C. Park, I. J Watson

Sungkyunkwan University, Suwon, Korea

Y. Choi, C. Hwang, Y. Jeong, J. Lee, Y. Lee, I. Yu

Riga Technical University, Riga, Latvia

V. Veckalns[32]

Vilnius University, Vilnius, Lithuania

V. Dudenas, A. Juodagalvis, A. Rinkevicius, G. Tamulaitis, J. Vaitkus

National Centre for Particle Physics, Universiti Malaya, Kuala Lumpur, Malaysia
Z. A. Ibrahim, F. Mohamad Idris[33], W. A. T. Wan Abdullah, M. N. Yusli, Z. Zolkapli

Universidad de Sonora (UNISON), Hermosillo, Mexico
J. F. Benitez, A. Castaneda Hernandez, J. A. Murillo Quijada, L. Valencia Palomo

Centro de Investigacion y de Estudios Avanzados del IPN, Mexico City, Mexico
H. Castilla-Valdez, E. De La Cruz-Burelo, I. Heredia-De La Cruz[34], R. Lopez-Fernandez, A. Sanchez-Hernandez

Universidad Iberoamericana, Mexico City, Mexico
S. Carrillo Moreno, C. Oropeza Barrera, M. Ramirez-Garcia, F. Vazquez Valencia

Benemerita Universidad Autonoma de Puebla, Puebla, Mexico
J. Eysermans, I. Pedraza, H. A. Salazar Ibarguen, C. Uribe Estrada

Universidad Autónoma de San Luis Potosí, San Luis Potosí, Mexico
A. Morelos Pineda

University of Montenegro, Podgorica, Montenegro
J. Mijuskovic, N. Raicevic

University of Auckland, Auckland, New Zealand
D. Krofcheck

University of Canterbury, Christchurch, New Zealand
S. Bheesette, P. H. Butler

National Centre for Physics, Quaid-I-Azam University, Islamabad, Pakistan
A. Ahmad, M. Ahmad, Q. Hassan, H. R. Hoorani, W. A. Khan, M. A. Shah, M. Shoaib, M. Waqas

AGH University of Science and Technology Faculty of Computer Science, Electronics and Telecommunications, Krakow, Poland
V. Avati, L. Grzanka, M. Malawski

National Centre for Nuclear Research, Swierk, Poland
H. Bialkowska, M. Bluj, B. Boimska, M. Górski, M. Kazana, M. Szleper, P. Zalewski

Institute of Experimental Physics, Faculty of Physics, University of Warsaw, Warsaw, Poland
K. Bunkowski, A. Byszuk[35], K. Doroba, A. Kalinowski, M. Konecki, J. Krolikowski, M. Misiura, M. Olszewski, M. Walczak

Laboratório de Instrumentação e Física Experimental de Partículas, Lisboa, Portugal
M. Araujo, P. Bargassa, D. Bastos, A. Di Francesco, P. Faccioli, B. Galinhas, M. Gallinaro, J. Hollar, N. Leonardo, T. Niknejad, J. Seixas, K. Shchelina, G. Strong, O. Toldaiev, J. Varela

Joint Institute for Nuclear Research, Dubna, Russia
S. Afanasiev, P. Bunin, M. Gavrilenko, I. Golutvin, I. Gorbunov, A. Kamenev, V. Karjavine, A. Lanev, A. Malakhov, V. Matveev[36,37], P. Moisenz, V. Palichik, V. Perelygin, M. Savina, S. Shmatov, S. Shulha, N. Skatchkov, V. Smirnov, N. Voytishin, A. Zarubin

Petersburg Nuclear Physics Institute, Gatchina (St. Petersburg), Russia
L. Chtchipounov, V. Golovtcov, Y. Ivanov, V. Kim[38], E. Kuznetsova[39], P. Levchenko, V. Murzin, V. Oreshkin, I. Smirnov, D. Sosnov, V. Sulimov, L. Uvarov, A. Vorobyev

Institute for Nuclear Research, Moscow, Russia
Yu. Andreev, A. Dermenev, S. Gninenko, N. Golubev, A. Karneyeu, M. Kirsanov, N. Krasnikov, A. Pashenkov, D. Tlisov, A. Toropin

Institute for Theoretical and Experimental Physics named by A.I. Alikhanov of NRC 'Kurchatov Institute', Moscow, Russia
V. Epshteyn, V. Gavrilov, N. Lychkovskaya, A. Nikitenko[40], V. Popov, I. Pozdnyakov, G. Safronov, A. Spiridonov, A. Stepennov, M. Toms, E. Vlasov, A. Zhokin

Moscow Institute of Physics and Technology, Moscow, Russia
T. Aushev

National Research Nuclear University 'Moscow Engineering Physics Institute' (MEPhI), Moscow, Russia
O. Bychkova, R. Chistov[41], M. Danilov[41], S. Polikarpov[41], E. Tarkovskii

P.N. Lebedev Physical Institute, Moscow, Russia
V. Andreev, M. Azarkin, I. Dremin, M. Kirakosyan, A. Terkulov

Skobeltsyn Institute of Nuclear Physics, Lomonosov Moscow State University, Moscow, Russia
A. Belyaev, E. Boos, V. Bunichev, M. Dubinin[42], L. Dudko, A. Ershov, A. Gribushin, V. Klyukhin, O. Kodolova, I. Lokhtin, S. Obraztsov, S. Petrushanko, V. Savrin

Novosibirsk State University (NSU), Novosibirsk, Russia
A. Barnyakov[43], V. Blinov[43], T. Dimova[43], L. Kardapoltsev[43], Y. Skovpen[43]

Institute for High Energy Physics of National Research Centre 'Kurchatov Institute', Protvino, Russia
I. Azhgirey, I. Bayshev, S. Bitioukov, V. Kachanov, D. Konstantinov, P. Mandrik, V. Petrov, R. Ryutin, S. Slabospitskii, A. Sobol, S. Troshin, N. Tyurin, A. Uzunian, A. Volkov

National Research Tomsk Polytechnic University, Tomsk, Russia
A. Babaev, A. Iuzhakov, V. Okhotnikov

Tomsk State University, Tomsk, Russia
V. Borchsh, V. Ivanchenko, E. Tcherniaev

University of Belgrade: Faculty of Physics and VINCA Institute of Nuclear Sciences, Belgrade, Serbia
P. Adzic[44], P. Cirkovic, M. Dordevic, P. Milenovic, J. Milosevic, M. Stojanovic

Centro de Investigaciones Energéticas Medioambientales y Tecnológicas (CIEMAT), Madrid, Spain
M. Aguilar-Benitez, J. Alcaraz Maestre, A. lvarez Fernández, I. Bachiller, M. Barrio Luna, J. A. Brochero Cifuentes, C. A. Carrillo Montoya, M. Cepeda, M. Cerrada, N. Colino, B. De La Cruz, A. Delgado Peris, C. Fernandez Bedoya, J. P. Fernández Ramos, J. Flix, M. C. Fouz, O. Gonzalez Lopez, S. Goy Lopez, J. M. Hernandez, M. I. Josa, D. Moran, Navarro Tobar, A. Pérez-Calero Yzquierdo, J. Puerta Pelayo, I. Redondo, L. Romero, S. Sánchez Navas, M. S. Soares, A. Triossi, C. Willmott

Universidad Autónoma de Madrid, Madrid, Spain
C. Albajar, J. F. de Trocóniz, R. Reyes-Almanza

Universidad de Oviedo, Instituto Universitario de Ciencias y Tecnologías Espaciales de Asturias (ICTEA), Oviedo, Spain
B. Alvarez Gonzalez, J. Cuevas, C. Erice, J. Fernandez Menendez, S. Folgueras, I. Gonzalez Caballero, J. R. González Fernández, E. Palencia Cortezon, V. Rodríguez Bouza, S. Sanchez Cruz

Instituto de Física de Cantabria (IFCA), CSIC-Universidad de Cantabria, Santander, Spain
I. J. Cabrillo, A. Calderon, B. Chazin Quero, J. Duarte Campderros, M. Fernandez, P. J. Fernández Manteca, A. García Alonso, G. Gomez, C. Martinez Rivero, P. Martinez Ruiz del Arbol, F. Matorras, J. Piedra Gomez, C. Prieels, T. Rodrigo, A. Ruiz-Jimeno, L. Russo[45], L. Scodellaro, I. Vila, J. M. Vizan Garcia

University of Colombo, Colombo, Sri Lanka
K. Malagalage

Department of Physics, University of Ruhuna, Matara, Sri Lanka
W. G. D. Dharmaratna, N. Wickramage

CERN, European Organization for Nuclear Research, Geneva, Switzerland

D. Abbaneo, B. Akgun, E. Auffray, G. Auzinger, J. Baechler, P. Baillon, A. H. Ball, D. Barney, J. Bendavid, M. Bianco, A. Bocci, P. Bortignon, E. Bossini, C. Botta, E. Brondolin, T. Camporesi, A. Caratelli, G. Cerminara, E. Chapon, G. Cucciati, D. d'Enterria, A. Dabrowski, N. Daci, V. Daponte, A. David, O. Davignon, A. De Roeck, M. Deile, M. Dobson, M. Dünser, N. Dupont, A. Elliott-Peisert, N. Emriskova, F. Fallavollita[46], D. Fasanella, S. Fiorendi, G. Franzoni, J. Fulcher, W. Funk, S. Giani, D. Gigi, A. Gilbert, K. Gill, F. Glege, L. Gouskos, M. Gruchala, M. Guilbaud, D. Gulhan, J. Hegeman, C. Heidegger, Y. Iiyama, V. Innocente, T. James, P. Janot, O. Karacheban[19], J. Kaspar, J. Kieseler, M. Krammer[1], N. Kratochwil, C. Lange, P. Lecoq, C. Lourenço, L. Malgeri, M. Mannelli, A. Massironi, F. Meijers, J. A. Merlin, S. Mersi, E. Meschi, F. Moortgat, M. Mulders, J. Ngadiuba, J. Niedziela, S. Nourbakhsh, S. Orfanelli, L. Orsini, F. Pantaleo[16], L. Pape, E. Perez, M. Peruzzi, A. Petrilli, G. Petrucciani, A. Pfeiffer, M. Pierini, F. M. Pitters, D. Rabady, A. Racz, M. Rieger, M. Rovere, H. Sakulin, C. Schäfer, C. Schwick, M. Selvaggi, A. Sharma, P. Silva, W. Snoeys, P. Sphicas[47], J. Steggemann, S. Summers, V. R. Tavolaro, D. Treille, A. Tsirou, G. P. Van Onsem, A. Vartak, M. Verzetti, W. D. Zeuner

Paul Scherrer Institut, Villigen, Switzerland

L. Caminada[48], K. Deiters, W. Erdmann, R. Horisberger, Q. Ingram, H. C. Kaestli, D. Kotlinski, U. Langenegger, T. Rohe, S. A. Wiederkehr

ETH Zurich-Institute for Particle Physics and Astrophysics (IPA), Zurich, Switzerland

M. Backhaus, P. Berger, N. Chernyavskaya, G. Dissertori, M. Dittmar, M. Donegà, C. Dorfer, T. A. Gómez Espinosa, C. Grab, D. Hits, T. Klijnsma, W. Lustermann, A.-M. Lyon, R. A. Manzoni, M. T. Meinhard, F. Micheli, P. Musella, F. Nessi-Tedaldi, F. Pauss, G. Perrin, L. Perrozzi, S. Pigazzini, M. G. Ratti, M. Reichmann, C. Reissel, T. Reitenspiess, D. Ruini, D. A. Sanz Becerra, M. Schönenberger, L. Shchutska, M. L. Vesterbacka Olsson, R. Wallny, D. H. Zhu

Universität Zürich, Zurich, Switzerland

T. K. Aarrestad, C. Amsler[49], D. Brzhechko, M. F. Canelli, A. De Cosa, R. Del Burgo, S. Donato, B. Kilminster, S. Leontsinis, V. M. Mikuni, I. Neutelings, G. Rauco, P. Robmann, K. Schweiger, C. Seitz, Y. Takahashi, S. Wertz, A. Zucchetta

National Central University, Chung-Li, Taiwan

T. H. Doan, C. M. Kuo, W. Lin, A. Roy, S. S. Yu

National Taiwan University (NTU), Taipei, Taiwan

P. Chang, Y. Chao, K. F. Chen, P. H. Chen, W.-S. Hou, Y. y. Li, R.-S. Lu, E. Paganis, A. Psallidas, A. Steen

Chulalongkorn University, Faculty of Science, Department of Physics, Bangkok, Thailand

B. Asavapibhop, C. Asawatangtrakuldee, N. Srimanobhas, N. Suwonjandee

ukurova University, Physics Department, Science and Art Faculty, Adana, Turkey

A. Bat, F. Boran, A. Celik[50], S. Cerci[51], S. Damarseckin[52], Z. S. Demiroglu, F. Dolek, C. Dozen[53], I. Dumanoglu, G. Gokbulut, EmineGurpinar Guler[54], Y. Guler, I. Hos[55], C. Isik, E. E. Kangal[56], O. Kara, A. Kayis Topaksu, U. Kiminsu, G. Onengut, K. Ozdemir[57], S. Ozturk[58], A. E. Simsek, D. Sunar Cerci[51], U. G. Tok, S. Turkcapar, I. S. Zorbakir, C. Zorbilmez

Middle East Technical University, Physics Department, Ankara, Turkey

B. Isildak[59], G. Karapinar[60], M. Yalvac

Bogazici University, Istanbul, Turkey

I. O. Atakisi, E. Gülmez, M. Kaya[61], O. Kaya[62], Ö. Özçelik, S. Tekten, E. A. Yetkin[63]

Istanbul Technical University, Istanbul, Turkey

A. Cakir, K. Cankocak, Y. Komurcu, S. Sen[64]

Istanbul University, Istanbul, Turkey

B. Kaynak, S. Ozkorucuklu

Institute for Scintillation Materials of National Academy of Science of Ukraine, Kharkov, Ukraine

B. Grynyov

National Scientific Center, Kharkov Institute of Physics and Technology, Kharkov, Ukraine
L. Levchuk

University of Bristol, Bristol, United Kingdom
E. Bhal, S. Bologna, J. J. Brooke, D. Burns[65], E. Clement, D. Cussans, H. Flacher, J. Goldstein, G. P. Heath, H. F. Heath, L. Kreczko, B. Krikler, S. Paramesvaran, B. Penning, T. Sakuma, S. Seif El Nasr-Storey, V. J. Smith, J. Taylor, A. Titterton

Rutherford Appleton Laboratory, Didcot, United Kingdom
K. W. Bell, A. Belyaev[66], C. Brew, R. M. Brown, D. J. A. Cockerill, J. A. Coughlan, K. Harder, S. Harper, J. Linacre, K. Manolopoulos, D. M. Newbold, E. Olaiya, D. Petyt, T. Reis, T. Schuh, C. H. Shepherd-Themistocleous, A. Thea, I. R. Tomalin, T. Williams, W. J. Womersley

Imperial College, London, United Kingdom
R. Bainbridge, P. Bloch, J. Borg, S. Breeze, O. Buchmuller, A. Bundock, GurpreetSingh CHAHAL[67], D. Colling, P. Dauncey, G. Davies, M. Della Negra, R. Di Maria, P. Everaerts, G. Hall, G. Iles, M. Komm, C. Laner, L. Lyons, A.-M. Magnan, S. Malik, A. Martelli, V. Milosevic, A. Morton, J. Nash[68], V. Palladino, M. Pesaresi, D. M. Raymond, A. Richards, A. Rose, E. Scott, C. Seez, A. Shtipliyski, M. Stoye, T. Strebler, A. Tapper, K. Uchida, T. Virdee[16], N. Wardle, D. Winterbottom, J. Wright, A. G. Zecchinelli, S. C. Zenz

Brunel University, Uxbridge, United Kingdom
J. E. Cole, P. R. Hobson, A. Khan, P. Kyberd, C. K. Mackay, I. D. Reid, L. Teodorescu, S. Zahid

Baylor University, Waco, USA
K. Call, B. Caraway, J. Dittmann, K. Hatakeyama, C. Madrid, B. McMaster, N. Pastika, C. Smith

Catholic University of America, Washington DC, USA
R. Bartek, A. Dominguez, R. Uniyal, A. M. Vargas Hernandez

The University of Alabama, Tuscaloosa, USA
A. Buccilli, S. I. Cooper, C. Henderson, P. Rumerio, C. West

Boston University, Boston, USA
A. Albert, D. Arcaro, Z. Demiragli, D. Gastler, C. Richardson, J. Rohlf, D. Sperka, I. Suarez, L. Sulak, D. Zou

Brown University, Providence, USA
G. Benelli, B. Burkle, X. Coubez[17], D. Cutts, Y. t. Duh, M. Hadley, U. Heintz, J. M. Hogan[69], K. H. M. Kwok, E. Laird, G. Landsberg, K. T. Lau, J. Lee, Z. Mao, M. Narain, S. Sagir[70], R. Syarif, E. Usai, D. Yu, W. Zhang

University of California, Davis, Davis, USA
R. Band, C. Brainerd, R. Breedon, M. Calderon De La Barca Sanchez, M. Chertok, J. Conway, R. Conway, P. T. Cox, R. Erbacher, C. Flores, G. Funk, F. Jensen, W. Ko, O. Kukral, R. Lander, M. Mulhearn, D. Pellett, J. Pilot, M. Shi, D. Taylor, K. Tos, M. Tripathi, Z. Wang, F. Zhang

University of California, Los Angeles, USA
M. Bachtis, C. Bravo, R. Cousins, A. Dasgupta, A. Florent, J. Hauser, M. Ignatenko, N. Mccoll, W. A. Nash, S. Regnard, D. Saltzberg, C. Schnaible, B. Stone, V. Valuev

University of California, Riverside, Riverside, USA
K. Burt, Y. Chen, R. Clare, J. W. Gary, S. M. A. Ghiasi Shirazi, G. Hanson, G. Karapostoli, E. Kennedy, O. R. Long, M. Olmedo Negrete, M. I. Paneva, W. Si, L. Wang, S. Wimpenny, B. R. Yates, Y. Zhang

University of California, San Diego, La Jolla, USA
J. G. Branson, P. Chang, S. Cittolin, S. Cooperstein, N. Deelen, M. Derdzinski, R. Gerosa, D. Gilbert, B. Hashemi, D. Klein, V. Krutelyov, J. Letts, M. Masciovecchio, S. May, S. Padhi, M. Pieri, V. Sharma, M. Tadel, F. Würthwein, A. Yagil, G. Zevi Della Porta

University of California, Santa Barbara-Department of Physics, Santa Barbara, USA
N. Amin, R. Bhandari, C. Campagnari, M. Citron, V. Dutta, M. Franco Sevilla, J. Incandela, B. Marsh, H. Mei, A. Ovcharova, H. Qu, J. Richman, U. Sarica, D. Stuart, S. Wang

California Institute of Technology, Pasadena, USA

D. Anderson, A. Bornheim, O. Cerri, I. Dutta, J. M. Lawhorn, N. Lu, J. Mao, H. B. Newman, T. Q. Nguyen, J. Pata, M. Spiropulu, J. R. Vlimant, S. Xie, Z. Zhang, R. Y. Zhu

Carnegie Mellon University, Pittsburgh, USA

M. B. Andrews, T. Ferguson, T. Mudholkar, M. Paulini, M. Sun, I. Vorobiev, M. Weinberg

University of Colorado Boulder, Boulder, USA

J. P. Cumalat, W. T. Ford, E. MacDonald, T. Mulholland, R. Patel, A. Perloff, K. Stenson, K. A. Ulmer, S. R. Wagner

Cornell University, Ithaca, USA

J. Alexander, Y. Cheng, J. Chu, A. Datta, A. Frankenthal, K. Mcdermott, J. R. Patterson, D. Quach, A. Ryd, S. M. Tan, Z. Tao, J. Thom, P. Wittich, M. Zientek

Fermi National Accelerator Laboratory, Batavia, USA

S. Abdullin, M. Albrow, M. Alyari, G. Apollinari, A. Apresyan, A. Apyan, S. Banerjee, L. A. T. Bauerdick, A. Beretvas, D. Berry, J. Berryhill, P. C. Bhat, K. Burkett, J. N. Butler, A. Canepa, G. B. Cerati, H. W. K. Cheung, F. Chlebana, M. Cremonesi, J. Duarte, V. D. Elvira, J. Freeman, Z. Gecse, E. Gottschalk, L. Gray, D. Green, S. Grünendahl, O. Gutsche, AllisonReinsvold Hall, J. Hanlon, R. M. Harris, S. Hasegawa, R. Heller, J. Hirschauer, B. Jayatilaka, S. Jindariani, M. Johnson, U. Joshi, B. Klima, M. J. Kortelainen, B. Kreis, S. Lammel, J. Lewis, D. Lincoln, R. Lipton, M. Liu, T. Liu, J. Lykken, K. Maeshima, J. M. Marraffino, D. Mason, P. McBride, P. Merkel, S. Mrenna, S. Nahn, V. O'Dell, V. Papadimitriou, K. Pedro, C. Pena, G. Rakness, F. Ravera, L. Ristori, B. Schneider, E. Sexton-Kennedy, N. Smith, A. Soha, W. J. Spalding, L. Spiegel, S. Stoynev, J. Strait, N. Strobbe, L. Taylor, S. Tkaczyk, N. V. Tran, L. Uplegger, E. W. Vaandering, C. Vernieri, R. Vidal, M. Wang, H. A. Weber

University of Florida, Gainesville, USA

D. Acosta, P. Avery, D. Bourilkov, A. Brinkerhoff, L. Cadamuro, A. Carnes, V. Cherepanov, F. Errico, R. D. Field, S. V. Gleyzer, B. M. Joshi, M. Kim, J. Konigsberg, A. Korytov, K. H. Lo, P. Ma, K. Matchev, N. Menendez, G. Mitselmakher, D. Rosenzweig, K. Shi, J. Wang, S. Wang, X. Zuo

Florida International University, Miami, USA

Y. R. Joshi

Florida State University, Tallahassee, USA

T. Adams, A. Askew, S. Hagopian, V. Hagopian, K. F. Johnson, R. Khurana, T. Kolberg, G. Martinez, T. Perry, H. Prosper, C. Schiber, R. Yohay, J. Zhang

Florida Institute of Technology, Melbourne, USA

M. M. Baarmand, M. Hohlmann, D. Noonan, M. Rahmani, M. Saunders, F. Yumiceva

University of Illinois at Chicago (UIC), Chicago, USA

M. R. Adams, L. Apanasevich, R. R. Betts, R. Cavanaugh, X. Chen, S. Dittmer, O. Evdokimov, C. E. Gerber, D. A. Hangal, D. J. Hofman, K. Jung, C. Mills, T. Roy, M. B. Tonjes, N. Varelas, J. Viinikainen, H. Wang, X. Wang, Z. Wu

The University of Iowa, Iowa City, USA

M. Alhusseini, B. Bilki[54], W. Clarida, K. Dilsiz[71], S. Durgut, R. P. Gandrajula, M. Haytmyradov, V. Khristenko, O. K. Köseyan, J.-P. Merlo, A. Mestvirishvili[72], A. Moeller, J. Nachtman, H. Ogul[73], Y. Onel, F. Ozok[74], A. Penzo, C. Snyder, E. Tiras, J. Wetzel

Johns Hopkins University, Baltimore, USA

B. Blumenfeld, A. Cocoros, N. Eminizer, A. V. Gritsan, W. T. Hung, S. Kyriacou, P. Maksimovic, J. Roskes, M. Swartz

The University of Kansas, Lawrence, USA

C. Baldenegro Barrera, P. Baringer, A. Bean, S. Boren, J. Bowen, A. Bylinkin, T. Isidori, S. Khalil, J. King, G. Krintiras, A. Kropivnitskaya, C. Lindsey, D. Majumder, W. Mcbrayer, N. Minafra, M. Murray, C. Rogan, C. Royon, S. Sanders, E. Schmitz, J. D. Tapia Takaki, Q. Wang, J. Williams, G. Wilson

Kansas State University, Manhattan, USA

S. Duric, A. Ivanov, K. Kaadze, D. Kim, Y. Maravin, D. R. Mendis, T. Mitchell, A. Modak, A. Mohammadi

Lawrence Livermore National Laboratory, Livermore, USA

F. Rebassoo, D. Wright

University of Maryland, College Park, USA

A. Baden, O. Baron, A. Belloni, S. C. Eno, Y. Feng, N. J. Hadley, S. Jabeen, G. Y. Jeng, R. G. Kellogg, J. Kunkle, A. C. Mignerey, S. Nabili, F. Ricci-Tam, M. Seidel, Y. H. Shin, A. Skuja, S. C. Tonwar, K. Wong

Massachusetts Institute of Technology, Cambridge, USA

D. Abercrombie, B. Allen, A. Baty, R. Bi, S. Brandt, W. Busza, I. A. Cali, M. D'Alfonso, G. Gomez Ceballos, M. Goncharov, P. Harris, D. Hsu, M. Hu, M. Klute, D. Kovalskyi, Y.-J. Lee, P. D. Luckey, B. Maier, A. C. Marini, C. Mcginn, C. Mironov, S. Narayanan, X. Niu, C. Paus, D. Rankin, C. Roland, G. Roland, Z. Shi, G. S. F. Stephans, K. Sumorok, K. Tatar, D. Velicanu, J. Wang, T. W. Wang, B. Wyslouch

University of Minnesota, Minneapolis, USA

R. M. Chatterjee, A. Evans, S. Guts[†], P. Hansen, J. Hiltbrand, Y. Kubota, Z. Lesko, J. Mans, R. Rusack, M. A. Wadud

University of Mississippi, Oxford, USA

J. G. Acosta, S. Oliveros

University of Nebraska-Lincoln, Lincoln, USA

K. Bloom, S. Chauhan, D. R. Claes, C. Fangmeier, L. Finco, F. Golf, R. Kamalieddin, I. Kravchenko, J. E. Siado, G. R. Snow[†], B. Stieger, W. Tabb

State University of New York at Buffalo, Buffalo, USA

G. Agarwal, C. Harrington, I. Iashvili, A. Kharchilava, C. McLean, D. Nguyen, A. Parker, J. Pekkanen, S. Rappoccio, B. Roozbahani

Northeastern University, Boston, USA

G. Alverson, E. Barberis, C. Freer, Y. Haddad, A. Hortiangtham, G. Madigan, B. Marzocchi, D. M. Morse, T. Orimoto, L. Skinnari, A. Tishelman-Charny, T. Wamorkar, B. Wang, A. Wisecarver, D. Wood

Northwestern University, Evanston, USA

S. Bhattacharya, J. Bueghly, T. Gunter, K. A. Hahn, N. Odell, M. H. Schmitt, K. Sung, M. Trovato, M. Velasco

University of Notre Dame, Notre Dame, USA

R. Bucci, N. Dev, R. Goldouzian, M. Hildreth, K. Hurtado Anampa, C. Jessop, D. J. Karmgard, K. Lannon, W. Li, N. Loukas, N. Marinelli, I. Mcalister, F. Meng, C. Mueller, Y. Musienko[36], M. Planer, R. Ruchti, P. Siddireddy, G. Smith, S. Taroni, M. Wayne, A. Wightman, M. Wolf, A. Woodard

The Ohio State University, Columbus, USA

J. Alimena, B. Bylsma, L. S. Durkin, B. Francis, C. Hill, W. Ji, A. Lefeld, T. Y. Ling, B. L. Winer

Princeton University, Princeton, USA

G. Dezoort, P. Elmer, J. Hardenbrook, N. Haubrich, S. Higginbotham, A. Kalogeropoulos, S. Kwan, D. Lange, M. T. Lucchini, J. Luo, D. Marlow, K. Mei, I. Ojalvo, J. Olsen, C. Palmer, P. Piroué, J. Salfeld-Nebgen, D. Stickland, C. Tully, Z. Wang

University of Puerto Rico, Mayaguez, USA

S. Malik, S. Norberg

Purdue University, West Lafayette, USA

A. Barker, V. E. Barnes, S. Das, L. Gutay, M. Jones, A. W. Jung, A. Khatiwada, B. Mahakud, D. H. Miller, G. Negro, N. Neumeister, C. C. Peng, S. Piperov, H. Qiu, J. F. Schulte, N. Trevisani, F. Wang, R. Xiao, W. Xie

Purdue University Northwest, Hammond, USA

T. Cheng, J. Dolen, N. Parashar

Rice University, Houston, USA

U. Behrens, K. M. Ecklund, S. Freed, F. J. M. Geurts, M. Kilpatrick, Arun Kumar, W. Li, B. P. Padley, R. Redjimi, J. Roberts, J. Rorie, W. Shi, A. G. Stahl Leiton, Z. Tu, A. Zhang

University of Rochester, Rochester, USA

A. Bodek, P. de Barbaro, R. Demina, J. L. Dulemba, C. Fallon, T. Ferbel, M. Galanti, A. Garcia-Bellido, O. Hindrichs, A. Khukhunaishvili, E. Ranken, R. Taus

Rutgers, The State University of New Jersey, Piscataway, USA

B. Chiarito, J. P. Chou, A. Gandrakota, Y. Gershtein, E. Halkiadakis, A. Hart, M. Heindl, E. Hughes, S. Kaplan, I. Laflotte, A. Lath, R. Montalvo, K. Nash, M. Osherson, H. Saka, S. Salur, S. Schnetzer, S. Somalwar, R. Stone, S. Thomas

University of Tennessee, Knoxville, USA

H. Acharya, A. G. Delannoy, S. Spanier

Texas A & M University, College Station, USA

O. Bouhali[75], A. Celik, M. Dalchenko, M. De Mattia, A. Delgado, S. Dildick, R. Eusebi, J. Gilmore, T. Huang, T. Kamon[76], S. Luo, S. Malhotra, D. Marley, R. Mueller, D. Overton, L. Perniè, D. Rathjens, A. Safonov

Texas Tech University, Lubbock, USA

N. Akchurin, J. Damgov, F. De Guio, S. Kunori, K. Lamichhane, S. W. Lee, T. Mengke, S. Muthumuni, T. Peltola, S. Undleeb, I. Volobouev, Z. Wang, A. Whitbeck

Vanderbilt University, Nashville, USA

S. Greene, A. Gurrola, R. Janjam, W. Johns, C. Maguire, A. Melo, H. Ni, K. Padeken, F. Romeo, P. Sheldon, S. Tuo, J. Velkovska, M. Verweij

University of Virginia, Charlottesville, USA

M. W. Arenton, P. Barria, B. Cox, G. Cummings, J. Hakala, R. Hirosky, M. Joyce, A. Ledovskoy, C. Neu, B. Tannenwald, Y. Wang, E. Wolfe, F. Xia

Wayne State University, Detroit, USA

R. Harr, P. E. Karchin, N. Poudyal, J. Sturdy, P. Thapa

University of Wisconsin-Madison, Madison, WI, USA

T. Bose, J. Buchanan, C. Caillol, D. Carlsmith, S. Dasu, I. De Bruyn, L. Dodd, F. Fiori, C. Galloni, B. Gomber[77], H. He, M. Grothe, M. Herndon, A. Hervé, U. Hussain, P. Klabbers, A. Lanaro, A. Loeliger, K. Long, R. Loveless, J. Madhusudanan Sreekala, D. Pinna, T. Ruggles, A. Savin, V. Sharma, W. H. Smith, D. Teague, S. Trembath-reichert, N. Woods

[†] **Deceased**

1: Also at Vienna University of Technology, Vienna, Austria
2: Also at IRFU, CEA, Université Paris-Saclay, Gif-sur-Yvette, France
3: Also at Universidade Estadual de Campinas, Campinas, Brazil
4: Also at Federal University of Rio Grande do Sul, Porto Alegre, Brazil
5: Also at UFMS, Nova Andradina, Brazil
6: Also at Universidade Federal de Pelotas, Pelotas, Brazil
7: Also at Université Libre de Bruxelles, Bruxelles, Belgium
8: Also at University of Chinese Academy of Sciences, Beijing, China
9: Also at Institute for Theoretical and Experimental Physics named by A.I. Alikhanov of NRC 'Kurchatov Institute', Moscow, Russia
10: Also at Joint Institute for Nuclear Research, Dubna, Russia
11: Also at Suez University, El-Suez, Egypt
12: Now at British University in Egypt, Cairo, Egypt
13: Now at Purdue University, West Lafayette, USA
14: Also at Université de Haute Alsace, Mulhouse, France
15: Also at Erzincan Binali Yildirim University, Erzincan, Turkey
16: Also at CERN, European Organization for Nuclear Research, Geneva, Switzerland
17: Also at RWTH Aachen University, III. Physikalisches Institut A, Aachen, Germany
18: Also at University of Hamburg, Hamburg, Germany
19: Also at Brandenburg University of Technology, Cottbus, Germany

20: Also at Institute of Physics, University of Debrecen, Debrecen, Hungary, Debrecen, Hungary

21: Also at Institute of Nuclear Research ATOMKI, Debrecen, Hungary

22: Also at MTA-ELTE Lendület CMS Particle and Nuclear Physics Group, Eötvös Loránd University, Budapest, Hungary, Budapest, Hungary

23: Also at IIT Bhubaneswar, Bhubaneswar, India, Bhubaneswar, India

24: Also at Institute of Physics, Bhubaneswar, India

25: Also at Shoolini University, Solan, India

26: Also at University of Visva-Bharati, Santiniketan, India

27: Also at Isfahan University of Technology, Isfahan, Iran

28: Now at INFN Sezione di Bari [a], Università di Bari [b], Politecnico di Bari [c], Bari, Italy

29: Also at Italian National Agency for New Technologies, Energy and Sustainable Economic Development, Bologna, Italy

30: Also at Centro Siciliano di Fisica Nucleare e di Struttura Della Materia, Catania, Italy

31: Also at Scuola Normale e Sezione dell'INFN, Pisa, Italy

32: Also at Riga Technical University, Riga, Latvia, Riga, Latvia

33: Also at Malaysian Nuclear Agency, MOSTI, Kajang, Malaysia

34: Also at Consejo Nacional de Ciencia y Tecnología, Mexico City, Mexico

35: Also at Warsaw University of Technology, Institute of Electronic Systems, Warsaw, Poland

36: Also at Institute for Nuclear Research, Moscow, Russia

37: Now at National Research Nuclear University 'Moscow Engineering Physics Institute' (MEPhI), Moscow, Russia

38: Also at St. Petersburg State Polytechnical University, St. Petersburg, Russia

39: Also at University of Florida, Gainesville, USA

40: Also at Imperial College, London, United Kingdom

41: Also at P.N. Lebedev Physical Institute, Moscow, Russia

42: Also at California Institute of Technology, Pasadena, USA

43: Also at Budker Institute of Nuclear Physics, Novosibirsk, Russia

44: Also at Faculty of Physics, University of Belgrade, Belgrade, Serbia

45: Also at Università degli Studi di Siena, Siena, Italy

46: Also at INFN Sezione di Pavia [a], Università di Pavia [b], Pavia, Italy, Pavia, Italy

47: Also at National and Kapodistrian University of Athens, Athens, Greece

48: Also at Universität Zürich, Zurich, Switzerland

49: Also at Stefan Meyer Institute for Subatomic Physics, Vienna, Austria, Vienna, Austria

50: Also at Burdur Mehmet Akif Ersoy University, BURDUR, Turkey

51: Also at Adiyaman University, Adiyaman, Turkey

52: Also at Şırnak University, Sirnak, Turkey

53: Also at Tsinghua University, Beijing, China

54: Also at Beykent University, Istanbul, Turkey, Istanbul, Turkey

55: Also at Istanbul Aydin University, Istanbul, Turkey

56: Also at Mersin University, Mersin, Turkey

57: Also at Piri Reis University, Istanbul, Turkey

58: Also at Gaziosmanpasa University, Tokat, Turkey

59: Also at Ozyegin University, Istanbul, Turkey

60: Also at Izmir Institute of Technology, Izmir, Turkey

61: Also at Marmara University, Istanbul, Turkey

62: Also at Kafkas University, Kars, Turkey

63: Also at Istanbul Bilgi University, Istanbul, Turkey

64: Also at Hacettepe University, Ankara, Turkey

65: Also at Vrije Universiteit Brussel, Brussel, Belgium

66: Also at School of Physics and Astronomy, University of Southampton, Southampton, United Kingdom

67: Also at IPPP Durham University, Durham, United Kingdom

68: Also at Monash University, Faculty of Science, Clayton, Australia

69: Also at Bethel University, St. Paul, Minneapolis, USA, St. Paul, USA

70: Also at Karamanoğlu Mehmetbey University, Karaman, Turkey

71: Also at Bingol University, Bingol, Turkey

72: Also at Georgian Technical University, Tbilisi, Georgia

73: Also at Sinop University, Sinop, Turkey

74: Also at Mimar Sinan University, Istanbul, Istanbul, Turkey

75: Also at Texas A&M University at Qatar, Doha, Qatar

76: Also at Kyungpook National University, Daegu, Korea, Daegu, Korea

77: Also at University of Hyderabad, Hyderabad, India